Engineering Library

JAN 25 '50

Journal of Research

of the

U.S. National Bureau of Standards

DECEMBER 1949

VOLUME 43 NUMBER 6

PERIODICALS OF THE NATIONAL BUREAU OF STANDARDS

Journal of Research

The National Bureau of Standards is the principal agency of the Federal Government for fundamental research in physics, chemistry, and engineering. It has the custody of the national standards of physical measurement in terms of which all working standards in research laboratories and industry are calibrated, and carries on necessary research leading to improvement in such standards and methods of measurement. It also has a general responsibility for basic research in physics, chemistry, and engineering, and for developments of improved methods for testing materials and equipment. It determines physical constants and properties of materials, tests and calibrates standard measuring apparatus and reference standards, and studies technical processes. The results of the Bureau's research and investigations are published in the JOURNAL OF RESEARCH.

Research Papers

Reprints of individual articles appearing in the JOURNAL OF RESEARCH. They are made available to serve the needs of research workers, technical groups, and others for the separate papers relating to the special subjects in which they are interested.

Technical News Bulletin

Contains short but complete summaries of research, development, and testing in progress at the Bureau, accounts of the Bureau's national and international activities, scientific and technical announcements of new plans and programs, and a list of publications by members of the staff. It is a prompt and reliable source of official information of value to those who desire to keep in touch with the general activities of the Bureau.

Basic Radio Propagation Predictions

The CRPL-D series, Basic Radio Propagation Predictions, is issued as a monthly publication for those concerned with radio communication in determining the best sky-wave frequencies over any path at any time of day for average conditions for the month of prediction, which is made 3 months in advance. Charts of extraordinary-wave critical frequency for the F2 layer, of maximum usable frequency for a transmission distance of 4,000 km, and of percentage of time occurrence for transmission by sporadic E in excess of 15 Mc, for a distance of 2,000 km, are included.

ANNUAL SUBSCRIPTION Send order, with remittance, to Superintendent of Documents, U. S. Government Printing Office, Washington 25, D. C.	United States, Canada, Cuba, Mexico, Newfoundland, Republic of Panama	Other countries
JOURNAL OF RESEARCH of the National Bureau of Standards:		
12 monthly issues (2 volumes), paper covers	$4.50	$5.50
Bound volume (½ year, 1 volume), blue buckram	3.00	3.50
RESEARCH PAPERS	(*)	(*)
TECHNICAL NEWS BULLETIN, 12 monthly issues	1.00	1.35
BASIC RADIO PROPAGATION PREDICTIONS, 12 monthly issues	1.00	1.25

*The prices of the separate Research Papers appearing in this JOURNAL are given in the Contents. If 100 or more copies of any separate are ordered a discount of 25 percent is allowed. Those who desire copies of separate Research Papers should send their orders and remittance without delay to the Superintendent of Documents, U. S. Government Printing Office, Washington 25, D. C. This will aid him to determine the number of copies to be printed for sale. Research Papers are not printed from electrotypes and usually no more reprints can be had when the first and only printing is exhausted.

The printing of this publication has been approved by the Director of the Bureau of the Budget, April 23, 1947

U. S. DEPARTMENT OF COMMERCE
Charles Sawyer, Secretary
NATIONAL BUREAU OF STANDARDS
E. U. Condon, Director

DECEMBER 1949
VOLUME • 43
NUMBER 6

JOURNAL OF RESEARCH

of the

NATIONAL BUREAU OF STANDARDS

Contents

RP		Page
2042	The freezing point of uranium. Andrew I. Dahl and Harold E. Cleaves. (Price 5 cents)	513
2043	Dissociation constants of weak bases from electromotive-force measurements of solutions of partially hydrolyzed salts. Roger G. Bates and Gladys D. Pinching. (Price 5 cents)	519
2044	A reduction-of-area gage for use at low temperatures. Glenn W. Geil and Nesbit L. Carwile. (Price 5 cents)	527
2045	Mass spectra of C_3H_8 isomers. Fred L. Mohler, Evelyn G. Bloom, Laura Williamson, C. E. Wise, and E. J. Wells. (Price 5 cents)	533
2046	A note on the numerical integration of differential equations. W. E. Milne. (Price 5 cents)	537
2047	Measurement of the disintegration rate of sodium^{22} by the coincidence method. J. L. Herson. (Price 5 cents)	543
2048	Submicroscopic structure of cellulose from nitrogen sorption measurements. Charles M. Hunt, Raymond L. Blaine, and John W. Rowen. (Price 5 cents)	547
2049	Vapor pressures and boiling points of sixty API-NBS hydrocarbons. Alphonse F. Forziati, William R. Norris, and Frederick D. Rossini. (Price 10 cents)	555
2050	Bond of concrete reinforcing bars. Arthur P. Clark. (Price 10 cents)	565
2051	Analysis of the direct-current bolometer bridge. David M. Kerns. (Price 10 cents)	581
2052	A method and apparatus for determining the ignition characteristics of plastics. Nicholas P. Setchkin. (Price 15 cents)	591
	Index to volume 43 (July to December 1949, Research Papers RP2000 to RP2052).	609

For sale by the Superintendent of Documents, U. S. Government Printing Office, Washington 25, D. C. - Price 75 cents
$4.50 per year on subscription

UNITED STATES GOVERNMENT PRINTING OFFICE, WASHINGTON : 1949

U. S. Department of Commerce
National Bureau of Standards

Research Paper RP2042
Volume 43, December 1949

Part of the Journal of Research of the National Bureau of Standards

The Freezing Point of Uranium

By Andrew I. Dahl and Harold E. Cleaves

The freezing temperature of uranium of about 99.99-percent purity was measured with an optical pyrometer and found to be 1,133° ± 2° C. Both the initial purity and the initial freezing temperature were lower than the foregoing values. However, holding the metal at temperatures just above the melting point for several hours resulted in a decrease in the content of several impurities and an increase in the freezing temperature to a final constant value.

The freezing temperature was not greatly affected by the crucible material, similar values being obtained in beryllia, thoria, and graphite crucibles.

I. Introduction

Concurrent with the great increase of interest in the metal, uranium, brought about by the role of this metal in the field of atomic energy, there has been an initiation of investigations to obtain more accurate values of certain physical properties of the element. Previously, the metal was of little practical importance and was not available in a state of sufficient purity to give a positive significance to the results of determinations of many of its physical properties. Only a few of the physical constants of uranium were listed in tables published before 1943, and those listed were highly discordant. As a result of the atomic energy program conducted by the Manhattan District, Corps of Engineers, United States Army, there became available a quantity of uranium of relatively high purity. This paper describes the work on the freezing point of uranium done at the National Bureau of Standards for the Manhattan Project.

II. Previous Work

A survey of various tables and handbooks published before 1943 shows the freezing point of uranium is listed as $<$1,850° C [1],[1] 1,860° C [2], 2,400° C [3], and 3,600° C (computed on the basis of the position formerly assigned to uranium in the periodic system) [4]. Information regarding the method of arriving at the values quoted is generally lacking. J. W. Mellor [5] cited values of 1,300° to 1,400° C, 1,600° and 1,850° C and made the statement "uranium melts less easily than platinum, chromium, and molybdenum but more easily than tungsten and vanadium". Driggs and Lilliendahl [6] reported observed values of 1,688° and 1,690° C. Fisher and Rideal [7] reported 1,300° to 1,400° C. In 1941 W. F. Roeser [8] observed 1,075° and 1,100° C for two samples of impure uranium melted in vacuum.

The large spread in values reported for the melting point of uranium probably may be explained by the fact that a casing or crust is formed on the surface of uranium when it is heated in the presence of certain gases. This casing encloses the molten metal until temperatures far above the melting point of uranium are reached. For example, in some experiments at this Bureau, a specimen of uranium did not melt down when heated to about 1,800° C in a furnace evacuated to about 3 mm of mercury, whereas other specimens cut from the same ingot melted below 1,200° C when heated in a furnace evacuated to a few microns pressure. The flat surfaces of the first specimen became convex during heating, which indicates that the casing was sufficiently plastic to distort at the higher temperatures reached but, nevertheless, it was not ruptured by the head pressure of the molten metal. Obviously, the melting point of uranium may be much lower than the temperature at which the molten metal breaks through the casing.

[1] Figures in brackets indicate the literature references at the end of this paper.

The melting or freezing of a pure or nearly pure metal is accompanied by the absorption or evolution of its latent heat of fusion. During the change of state the temperature remains essentially constant. Thus, the heating or cooling curves of the metal will indicate the true melting or freezing point.

III. Present Work

1. Materials

Three samples of uranium designated as A_1, A_2, and B were used in the present work. Samples A_1 and A_2 were cut from the same extruded rod, sample B was cut from a cast ingot. The initial purity of samples A_1 and A_2 was about 99.94 percent, that of sample B was about 99.96 percent. Carbon and iron were the major impurities.

2. Experimental Procedure

The so-called crucible method was followed in the freezing-point determinations. In this method a hollow enclosure, or black body, is immersed in a bath of the metal, and observations on the radiation from the black body are made with an optical pyrometer during the time the metal is freezing. The uranium was melted in a high-frequency induction furnace. This type of heating provides stirring and consequently a high degree of temperature uniformity throughout the molten sample and minimizes the probability of contamination of the sample by the furnace elements.

Each of the uranium samples was melted in a different refractory—sample A_1 in beryllia, sample A_2 in graphite, and sample B in thoria. All of the crucibles were identical in size and shape. The beryllia and thoria crucibles were prepared by the general method described by Swanger and Caldwell [9]. The graphite crucible and accessory parts were made by machining. In each case the sight tube and the powdered material at the bottom of the tube were made of the same material as the crucible.

The uranium ingots, about 380 g in weight, were formed to the desired shape by hot forging. An axial hole was drilled in each ingot to accommodate the sight tube. Each sample was placed in its crucible and mounted in a larger porcelain container, as shown in figure 1. In the case of the samples contained in the beryllia and the graphite crucibles, lampblack was used as thermal insulation. The crucible assembly containing sample A_2 was heated in an Arsem furnace evacuated to about 2 mm for 16 hr at about 1,000° C to eliminate volatile products from the carbon insulation. Thoria powder was used as insulation for the sample in the thoria crucible. The assembly shown in figure 1 was placed inside a Pyrex glass

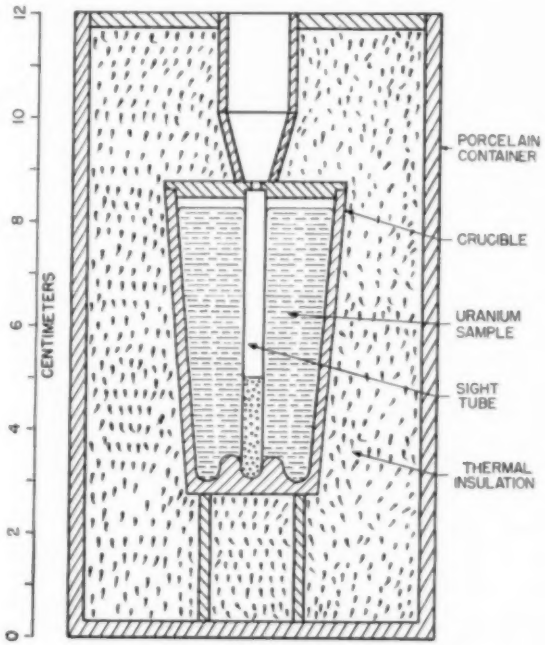

FIGURE 1. *Crucible assembly*

enclosure, shown in figure 2. The tube was closed at the top with a pyrex window sealed to the tube with propylene phthalate. The Pyrex tube fitted closely inside the water-cooled coils of the induction furnace.

Since uranium oxidizes rapidly even at moderate temperatures, the metal must be melted either in an inert atmosphere or in vacuum. Previously, melting uranium in vacuum had been found to produce an evolution of volatile material that deposited on the window and interfered with temperature measurements with an optical pyrometer. Use of an inert gas at atmospheric pressure would be expected to minimize this interference. Purified helium was selected as the protective atmosphere in the present work.

The optical pyrometer used has been previously described by Fairchild and Hoover [10]. It was

fitted with a 45-deg totally reflecting prism for sighting vertically into the black body. The current-temperature relation of the pyrometer lamp was obtained by a calibration method based on the definition of the International Temperature Scale.[2] The identical prism and window employed in the freezing-point determinations were used in the calibration.

The Pyrex enclosure was flushed out with helium for about 2 hr before heating of the sample was started, and a helium atmosphere was maintained during the actual heating. A freezing-point observation consisted in heating the metal to a temperature about 50 deg C above its melting point and then allowing the sample to cool slowly. Observations were made during the time the metal was freezing, as indicated by the halt in the cooling process. The average number of pyrometer readings obtained during one freeze was seven. The uranium samples exhibited no undercooling prior to solidification.

3. Results

The initial freeze on uranium sample A_1 indicated a freezing temperature of 1124.9° C. Subsequent freezes indicated a progressive rise in the freezing temperature, the fifth freeze indicating a freezing point of 1126.8° C. Following the fifth freeze the sample was melted and maintained at a temperature about 50 deg C above the melting point for a period of 30 min. The next two freezes indicated a freezing temperature of 1128.0° C. Thereafter the sample was held in the molten state for periods of 1 to 5 hr between sets of freezing-point observations until the heating period totaled 22 hr. A constant freezing-point limiting value of 1131.5° C for the freezing point was observed after about 15 hr of heating. In reckoning the total heating period, each set of freezing-point observations was regarded as the equivalent of 6 min of heating in the molten state. The change in the freezing temperature of uranium sample A_1 with time of heating is shown graphically in figure 3.

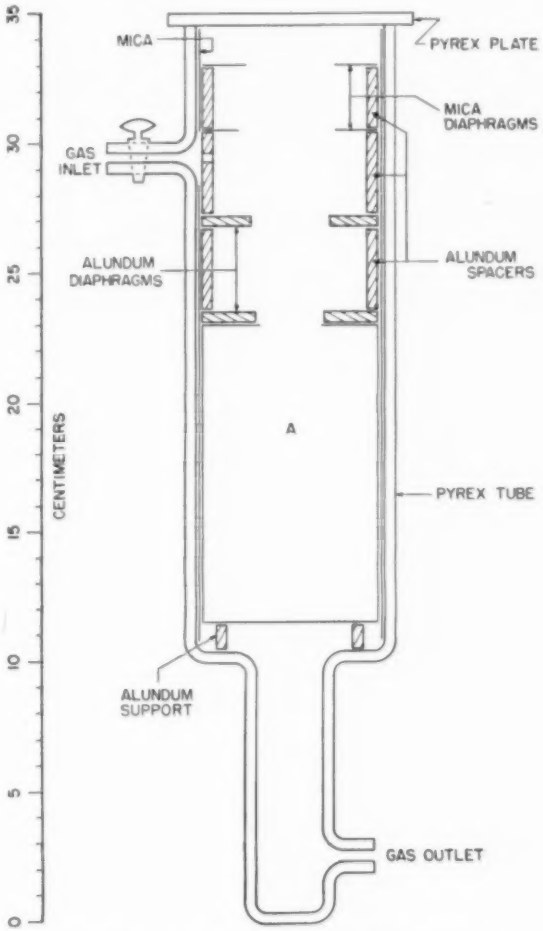

FIGURE 2. *Crucible assembly in Pyrex envelope*

A, Porcelain container with sample as shown in figure 1.

Observations of the freezing points of uranium samples A_2 and B also indicated a progressive rise in the freezing temperature with increase in the time the material was held in the molten state. A summary of the freezing-point observations on the three samples of uranium is given in table 1.

[2] In this method, the lamp current corresponding to the gold point (1,063° C) is determined by matching the brightness of a portion of the lamp filament with that of a black body in freezing gold. The apparatus used is similar to that shown in figure 1, but an inert atmosphere is not required. The calibration is extended to higher temperatures by using a black body furnace and rotating sector disks of known transmission [11]. The temperature of the furnace is adjusted until its brightness, when viewed through a given rotating sector disk, is equal to that of the black body at the gold point. The temperature of the black body furnace, $T°$ K, may be calculated with sufficient accuracy using the following formula derived from Wien's law

$$\ln t = \frac{1.438}{\lambda_e}\left(\frac{1}{T}-\frac{1}{T_{Au}}\right),$$

where t is the fractional transmission of the sector disk; λ_e is the effective wavelength of the optical pyrometer in centimeters; and T_{Au} is the absolute temperature of the gold point. The sector disk is then removed and the current increased to obtain a brightness match between pyrometer lamp and black body furnace. This current corresponds to the temperature, T. By utilizing sector disks having different angular openings, the lamp current for various temperatures higher than the gold point may be determined and a complete calibration obtained by interpolation.

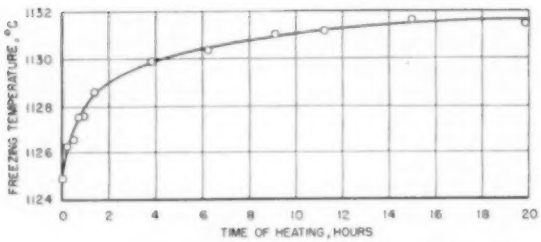

FIGURE 3. *Freezing temperature versus time of heating for uranium sample A_1.*

TABLE 1. *Summary of freezing-point observations*

Time held in molten state	Freezing Temperature		
	Sample A_1 (in BeO)	Sample A_2 (in graphite)	Sample B (in ThO_2)
hr	° C	° C	° C
0	1125.	1128.	1128.
½	1127.	----------	1128.5
1	1128.	----------	1129.
2	1129.	1129.5	1130.
5	1130.	----------	1131.5
7	----------	1131.	----------
10	1131.	----------	1133.
15	1131.5	1131.5	1133.5
20	1131.5	----------	1133.5

Each of the temperature values in the above table for heating periods of 5 hr or greater is the mean of the value of three to five successive freezes. The uncertainty in the temperature values, resulting from uncertainties in photometric matching and lamp calibration, is believed to be within ± 2 deg C.

The factors that cause inaccuracies in melting- and freezing-point determinations tend to produce low values; hence the highest value obtained in the three determinations, rounded to $1{,}133° \pm 2°$ C is believed to best represent the freezing point of uranium.

IV. Discussion of Results

Uranium samples A_1 and A_2, from the same source, exhibited a difference in freezing temperature during the initial portion of the heating period but attained the same final value of 1,131.5° C after a 15-hr heating period. This initial difference may have resulted from the preliminary heating for 16 hr in vaccuum, given sample A_2 but not A_1. The higher initial purity of sample B may account for its initial freezing point being higher than that of sample A_1.

Analysis of the ingots after the freezing temperature determinations showed a substantial increase in the purity of the metal, to about 99.99 percent for samples A_1 and B and slightly less for sample A_2. The content of some impurities, including oxygen, remained about the same. Iron was increased about 15 ppm. Some impurities, notably carbon and nitrogen, were decreased in amount, some were completely eliminated.

The outstanding decrease was in the carbon content, which was reduced from about 400 to 5 ppm in ingot A_1 and from 150 to 7 ppm in ingot B. The melting and freezing procedure resulted in a reduction of the carbon content of ingot A_2 from about 400 to 110 ppm for a sample representing the full cross section of the ingot, even though a graphite crucible was used.

Metallographic examination of the ingots after the melting-point determination gave a qualitative confirmation of these low carbon contents and indicated the mechanism by which the carbon was eliminated from the body of the ingot. Ingots A_1 and B, melted in beryllia and thoria, respectively, were substantially free from carbide inclusions except for the extreme top where the carbide inclusions had concentrated, largely as a crust. Analysis of the crust showed a carbon content of 1,100 ppm. The section just below the crust contained 16 ppm of carbon. A few carbide inclusions that were observed embedded in the side wall of ingots A_1 and B probably account for the carbon contents of 5 and 7 ppm obtained on samples of these ingots.

Ingot A_2 had a similar concentration of carbide inclusions in the extreme top and the same freedom from carbide inclusions in the body of the ingot but differed from the other ingots in having a considerable concentration of very fine carbide inclusions in the side wall.

It is apparent that the elimination of carbon from the body of the ingot was the result of agglomeration and migration of the carbide inclusions to the top of the ingots during the periods that the metal was held quietly molten at temperatures just above the freezing point.

The analytical and metallographic data indicate that the increase in freezing temperature with increase in the time during which the metal was held molten was the result of increase in the purity of the metal.

V. Summary

1. The data obtained in this investigation indicate that the freezing temperature of uranium of about 99.99-percent purity is 1,133°±2° C.

2. The freezing temperature was not greatly affected by the crucible material, similar values for the freezing temperature being obtained in beryllia, thoria, and graphite crucibles.

3. Holding the metal at temperatures just above the melting point for several hours resulted in a decrease in the content of several impurities, by volatilization and by migration to the top and side walls. This increase in the purity of the metal was accompanied by an increase in the freezing temperature to a final constant value, 5° or 6° C above the initial freezing temperature.

VI. References

[1] International Critical Tables **1,** 105 (1926); Van Nostrand's Chemical Annual, p. 294 (1926); Smithsonian Physical Tables, p. 198 (1927); Kent's Mechanical Engineers Handbook, p. 596 (1933); General Engineering Handbook (O'Rourke), p. 126 (1940); Machinery's Handbook, p. 1579 (1943); Handbook of Chemistry and Physics, p. 1712 (1943).

[2] Brady's Materials Handbook, p. 502 (1940).

[3] Mark's Handbook (Mechanical Engineers), p. 546 (1924).

[4] NBS Misc. Pub. M126 (1937).

[5] Comprehensive Treatise on Inorganic and Theoretical Chemistry **12,** 15 (Longmans Green & Co., New York, N. Y., 1932).

[6] Ind. Eng. Chem. **22,** 516 (1930).

[7] Z. anorg. chem. **81,** 170 (1913).

[8] Unpublished work, Pyrometry Laboratory of the National Bureau of Standards.

[9] W. H. Swanger and F. R. Caldwell, BS J. Research **6,** 1131 (1931) RP327.

[10] C. O. Fairchild and W. H. Hoover, J. Opt. Soc. Am. and Rev. Sci. Instr. **7,** No. 7, p. 543 (1923).

[11] W. F. Roeser, F. R. Caldwell, and H. T. Wensel, BS J. Research **6,** 1119 (1931) RP326.

Washington, August 11, 1949.

U. S. Department of Commerce
National Bureau of Standards

Research Paper RP2043
Volume 43, December 1949

Part of the Journal of Research of the National Bureau of Standards

Dissociation Constants of Weak Bases from Electromotive-Force Measurements of Solutions of Partially Hydrolyzed Salts

By Roger G. Bates and Gladys D. Pinching

A method for the determination of dissociation constants of weak electrolytes by electromotive-force measurements of solutions of partially hydrolyzed salts of a weak acid and a weak base is described. Although the precision is only half that of the conventional emf method, this procedure has particular advantage in determining the dissociation constants of certain bases, for some of the experimental difficulties encountered in adapting the usual method to solutions containing these bases can be overcome or reduced. The hydrogen-ion concentration of a solution of a salt of this type depends upon the constants of the weak acid, the weak base, and water. If two of these are known, the third can be evaluated by means of emf measurements without the necessity of knowing the exact hydrogen-ion concentration, which is usually difficult to obtain. Hydrogen electrodes and silver-silver chloride electrodes are used in the cells, and the solutions are aqueous mixtures containing the ions of the salt and an alkali chloride. The equations for the calculation of dissociation constants are developed. The method was tested by a determination of the basic dissociation constant of tris(hydroxymethyl)aminomethane at 20°, 25°, and 30° C from three series of measurements: (a) by the conventional emf method; (b) by emf studies of the hydrolysis of mixtures of the amine and primary potassium phosphate; and (c) by emf studies of the hydrolysis of mixtures of the amine and potassium *p*-phenolsulfonate. The three determinations were in acceptable agreement. The negative logarithm of the basic dissociation constant, pK_b, was found to be 5.946 at 20°, 5.920 at 25°, and 5.896 at 30° C.

I. Introduction

Although the experimental difficulties met in the study of most weak bases are not insurmountable, they have been in large part responsible for the failure of this important class of substances to receive the attention it deserves. The hydrogen-silver chloride cell, so useful in precise determinations of the dissociation constants of weak acids by the electromotive-force method [1, 2, 3] [1] can be successfully applied to a measurement of the constant of ammonia only under special conditions [4]. Thus, if equimolal mixtures of ammonia and ammonium chloride are to be investigated by this method, one must not only determine and apply corrections for the volatility of ammonia and for the solubility of silver chloride but must retard the diffusion of silver to the hydrogen electrode as well.

Replacement of the silver-silver chloride electrode by a type less susceptible to reaction with ammonia bases has been suggested [5, 6], but some sacrifice of reproducibility may be expected [7]. Furthermore, it is desirable in the interest of consistency that dissociation constants of bases should relate to the same cell used extensively in studies of weak acids and in measuring the ionization constant of water. Nevertheless, the extrapolation to infinite dilution to obtain the thermodynamic constant of a monoacidic base entails a greater uncertainty than for a monobasic acid, where the activity-coefficient term is practically zero, or at worst a linear function of ionic strength.

[1] Figures in brackets indicate the literature references at the end of this paper.

859368—49——2

It is well known that the pH of an aqueous solution of a salt of "two-sided weakness", that is, a salt formed by neutralization of a weak acid with a weak base, is fixed by the concentration and by the dissociation constants of the acid, the base, and water. These three constants are designated by the symbols K_a, K_b, and K_w, respectively. Unfortunately, the pH cannot be uniquely determined [8]. However, these dissociation constants can be expressed in terms of the measured electromotive force of galvanic cells composed of hydrogen and silver-silver chloride electrodes immersed in solutions of the weak salt with added chloride. The value of K_aK_w/K_b can be obtained by a suitable extrapolation to zero concentration of salt ions. A knowledge of the hydrogen-ion concentration or activity is then unnecessary.

The extent of hydrolysis of the salt depends upon the relative magnitudes of K_a and K_w/K_b. For best results, the acid and base should be of such strengths that at least 5 percent of each of the two salt ions is hydrolyzed, thus assuring an adequate buffer capacity. Similarly, degrees of hydrolysis greater than 95 percent should be avoided. In general, this restriction means that log K_a and log (K_w/K_b) should differ by no more than 2.

This emf-hydrolysis method is often better suited to the determination of the dissociation constants of weak bases than is the conventional emf method. The low buffer capacity near the ends of the pH-neutralization curve and the difficulty of evaluating the buffer ratio precisely in these regions usually restrict the application of the conventional method to solutions with buffer ratios between 0.2 and 5. Nevertheless, a low ratio of free base to salt is sometimes desired in order to minimize losses by volatilization and errors caused by the high solubility of silver chloride in the cell solutions. If K_a for the acid selected is larger than K_w/K_b, less than half of the base ion will usually be transformed into free base, and these errors may be of little or no consequence. Under these conditions the buffer ratio may depart widely from unity, but this disadvantage is offset by the double buffering action offered by the two systems set up by the incomplete reaction of the salt ions with water. Furthermore, the buffer ratio need not be established with great accuracy. If the free base is uncharged and the acid chosen is a singly charged anion, the activity-coefficient term is usually small and the extrapolation to zero salt concentration is easily effected.

The solutions needed to determine the dissociation constant of a weak base by the emf-hydrolysis method are usually not difficult to prepare. If the free base is a solid and is readily obtained in the pure state, it is weighed and combined in solution with an equivalent amount of the weak acid and the desired amount of alkali chloride. If the acid is not a solid, and if the weak base is most conveniently added in the form of its hydrochloride, the solutions are made from equivalent amounts of base hydrochloride and an alkali salt of the weak acid.

The chief disadvantage of this method results from the dependence of the emf of the cell upon the geometric mean of two constants, that is upon $\sqrt{K_a(K_w/K_b)}$, instead of upon K_a/K_b alone, as in the usual emf method. Consequently the precision of determining K_b with the aid of known values of K_w and K_a is reduced by one-half.

Tris(hydroxymethyl)aminomethane was chosen for a comparison of the new procedure with the earlier method. This primary amine can be obtained as a pure solid readily soluble in water and not appreciably volatile. It does not react with silver ion so extensively as to prohibit the use of the silver-silver chloride in equimolal mixtures of the amine and its hydrochloride. Electromotive-force measurements were made at 20°, 25°, and 30° C on solutions of partially hydrolyzed salts of this amine with primary phosphate ion ($H_2PO_4^-$) and with *p*-phenolsulfonate ion ($HOC_6H_4SO_3^-$), and the dissociation constant of the base was calculated from the results. The constant was also found by the customary emf method [1, 3]. The three determinations were in acceptable agreement.

II. Description of the Method

If the standard potential, $E°$, is known, each emf measurement of the hydrogen-silver chloride cell yields a value of $-\log (f_H f_{Cl} m_H)$, where m is molality, f is the activity coefficient on the molal scale, and H designates the total hydrogen-ion species, hydrated or otherwise. This quantity has been called pwH for convenience and to suggest its status as a practical unit of acidity susceptible of exact definition [8]. The pwH is calculated from the emf E by

$$\text{pwH} \equiv -\log (f_H f_{Cl} m_H) = \frac{(E-E°)F}{2.3026\,RT} + \log m_{Cl}, \quad (1)$$

where $\boldsymbol{F}$, R, and T are respectively the faraday, gas constant, and temperature on the Kelvin scale. The values of E° and $2.3026\ RT/\boldsymbol{F}$ are summarized in another publication [4]. Thermodynamic dissociation constants are derived from experimental values of pwH by expression of m_H or $f_H m_H$ in terms of the constants that fix their values in the cell solutions, and extrapolation of a suitable function of the dissociation constants to zero concentration where the activity coefficients become unity.

Three equilibria are of significance in determining the hydrogen-ion concentration in a solution of a salt of a weak acid anion, HA^-, and weak monoacidic base, B.[2] These are the acidic dissociation of the weak acid,

$$HA^- + H_2O = H_3O^+ + A^-;\ K_a \qquad (2a)$$

the basic dissociation of the weak base,

$$B + H_2O = BH^+ + OH^-;\ K_b \qquad (2b)$$

and the ionization of water,

$$2H_2O = H_3O^+ + OH^-;\ K_w \qquad (2c)$$

The equilibria among water and the salt ions BH^+ and A^- are expressed in terms of the three above:

$$BH^+ + H_2O = B + H_3O^+;\ K_{bb} = K_w/K_b, \qquad (3a)$$

and

$$A^- + H_2O = HA^- + OH^-;\ K_w/K_a. \qquad (3b)$$

In terms of the Brønsted-Lowry theory of acids and bases [9, 10], eq 3a represents the acidic dissociation of BH^+, the conjugate acid of the base B, and eq 3b represents the dissociation of the (hydrated) anion A^- as a base. Evidently the extent to which the separate reactions 3a and 3b proceed to establish equilibrium is largely dependent upon the acidic and basic strengths of BH^+ and A^- in comparison with the amphiprotic solvent. If B is a rather strong base (and its conjugate acid BH^+ correspondingly weak), the hydrolysis of BH^+ by eq 3a will proceed but slightly unless one of the products, hydrogen ion or free base, is removed. Similarly, if HA^- is a stronger acid than is water, A^- will be a weak base, and eq 3b will also show little tendency to take place. However, when both BH^+ and A^- are part of the same aqueous system, the several acids and bases present interact, and hydrolysis is no longer dependent solely upon the acidic and basic properties of water. For example, BH^+ will be hydrolyzed to a larger extent in the presence of A^- than by water alone, if A^- is a stronger base than water. The acid strength of BH^+ has a similar influence upon the extent to which eq 3b proceeds. This behavior is quite adequately explained by eq 3a and 3b, for the concentrations of hydronium and hydroxyl ions cannot be varied independently in the same solution.

By combination of eq 3a with 3b, one can write the complete equation for the simultaneous hydrolysis of the ions BH^+ and A^-:

$$BH^+ + A^- + 2H_2O = B + HA^- + H_3O^+ + OH^-;\ K_w^2/K_aK_b. \qquad (4)$$

It is clear that the two ions will not usually hydrolyze to equal extents, for K_a and K_b (and consequently the constants of eq 3a and 3b) will ordinarily be different. Hence, it is incorrect to apply the term "degree of hydrolysis" to a salt of a weak acid and a weak base. It should rather be applied to each of the salt ions individually. If K_a and K_b were indeed equal, and thus the degrees of hydrolysis of the individual ions as well, hydronium and hydroxyl ions would be produced in equal numbers upon dissolving the salt in water, as equilibrium 4 indicates; and the solution would remain neutral, or substantially so, at all concentrations. The inequality of K_a and K_b not only causes the solution to be acidic or alkaline but also gives rise to a change of pH with concentration [11].

In order to calculate m_H or $f_H m_H$ in a solution of this type, the fraction of BH^+ hydrolyzed will be designated α_1, and the corresponding degree of hydrolysis of the acid anion A^- will be called α_2. Hence, from the mass-law expression for equilibrium 3a one can write

$$-\log K_{bb} = -\log f_H m_H + \log \frac{1-\alpha_1}{\alpha_1} + \log \frac{f_{BH^+}}{f_B}, \qquad (5a)$$

and from eq 2a

$$-\log K_a = -\log f_H m_H + \log \frac{\alpha_2}{1-\alpha_2} + \log \frac{f_{HA^-}}{f_{A^-}}. \qquad (5b)$$

[2] The equations can be derived in a similar manner for acids and bases of other electric types.

These equations, together with that for the water equilibrium, regulate the hydrogen-ion concentration. By combination of eq 1, 5a, and 5b we obtain

$$\frac{pK_{bh}+pK_a}{2}=-\log \sqrt{K_{bh}K_a}=pwH+$$
$$1/2 \log \frac{\alpha_2(1-\alpha_1)}{\alpha_1(1-\alpha_2)}+1/2 \log \frac{f_{BH^+}f_{HA}f_{Cl^-}^2}{f_B f_{A^-}}. \quad (6)$$

As usual, $pK \equiv -\log K$. The analogy with the equations for the product of the constants for overlapping successive dissociation steps of polybasic acids [12] is evident.

1. Calculation of the α Term

From a consideration of eq 3a and 3b, the relationship between α_1 and α_2 can be derived. Hydronium ion and hydroxyl ion are produced by these reactions in the molal amounts $\alpha_1 m$ and $\alpha_2 m$, respectively, where m is again the stoichiometric molality of each of the ions of the salt, usually not less than 0.01. By reaction with the other ion, either hydronium or hydroxyl is reduced to a negligible concentration. If the salt solution is neutral, $\alpha_1 \approx \alpha_2$. If acidic,

$$\alpha_1-\alpha_2 \approx m/m_H. \quad (7a)$$

If alkaline,

$$\alpha_2-\alpha_1 \approx m/m_{OH}. \quad (7b)$$

In the determination of basic dissociation constants, an acid of known dissociation is selected. Equation 5b can be converted to a form convenient for calculating α_2:

$$\log \frac{1-\alpha_2}{\alpha_2} \approx pwH-pK_a+\frac{2A\sqrt{\mu}}{1+Ba^*\sqrt{\mu}}, \quad (8)$$

where A and B are constants of the Debye-Hückel theory [13], μ is the ionic strength, and a^* is an adjustable parameter whose value usually lies between 0 and 10. An average value, for example 4, suffices for the purpose. It is desirable that α_2 should not be much less than 0.1. Hence pwH should not be more than about 1 unit greater than pK_a.

An approximate α_2 with which to evaluate the ionic strength is obtained from eq 7. For the first approximation, the ionic strength of mixtures of base, acid, and potassium chloride, each at molality m, is taken as $4m$. Then a more accurate value is obtained by

$$\mu=4m-m(3\alpha_2+\alpha_1)/2+(m_H+m_{OH})/2 \approx 4m(1-\alpha_2/2). \quad (9)$$

The simpler expression for μ given in the last part of eq 9 is adequate when pwH is between 4 and 10. With α_2 from eq 8 and m_H or m_{OH} (depending upon whether the solution is acidic or alkaline) calculated from pwH by

$$-\log m_H=pwH-\frac{2A\sqrt{\mu}}{1+Ba^*\sqrt{\mu}} \quad (10)$$

and

$$-\log m_{OH} \approx pK_w-pwH, \quad (11)$$

α_1 can be obtained by eq 7a or 7b, and the second term on the right of eq 6 can be evaluated. This term is quite small if α_2 exceeds 0.1 and the pH lies between 4 and 10. It is less than 0.0001 for equimolal mixtures of tris(hydroxymethyl)aminomethane and primary potassium phosphate at 20° to 30° C when m is 0.01 or greater. For a corresponding mixture of the amine and potassium *p*-phenolsulfonate, it amounts to 0.0004 at m= 0.01.

2. The Extrapolation

If the Debye-Hückel relation between ionic charge and activity coefficient were valid for these mixtures, the last term of eq 6 would be zero. The data presented in a later section indicate that this is not the case for equal molal mixtures of tris (hydroxymethyl)aminomethane, potassium dihydrogen phosphate (or potassium *p*-phenolsulfonate), and potassium chloride.

The last term of eq 6 can be divided into two parts. The first, $f_{BH^+}f_{Cl^-}/f_B$, pertains to the base, and the second, $f_{HA}f_{Cl^-}/f_{A^-}$, to the weak acid. It has been found that an activity-coefficient term of the first type (where B is NH_3) can be represented satisfactorily by

$$\tfrac{1}{2} \log \frac{f_{BH^+}f_{Cl^-}}{f_B}=-\frac{A\sqrt{\mu}}{1+Ba_1\sqrt{\mu}}+\beta_1\mu, \quad (12)$$

where β_1 is a second parameter [4]. Likewise, the term for the acid system can be expressed similarly, as studies of the phosphate and phenolsulfonate buffers [14, 15] have shown.

$$\tfrac{1}{2} \log \frac{f_{HA}f_{Cl^-}}{f_{A^-}}=\frac{A\sqrt{\mu}}{1+Ba_2\sqrt{\mu}}+\beta_2\mu. \quad (13)$$

If a_1 and a_2 were equal, the last term of eq 6 would be a linear function of ionic strength. That it was not found to be so suggests that a_1 differs from a_2.[3]

It is desired simply to find an empirical expression that will reduce the last term of eq 6 to a linear function of ionic strength and hence facilitate the extrapolation to zero concentration. From eq 12 and 13,

$$\frac{AB(a_1-a_2)\mu}{(1+Ba_1\sqrt{\mu})(1+Ba_2\sqrt{\mu})} = \tfrac{1}{2}\log\frac{f_{BH^+}f_{HA^-}f_{Cl^-}^2}{f_B f_{A^=}} + \beta'_\mu \approx \frac{AB(a_1-a_2)\mu}{(1+B\bar{a}\sqrt{\mu})^2}, \quad (14)$$

where $\bar{a}$ is $(a_1+a_2)/2$, and β' is the slope of a plot of the left (or extreme right) side of eq 14 as a function of μ. The approximate form (extreme right of eq 14) was found to yield a satisfactory straight line and was somewhat easier to compute than the exact left-hand term. The value of β' differs, of course, with the form of equation chosen.

"Apparent" values of the mean of pK_{bh} and pK_a, namely $[(pK_{bh}+pK_a)/2]'$, are therefore computed by eq 6 for various values of a_1 and a_2 with ionic strengths established as described in the foregoing section. These values are plotted as a function of μ, and the shape of the curve is examined. If necessary, $\bar{a}$ is varied until a straight line results. It is evident that a_1-a_2 in the numerator of eq 14 can be adjusted to alter the slope of the extrapolation plot if desired without affecting its curvature, so long as $\bar{a}$ remains unchanged. At zero ionic strength the activity-coefficient term is zero, and the intercept is the true mean of the thermodynamic constants, $\frac{1}{2}(pK_{bh}+pK_a)$. Inasmuch as $pK_{bh}=pK_w-pK_b$, and both K_a and K_w are known, the basic constant is readily obtained.

III. Experimental Procedures

Purified tris(hydroxymethyl)aminomethane was obtained through the courtesy of Commercial Solvents Corporation. The commercial grade of amine had been decolorized and crystallized three times from a mixture of methanol and water.[4] Two samples, titrated with a standard solution of hydrochloric acid, required amounts of acid equivalent to 100.02 percent of the base. A mixture of bromcresol green and alizarin red *S* was used as indicator for one sample (see footnote 4) and the sodium salt of methyl red for the other. Color standards, adjusted to pH 4.8, the theoretical end-point in 0.05-*M* solution computed from the dissociation constant found by Glasstone and Schram [16], were used. The solubility of freshly precipitated silver chloride in two solutions of the amine was determined at room temperature. A 0.1-*M* solution of the amine dissolved 0.0021 mole of silver chloride per liter, and a 0.1-*M* solution that was also 0.01 *M* with respect to potassium chloride dissolved 0.0007 mole. Hence, the solubility of silver chloride is considerably less than in solutions of ammonia, and it is safe to conclude that no correction is necessary for the solubility in equimolal solutions of the amine and its hydrochloride.

The potassium dihydrogen phosphate was NBS Standard Sample 186 I. Potassium *p*-phenolsulfonate was decolorized and then crystallized four times. The last crystallization was from freshly boiled conductivity water. The salt was dried at 90° to 110° C. The pH of the 0.1-*M* solutions was found by glass-electrode measurement to be about 5.1. This is close to the inflection point. The potassium chloride had been purified by treatment with chlorine, precipitation with gaseous hydrogen chloride, and fusion [17]. Hydrochloric acid was distilled and the middle fraction collected and diluted to about 0.1 *M*. Five separate determinations of the concentration of this standard solution by weighing silver chloride gave a mean deviation from the mean of less than 0.02 percent.

For the mixtures of amine and weak acid, the cell vessels were of the type ordinarily used for studies of weak-acid systems [18], that is, with a single saturator and no stopcock between the electrode compartments. Those employed previously in the investigation of ammonia solutions [4] were used for mixtures of amine and hydrochloric acid. In view of the low volatility of the amine, however, the presaturator was not required. Air was removed from the solutions by passage of nitrogen before the final weighing.

[3] Actually a_1 for the ammonia system was found to be about 2 [4], and values of 4.4 and 8 for a_2 were found for phosphate and phenolsulfonate buffer solutions [14, 15]. However, it would be surprising if the parameters remained unchanged in these solutions of partially hydrolyzed salts.

[4] Communication from John A. Riddick.

IV. Results

The electromotive force of cells with hydrogen electrodes and silver-silver chloride electrodes and containing equimolal mixtures of tris(hydroxymethyl)aminomethane, potassium dihydrogen phosphate (or potassium *p*-phenolsulfonate), and potassium chloride is listed in table 1. The emf has been corrected in the usual manner to a partial pressure of 1 atm of hydrogen. Table 2 gives the electromotive force of the same cell containing 15 aqueous mixtures of tris(hydroxymethyl)aminomethane and its hydrochloride. These data were obtained in order that the constant of the amine might be evaluated by the earlier or "conventional" method to furnish a test of the newer method based upon emf studies of partially hydrolyzed salts.

TABLE 1. *Electromotive force of hydrogen-silver chloride cells containing solutions of tris(hydroxymethyl)aminomethane, weak acid, and potassium chloride, each at molality m*

m	Electromotive force at—		
	20°	25°	30°
AMINE+POTASSIUM DIHYDROGEN PHOSPHATE			
0.08438	0.73985	0.74088	0.74189
.05526	.74892	.75019	.75124
.03555	.75980	.76106	.76230
.02025	.77369	.77524	.77678
.011629	.78737	.78915	.79085
AMINE+POTASSIUM *p*-PHENOLSULFONATE			
0.08111	0.79604	0.79687	0.79761
.05667	.80452	.80546	.80637
.03622	.81525	.81634	.81741
.019945	.82968	.83104	.83240
.010458	.84545	.84705	.84863

Table 3 lists the mean of pK_{bh} and pK_a calculated from the data in table 1 by the method described in earlier sections. The values of pK_{bh} obtained from these two series of measurements are listed in the last column. The values of pK_a were taken as 7.213, 7.198, and 7.189 for primary phosphate ion at 20°, 25°, and 30° C, respectively [14, 18]; and 9.105, 9.053, and 9.005 for *p*-phenolsulfonate ion at the same temperatures [15]. The mean value of pK_{bh} obtained by the earlier method of Roberts [1] and Harned and Ehlers [3] from the data given in table 2 is also listed in the last column. The following equation was used:

TABLE 2. *Electromotive force of hydrogen-silver chloride cells containing solutions of tris(hydroxymethyl)aminomethane (m_1) and its hydrochloride (m_2)*

m_2	Electromotive force at—		
	20°	25°	30°
$m_1 = m_2$			
0.08814	0.77789	0.77594	0.77376
.07097	.78240	.78050	.77838
.05089	.78940	.78757	.78557
.02886	.80002	.79923	.79741
.02564	.80436	.80266	.80099
.015268	.81585	.81432	.81283
.006662	.82541	.82414	.82273
.009785	.82593	.82455	.82329
.006092	.83099	.83560	.83445
.003924	.84097	.84574	.84477
$m_1 = 0.3630\ m_2$			
0.09959	0.74988	0.74738	0.74474
.07933	.75472	.75220	.74980
.05982	.76066	.75819	.75569
.03974	.76931	.76694	.76458
.02024	.78415	.78201	.77985

$$-\log K' \equiv -\log K_{bh} - \beta m_2 = \mathrm{pwH} + \log \frac{m_2}{m_1} - \frac{2A\sqrt{m_2}}{1+Ba^*\sqrt{m_2}}. \quad (15)$$

TABLE 3. *Values of* $1/2\ (pK_{bh}+pK_a)$ *and* pK_{bh} *derived from three series of emf measurements*

Acid	$\frac{pK_{bh}+pK_a}{2}$	pK_{bh}
20°		
KH_2PO_4	7.7175±0.0006	8.2220±0.0012
KH Phenolsulfonate	8.6630±.0002	8.2210±.0004
HCl		8.2214±.0009
25°		
KH_2PO_4	7.6370±0.0004	8.0760±0.0009
KH Phenolsulfonate	8.5642±.0004	8.0755±.0007
HCl		8.0766±.0007
30°		
KH_2PO_4	7.5622±0.0008	7.9355±0.0017
KH Phenolsulfonate	8.4710±.0004	7.9371±.0009
HCl		7.9391±.0010

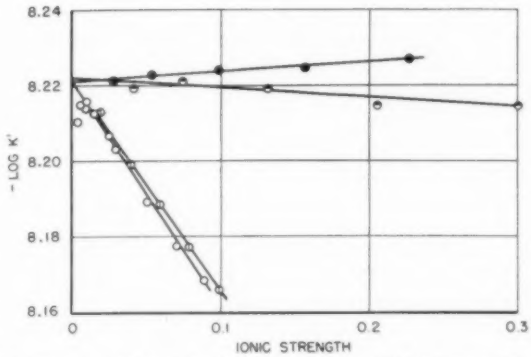

FIGURE 1. *Determination of K_{bh} for tris(hydroxymethyl)-aminomethane at 20° C.*

Dots, hydrolysis of amine-phenolsulfonate mixtures; half-shaded circles, hydrolysis of amine-phosphate mixtures; open circles and marked circles, amine-HCl mixtures.

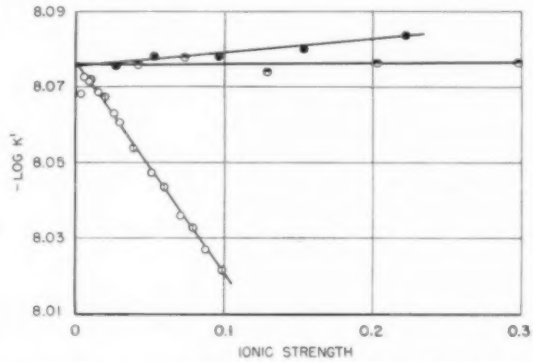

FIGURE 2. *Determination of K_{bh} for tris(hydroxymethyl)-aminomethane at 25° C.*

Dots, hydrolysis of amine-phenolsulfonate mixtures; half-shaded circles, hydrolysis of amine-phosphate mixtures; open circles and marked circles, amine-HCl mixtures.

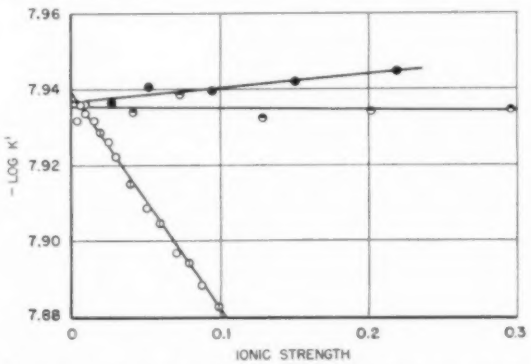

FIGURE 3. *Determination of K_{bh} for tris(hydroxymethyl)-aminomethane at 30° C.*

Dots, hydrolysis of amine-phenolsulfonate mixtures; half-shaded circles, hydrolysis of amine-phosphate mixtures; open circles and marked circles, amine-HCl mixtures.

Figures 1, 2, and 3 illustrate the change with ionic strength of the apparent value of pK_{bh}, denoted $-\log K'$, as derived from the three series of measurements. The open circles represent points computed from the first ten rows of table 2 and the marked circles from the last five rows. The dots represent amine-phenolsulfonate mixtures and the half-shaded circles mixtures of amine and potassium dihydrogen phosphate. A value of 1 for a^* in eq 15 gave the lower lines of each figure. The phosphate points correspond to $a_1=3$ and $a_2=5$ in the right-hand term of eq 14, and the phenolsulfonate points were computed with $a_1=4$ and $a_2=10$. The apparent K_{bh} was obtained by the following formula from the apparent values of the mean given by eq 6 with substitution of the right-hand member of eq 14 for the activity-coefficient term:

$$-\log K' = 2[(pK_{bh}+pK_a)/2]' - pK_a \qquad (16)$$

The agreement between the three determinations of pK_{bh} is satisfactory, in view of the dependence of the results furnished by the emf-hydrolysis method upon K_a values from other independent investigations. This procedure gives promise of usefulness in other studies of basic dissociation.

A summary of the average values of pK_{bh} and K_{bh} and of pK_b and K_b is given in table 4. For a calculation of the basic constant, K_b (which equals K_w/K_{bh}), pK_w was taken to be 14.167 at 20°, 13.996 at 25°, and 13.833 at 30° C [19]. The value of $-\log K_b$ at 25° C (5.920) is to be compared with 5.97 found by Glasstone and Schram [16] from measurements with the glass electrode.

TABLE 4. *Summary of dissociation constants for tris-(hydroxymethyl)aminomethane*

Temperature	pK_{bh}	$K_{bh}\times 10^6$	pK_b	$K_b\times 10^6$
°C				
20	8.221	6.00	5.946	1.133
25	8.076	8.40	5.920	1.202
30	7.937	11.55	5.896	1.272

V. References

[1] E. J. Roberts, J. Am. Chem. Soc. **52,** 3877 (1930).
[2] H. S. Harned and B. B. Owen, J. Am. Chem. Soc. **52,** 5079 (1930).
[3] H. S. Harned and R. W. Ehlers, J. Am. Chem. Soc. **54,** 1350 (1932).

[4] R. G. Bates and G. D. Pinching, J. Research NBS **42,** 419 (1949) RP1982.
[5] E. J. Roberts, J. Am. Chem. Soc. **56,** 878 (1934).
[6] B. B. Owen, J. Am. Chem. Soc. **56,** 2785 (1934).
[7] E. W. Kanning and A. F. Schmelzle, Proc. Indiana Acad. Sci. **51,** 150 (1941).
[8] R. G. Bates, Chem. Rev. **42,** 1 (1948).
[9] T. M. Lowry, J. Soc. Chem. Ind. **42,** 43 (1923).
[10] J. N. Brønsted, Rec. trav. chim. **42,** 718 (1923).
[11] R. O. Griffith, Trans. Faraday Soc. **17,** 525 (1922).
[12] R. G. Bates, J. Am. Chem. Soc. **70,** 1579 (1948).
[13] G. G. Manov, R. G. Bates, W. J. Hamer, and S. F. Acree, J. Am. Chem. Soc. **65,** 1765 (1943).
[14] R. G. Bates and S. F. Acree, J. Research NBS **34,** 373 (1945) RP1648.
[15] R. G. Bates, G. L. Siegel, and S. F. Acree, J. Research NBS **31,** 205 (1943) RP1559.
[16] S. Glasstone and A. F. Schram, J. Am. Chem. Soc. **69,** 1213 (1947).
[17] G. D. Pinching and R. G. Bates, J. Research NBS **37,** 311 (1946) RP1749.
[18] R. G. Bates and S. F. Acree, J. Research NBS **30,** 129 (1943) RP1524.
[19] H. S. Harned and B. B. Owen, The physical chemistry of electrolytic solutions, p. 485. (Reinhold Publishing Corp., New York, N. Y. 1943.)

Washington, July 15, 1949.

U. S. Department of Commerce
National Bureau of Standards

Research Paper RP2044
Volume 43, December 1949

Part of the Journal of Research of the National Bureau of Standards

A Reduction-of-Area Gage for Use at Low Temperatures

By Glenn W. Geil and Nesbit L. Carwile

A reduction-of-area gage for measuring the change in diameter of cylindrical or notched tension specimens during tests at controlled temperatures is described. The gage was designed especially for use in tests of specimens completely submerged in a temperature-controlled bath at temperatures ranging from −196° to +100° C. The calibration of this gage showed that measurements can be made with an accuracy of 0.0001 inch. Some results obtained with the use of this gage are illustrated by true stress-true strain curves for annealed ingot iron, cold-worked nickel and cold-worked 18:8 chromium nickel steel tested in tension at −188° and −196° C.

I. Introduction

During the course of an investigation of the mechanical properties of metals at low and moderately elevated temperatures, it became evident that an instrument was needed that could be used to measure accurately the change in diameter of cylindrical specimens submerged in liquid baths during tension tests at various temperatures. The portion of the true stress-true strain curve from maximum load to fracture cannot be determined from extension measurements. Moreover, for some metals, an accurate determination of the curve from yield to maximum load cannot be made from extension measurements, as the metal may contract locally before reaching the maximum load. Simultaneous load and diameter measurements are essential for the determination of the complete true stress-true strain curves for metals tested in tension, as pointed out by MacGregor.[1]

Ordinary reduction of area gages cannot be used satisfactorily on specimens submerged in liquid baths. The photographic method described by Seigle [2] for determining the change in diameter of a specimen submerged in a liquid bath during a tension test at low temperature was unsatisfactory at temperatures below −130° C. The reported accuracy of 0.0007 in. from the photographs obtained under the most favorable conditions is considered inadequate. It was deemed advisable to design a mechanical gage suitable for use in the temperature range of −196° to 100° C.

[1] C. W. MacGregor, Proc. Am. Soc. Testing Mat. **40**, 508 (1940).

[2] L. Seigle, Effect of ferritic grain size on the true stress-strain tensile properties and notched impact strength of ingot iron at low temperatures, a thesis presented to the graduate school, University of Pennsylvania (1948).

II. Design of the Gage

The reduction-of-area gage is shown in figure 1. The change in diameter of the test specimen during a tension test is followed by the movement of the sliding anvil, *A*, which is held against the specimen with slight pressure exerted by the tension spring, *F*. The movement of this anvil is transmitted to the spindle of the dial indicator by means of the simple lever, *B*. The pivot, or fulcrum, of this lever is a knife edge located at position *C* (not visible in fig. 1). To maintain the lever in position, it is supported by the four flexure strips, *D*. These thin strips are sufficiently flexible to permit rotation of the lever about the knife edge through an angle considerably greater than that required to follow the change in diameter of the test specimen. The two guide bars, *E*, are adjusted to give a clearance of 0.01 in. to the lever, *B*, and serve to hold the lever in position and prevent any excessive twisting of the flexure strips while the instrument is not in use. A lubricated bearing, such as roller or ball bearings or a sleeve type bearing, could not be used as the fulcrum for the lever as this portion of the instrument is submerged in the temperature-controlled liquid bath.

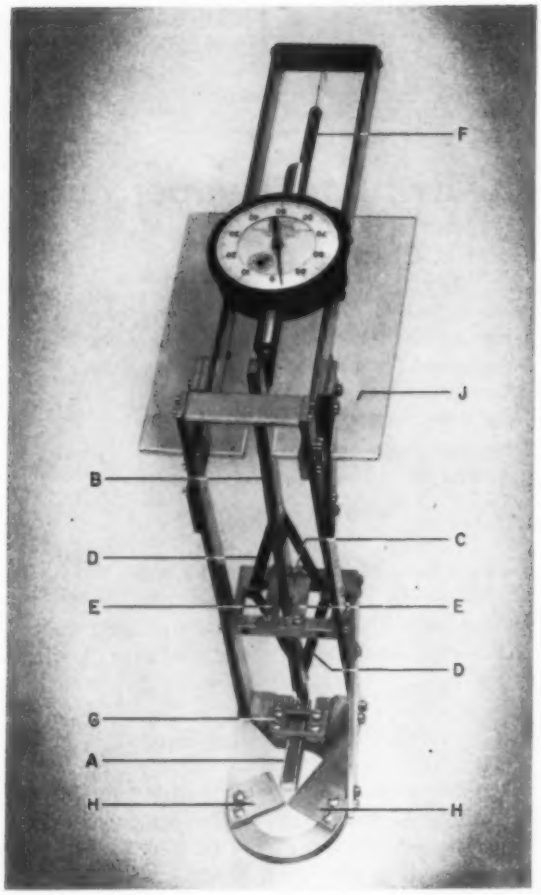

FIGURE 1. *Reduction of area gage;* ×0.4

Designation	Part	Material	Remarks
A	Sliding anvil	SAE 52100	Hardness of Rc 63.
B	Lever	AISI 440-C	Hardness of Rc 55.
C	Pivot	AISI 440-C	Hardness of Rc 55.
D	Flexure strips	Phosphor bronze	Cold rolled 0.003-in. sheet.
E	Guide bars	Monel	Cold rolled.
F	Tension spring	Phosphor bronze	Cold drawn.
G	Retainer caps	Monel	Cold rolled.
H	Fixed anvils	SAE 52100	Hardness of Rc 63.
J	Shield	Plastic	

An enlarged view of the measuring anvils is shown in figure 2. The six ribs (two each on top and bottom and one on each side) on the sliding anvil serve as the bearing surfaces. To minimize the area of contact of the bearing surfaces, the ribs of the retainer caps, *G*, are at right angles to the direction of movement of the anvil, *A*. A clearance of 0.002 in. between these caps and the sliding anvil is sufficient to allow for unequal contraction of the component parts on cooling to low temperatures.

The sliding anvil is attached to the lever arm with a small tension spring, *I*, to facilitate installation of the gage on the tensile specimen while immersed in the liquid bath. The anchor pin, *K*, for this spring also serves as a stop against the retainer caps, *G*, to prevent the measuring edge of the sliding anvil hitting the contact edges of the fixed anvils, *H*, when the tensile specimen breaks. Both ends of the sliding anvil and the contact ends of the fixed anvils were machined to a dihedral angle of 50° and a radius of 0.02 in. This design provides for the free access of the measuring contact edges of the anvils to the minimum diameter portion of the necked section of the tensile specimen.

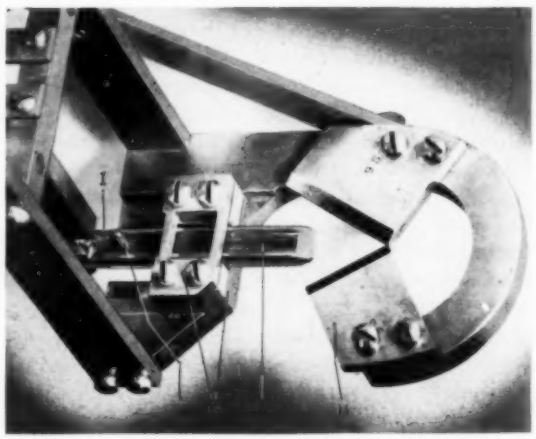

FIGURE 2. *Design of the sliding and fixed anvils of the reduction of area gage.*

Designation	Part	Material	Remarks
A	Sliding anvil	SAE 52100	Hardness of Rc 63
H	Fixed anvils	SAE 52100	Hardness of Rc 63
G	Retainer caps	Monel	Cold rolled
I	Tension spring	Phosphor bronze	Cold drawn
K	Anchor pin	Monel	Cold rolled

The contact edges of the anvils are co-planar and at an angle of 60° to each other. With this arrangement, the movement of the sliding anvil is 1.5 times the change in diameter of the test

specimen. The length of the lever arm between the pivot knife edge and the anvil knife edge is approximately 2.5 in.; the length of the lever arm between the pivot knife edge and the contact point of the dial indicator is approximately 5 in. Thus the total magnification of the instrument is approximately 3, or actually 2.985, by calibration.

The dial indicator is a jeweled low-friction type indicator and is mounted on the framework so that it is adjustable. The choice of the dial indicator depends upon the ductility of the metal to be tested. If the ductility is very low, a dial indicator with a small range of approximately 0.25 in. and dial divisions to 0.0001 in. can be used. If the metal to be tested has high ductility, a dial indicator with a range of approximately 1· in. is required in order to follow the larger change in diameter of the specimen.

The anvils are made of SAE 52100 steel, and the lever and pivot knife edge are made of AISI type 440C stainless steel, heat-treated for hardness values of Rockwell C63 and C55, respectively. The flexure strips and the tension springs are phosphor bronze. The framework of the instrument is constructed of cold-rolled Monel, which has suitable corrosion resistance and strength. A plastic shield, *J*, is used to insulate the dial indicator from the vapors of the temperature-controlled liquid baths, and it also serves as a convenient handle for manipulation of the instrument.

III. Calibration of the Gage

The gage was calibrated at room temperature to check the linearity of the dial readings with diameters. A series of six cylindrical test standards, each machined with a circumferential groove of 0.03-in. radius, were measured with an optical comparator to an accuracy of 0.0001 in. The diameters of the standards ranged from 0.1484 to 0.4864 in. The dial readings, obtained with the test standards, were plotted against the diameters of the test standards, and a linear relationship was obtained throughout the entire range. The slope of this line is equal to the magnification factor of the instrument and, as mentioned previously, is 2.985. The zero reading of the instrument, R_0, is obtained by determining the dial reading at the intercept of this straight line with the zero diameter axis of the graph. The actual diameter, measurement D, for any reading is given by the following equation: $D=(R_0-R)/F$, in which R_0 represents the zero reading, R the actual dial reading, and F the magnification factor for the instrument. The diameters obtained from the dial readings of this gage on the test standards were identical, to the nearest 0.0001 in., with the diameter measurements obtained with the optical comparator.

The instrument was also calibrated under simulated test conditions to obtain the temperature correction curve. Test standards of fused quartz were used. The standard was placed in position in the gage and the diameter reading obtained at room temperature. The gage and specimen then were placed in the temperature-controlled liquid bath and submerged to the depth at which the gage is used during a tension test. Diameter readings were taken after temperature equilibrium was attained. The time to reach temperature equilibrium ranged from 10 to 15 min., and observations for greater periods up to 1 hour showed no further changes in the diameter readings. Calibration tests were made at +100°, +27°, −78°, −120°, and −196° C. Because of the very small coefficient of thermal expansion of fused quartz, the change in diameter of the quartz test standard did not exceed 0.00003 in. Therefore the changes in the dial readings were attributed to dimensional changes in the instrument. Data showing the relation between temperature and the indicated correction to be applied to the diameter measurement are shown in figure 3.

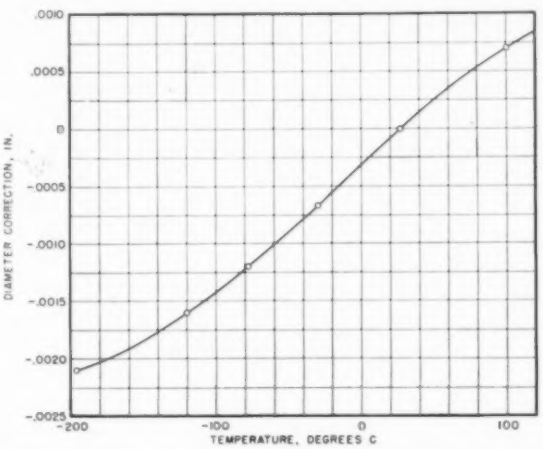

FIGURE 3. *Curve for the gage showing the relation between the diameter corrections and the temperature.*

The dial reading corrections are 2.985 times the diameter corrections.

The change in the observed dial readings is 2.985 times the correction (actual diameter values) shown in this figure.

IV. Applications of the Gage

The manipulation of this gage to determine the change in diameter of an unnotched cylindrical specimen during a tension test at low or moderately elevated temperatures is very simple. The test specimen supported vertically between the adapters of the tensile-testing machine is completely submerged in the temperature-controlled liquid bath. The gage is placed in position on the specimen with the measuring anvils at any position along the gage length of the specimen, and a time interval of about 15 min. is allowed for the gage to come to temperature equilibrium. The alinement of the gage with respect to the specimen is adjusted until a minimum diameter reading is obtained, indicating that the plane of the measuring anvils is perpendicular to the axis of the specimen. While maintaining this alinement, the gage, supported by hand, is moved up and down through the gage length of the test specimen to find the diameter at the area of minimum cross section. Numerous simultaneous load and diameter readings are made during the tension test.

This gage also can be used for following the change in diameter of circumferentially notched cylindrical specimens during test in tension at low or moderately elevated temperatures. For this purpose a set of anvils is required in which the measuring edges are machined to an angle less than the smallest notch angle of the test specimens. The radius of the measuring edges of the anvils likewise must be less than the smallest radius at the root of the notch.

An example of the use of this gage in following the change in diameter of a metal specimen that has very little ductility at low temperature is illustrated in figure 4. This figure summarizes the results obtained in a tension test at −196° C with

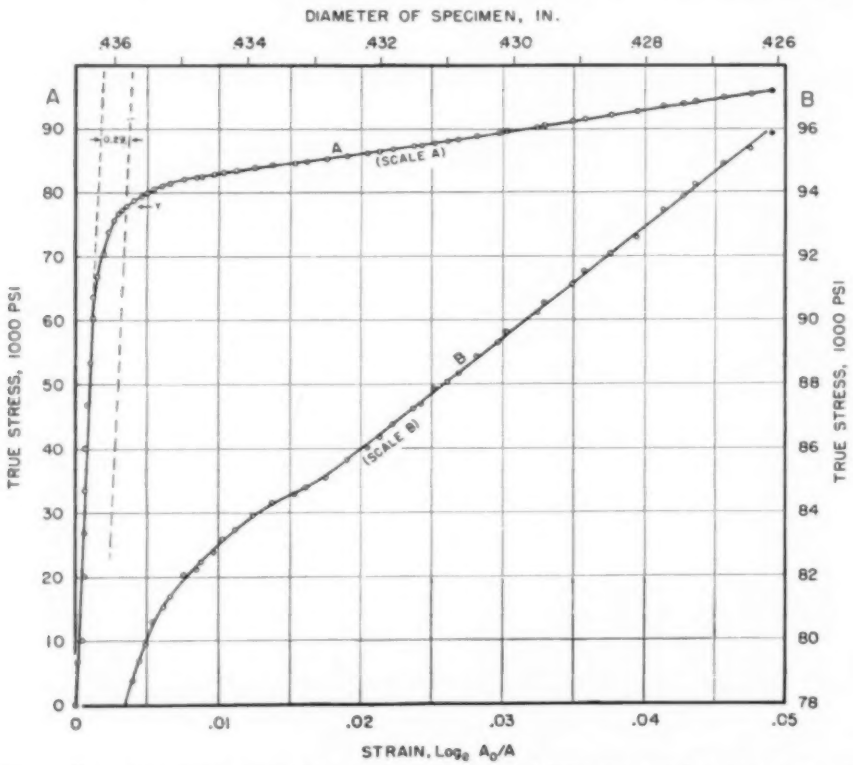

FIGURE 4. *True stress-strain curves for a specimen of annealed ingot iron tested in tension at −196° C.*

A, Complete true stress-true curve; B, portion of the true stress-true strain curve from yield to fracture on a more open stress scale. Y, Yield strength, 0.2-percent offset (reduction of area); ●, fracture.

a cylindrical tensile specimen of annealed ingot iron. The true stress is plotted against the true strain. The true stress is the current load divided by the current minimum cross-sectional area, and the true strain is the $\log_e(A_0/A)$, in which A_0 and A represent the initial and current minimum cross-sectional areas, respectively. Curve A is the entire true stress-true strain curve for this specimen. The portion of curve A extending from yield to fracture is replotted on an expanded stress scale as curve B. The maximum deviation of any point from the curve corresponds to a change in diameter of the specimen of less than 0.0001 in. The bulge in the lower portion of curve B is connected with a tendency to a drop of beam at yielding for the initially annealed ingot iron at this temperature.

An example of a complete true stress-true strain curve obtainable by the use of this instrument in a tension test in which the metal retains high ductility at low temperatures and contracts locally after reaching the maximum load is illustrated in figure 5. This figure shows the results obtained in a tension test at $-188°$ C with a cylindrical test specimen of nickel (99.4% Ni) that had received prior cold work by extending in tension to a 25-percent reduction of area.

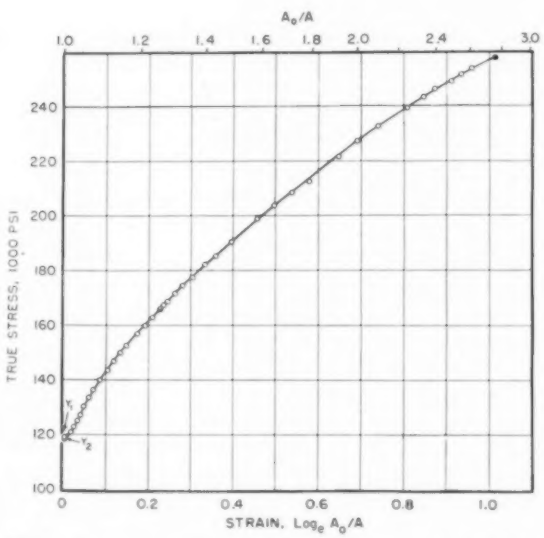

FIGURE 5. *True stress-strain curve for a specimen of cold-worked nickel tested in tension at $-188°$ C.*

Y_1, upper yield; Y_2, lower yield; ◒, maximum load, ●, fracture.

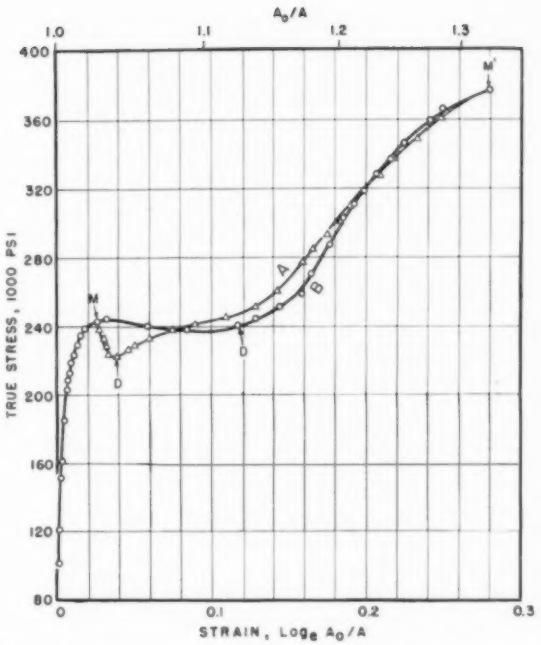

FIGURE 6.—*Portion of the stress-strain curves for a specimen of cold-drawn (49% reduction of area) 18:8 chromium-nickel steel, "EBM", tested in tension at $-196°$ C.*

Curve A, based on extension measurements; curve B, based on diameter measurements; D, minimum load, M, first maximum load, M', final maximum load.

The determination of true stress-true strain curves in cases where local contraction occurs before the load reaches a final maximum value is also possible by the use of this instrument, as illustrated by the results given in figure 6. Portions of the curves from the points representing initial yielding to the final maximum load, as obtained by two different types of measurements during a tension test with a cold-worked 18:8 chromium-nickel steel at $-196°$ C, are shown in this figure. Curve A is based upon measurements of the extension of the specimen during the test as obtained from the automatic load-extension chart and on the assumption that the specimen remains cylindrical (no local contraction) with deformation to the final maximum load, represented by the point M'. The actual true stress-true strain curve determined from the change in diameter of the same specimen during the tension test as measured with this gage is shown as curve B. Curve B shows that the local contraction at

the minimum load, represented by point D (true strain of approximately 0.12) corresponds to an actual reduction of area of approximately 11 percent whereas the curve A based on extension measurements, indicates an apparent true strain of about 0.04, corresponding to a reduction of area of approximately 4 percent. Thus curves A and B are not quantitatively similar.

V. Summary

A reduction-of-area gage was designed and constructed for measuring the change in diameter of test specimens submerged in liquid baths during tension tests at temperatures within the range of $-196°$ to $+100°$ C. The performance of the gage has been very satisfactory, as indicated by the test results shown for ingot iron, cold-worked nickel and 18:8 chromium-nickel steel.

The authors gratefully acknowledge the assistance of Mrs. F. A. Wilkinson and Miss L. B. Weinrich in the experimental testing and the preparation of illustrations, and the assistance of H. S. Miller of the Shop Division in the construction of the gage.

U. S. Department of Commerce
National Bureau of Standards

Research Paper RP2045
Volume 43, December 1949

Part of the Journal of Research of the National Bureau of Standards

Mass Spectra of C_5H_8 Isomers

By Fred L. Mohler, Evelyn G. Bloom, Laura Williamson, C. E. Wise, and E. J. Wells

Mass spectra of ten C_5H_8 isomers are described. These comprise spiropentane, methylenecyclobutane, cyclopentene, six dienes and 1-pentyne. The mass spectrum of each of these compounds has distinctive characteristics, but these are not correlated with the molecular structure in an obvious manner. The ratio of total ionization to that of *n*-butane covers a small range of values from 0.96 to 1.09, and the same range of values is found in other C_5 hydrocarbons. The doubly charged ion spectrum is very prominent in some pentadienes, with $C_3H_2^{++}$ the largest peak.

I. Introduction

The Mass Spectrometry Section has obtained mass spectra of ten C_5H_8 isomers as part of a systematic program of measuring mass spectra of pure hydrocarbons for inclusion in the API Catalog of Mass Spectral Data.[1] Spectra of these isomers have some interesting features in common, although they include compounds that differ greatly in their chemical properties.

Mass spectra have been obtained on a 180° Consolidated mass spectrometer using automatic electron current control and automatic temperature control of the ionization chamber at 245° C. Standard procedures have been followed (see footnote 1) in obtaining mass spectra, and spectra have been measured at both 50- and 70-v ionizing voltage. Data at 70v are quoted here. Intensities are expressed relative to the maximum peak in the spectrum taken as 100, and the sensitivity at the maximum peak (current per unit pressure) is measured in arbitrary units. On the same day the sensitivity of *n*-butane at the mass 43 peak is measured, and the ratio of the two sensitivities affords a measure of sensitivity that is independent of the units used.

We are indebted to the NACA Cleveland Laboratory for making available to us the samples of the rare compounds, spiropentane and methylenecyclobutane. These were considered to be about 99 percent pure, and no recognizable impurities were found in them. 1-Pentyne was made under the direction of Frank Howard in the fuel laboratory of this Bureau and was estimated to be better than 99 percent pure. The NBS standard samples are in general 99.9 percent pure or better.

[1] Catalog of Mass Spectral Data, American Petroleum Institute, Research Project 44, National Bureau of Standards.

II. Experimental Results

Table 1 lists the peak heights of some of the more distinctive mass peaks in these spectra. The last two rows give the sensitivity of the maximum peak relative to normal butane and the total ionization relative to *n*-butane. Figures 1 and 2 are plots of the mass spectra, omitting peaks that are less than 2 percent of the maximum peak. Figure 1 includes the cyclics and 1-pentyne, whereas figure 2 gives the dienes except *trans*-1,3-pentadiene, which is almost identical with *cis*-1,3-pentadiene (table 1). In these spectra there are many ions that cannot be obtained by simple dissociation but require a rearrangement of atoms in the dissociation process, and these are marked by asterisks in table 1 and in the figures.

All these compounds give CH_3^+ peaks of the magnitude usually found in hydrocarbons, although four of them (peaks marked by asterisks) do not contain CH_3 radicals. These include the three cyclics that give the smallest CH_3 peaks and also 1,4-pentadiene, which gives a relatively large peak.

The complementary process to production of CH_3^+ is the production of $C_4H_5^+ + CH_3$. For

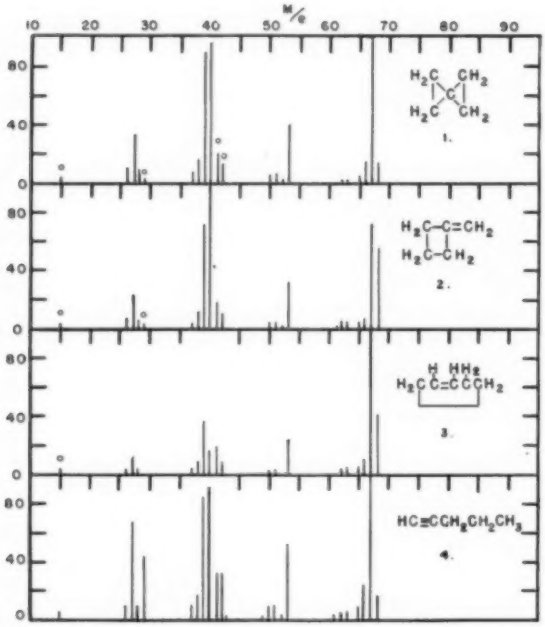

FIGURE 1. *Mass spectra of cyclic C_5H_8 isomers and 1-pentyne.*

Ordinates are peak heights relative to a maximum peak height of 100. Dots indicate ions that involve a rearrangement of atoms for their production.

nearly all hydrocarbons, ionization with loss of one carbon atom involves loss of at least three H atoms, and loss of CH_3 is most probable. This is true whether or not CH_3 radicals are contained in the molecule. There is some correlation in these molecules between the height of the CH_3^+ peak and the $C_4H_5^+$ peak; but C_4H_5 is always fairly large, and $C_4H_6^+$ is completely missing even in cases where the terminal radicals are CH_2.

$C_2H_3^+$ is always the largest peak in the C_2 group, and the height does not depend on whether or not this ion can be formed by simple dissociation. The peak is largest in 1,2-pentadiene and in 1-pentyne, which do not yield $C_2H_3^+$ by a single dissociation. By contrast, $C_2H_5^+$ is correlated with the structure and is largest in 1-pentyne and 1,2-pentadiene, which contain ethyl radicals.

The C_3 group of ions shows very distinctive differences. $C_3H_3^+$ is the maximum peak in 1,4-pentadiene and the largest of the C_3 ions in six other compounds. In all but one of these cases it requires multiple dissociation or rearrangement to obtain this ion. $C_3H_4^+$ is the maximum peak in methylenecyclobutane and a large peak in spiropentane and 1-pentyne. $C_3H_5^+$ is larger in the pentadienes than in the other compounds, and its height is roughly correlated with the complementary peak $C_2H_3^+$. Other ions of the C_3 group are not correlated with their complementary C_2 ions. $C_3H_7^+$ is permitted only in 1-pentyne and is observed in this case and is absent or very small in all the other molecules.

The relative heights of $C_5H_7^+$ and $C_5H_8^+$ are also very distinctive for these isomers. In six cases $C_5H_7^+$ is the maximum peak in the spectrum. It is quite unusual in hydrocarbons for ionization with loss of H to be the most probable ionization process, and in our experience propene and toluene are the only other hydrocarbons in which this is true. The molecule ion $C_5H_8^+$ is the maximum peak in two of the pentadienes.

All of these isomers have a metastable transition peak at mass 66 arising from the transition $68^+ \rightarrow 67^+ + 1$. Loss of H in a metastable transition is very rare and is evidently correlated with

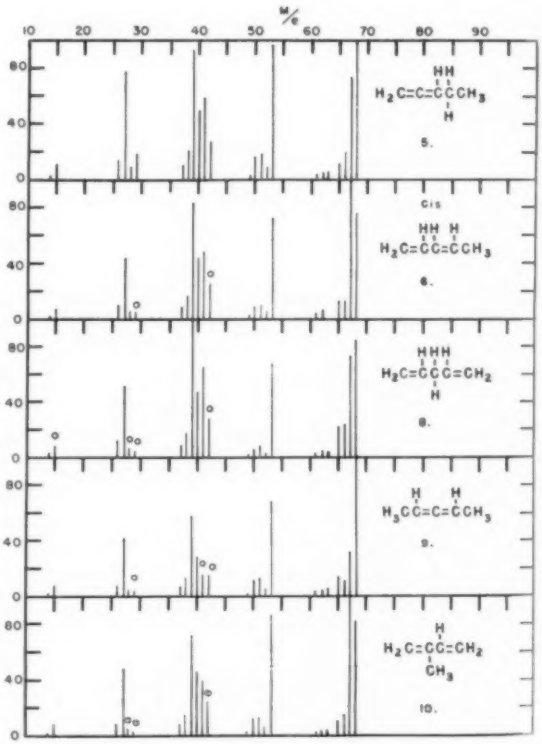

FIGURE 2. *Mass spectra of pentadienes.*

Ordinates are peak heights relative to a maximum peak height of 100. Dots indicate ions that involve a rearrangement of atoms for their production.

TABLE 1. *Relative peak heights in mass spectra of* C_5H_8 *isomers*

Ion	Reference number									
	1	2	3	4	5	6	7	8	9	10
	Spiropentane	Methylene cyclobutane	Cyclopentane	1-pentyne	1,2-pentadiene	1-*cis*-3-pentadiene	1-*trans*-3-pentadiene	1,4-pentadiene	2,3-pentadiene	Isoprene
CH_3^+	*3.75	*3.11	*3.21	5.96	10.7	7.29	7.17	*8.16	7.93	6.41
$C_2H_3^+$	33.9	23.0	14.8	68.4	78.7	42.7	41.6	50.9	41.0	47.6
$C_2H_4^+$	8.24	5.64	1.92	7.56	9.2	5.42	5.59	*6.00	5.45	*5.69
$C_2H_5^+$	*2.65	*2.22	*0.90	42.4	18.0	*4.72	*4.85	*4.70	*4.36	*3.77
$C_3H_3^+$	88.8	70.7	36.4	83.9	94.0	82.5	83.7	100	58.6	70.8
$C_3H_4^+$	95.6	100	15.9	89.5	49.3	43.4	45.3	47.3	29.6	44.5
$C_3H_5^+$	*20.3	18.8	19.0	32.0	59.4	48.4	50.6	63.5	*50.2	39.9
$C_3H_6^+$	*12.1	10.4	8.38	31.5	28.0	*24.9	*26.2	*26.6	*15.5	*22.4
$C_3H_7^+$	0	0	0	2.35	*0.30	0	0	0	*0.15	0
$C_4H_5^+$	39.7	31.3	23.4	52.9	97.4	71.9	74.5	68.6	68.5	86.2
$C_4H_7^+$	100	71.6	100	100	75.9	100	100	74.5	31.1	100
$C_4H_8^+$	15.2	56.6	41.6	17.4	100	75.8	79.6	83.6	100	83.2
$C_5H_2^{++}$	2.96	3.29	2.43	5.23	8.21	7.24	7.62	4.91	7.93	4.31
Sensitivity *	0.58	0.67	0.99	0.50	0.39	0.526	0.518	0.47	0.62	0.48
Total *	.958	.998	1.058	1.060	1.014	1.081	1.087	1.001	1.075	.974

*Ions involving rearrangement of atoms in the dissociation process.
* Sensitivity and total ionization relative to *n*-butane.

the relatively high intensity of both the 68 and 67 peaks. Other metastable transitions found in these compounds are of types that recur in many hydrocarbons.[2]

Nine peaks at half integer intervals from mass 30 to 34 come from doubly charged ions C_5^{++}, C_5H^{++}, $C_5H_2^{++}$, etc., to $C_5H_8^{++}$. $C_5H_2^{++}$ is the maximum peak in the doubly charged spectrum, and the relative intensity of this peak is included in table 1. The value 8.21 for 1,2-pentadiene is the highest value ever reported for doubly charged ions in hydrocarbons at 70-v ionizing voltage. The intensity distribution in these doubly charged spectra is similar to that found in all other C_5 hydrocarbons, but the relative intensity is greater than in C_5H_{10} and C_5H_{12} isomers.[3] In other C_5 hydrocarbons, the C_5^{++} peak at 30 is completely masked by the heavy isotope of $C_2H_5^+$; but in most of these compounds the heavy isotope contribution is less than 0.1 percent, and the reality of the C_5^{++} contribution (also about 0.1%) can be established. It is of interest that such an ion exists.

The next to the last row of table 1 gives the sensitivity (ion current per unit pressure) at the maximum peak relative to the sensitivity for the mass 43 peak of *n*-butane. It covers a large range of values from 0.39 to 0.99 and is in general small when there are many large peaks, and large when there are few. Adding the height of all the peaks in the spectrum and multiplying by the sensitivity gives a number proportional to the total ionization. The total ionization relative to the total ionization of *n*-butane is a number that has a small range of values from 0.96 to 1.09, with a mean value of 1.03. For comparison, the three pentanes give values ranging from 0.99 to 1.17, mean 1.09, and the six pentanes have values 0.96 to 1.06, with a mean value of 1.02. It is interesting that C_5H_8 isomers are much like other C_5 hydrocarbons in this respect and all have roughly the same total ionization at constant pressure. Instrumental characteristics may account for some of the small variations observed.

III. Conclusion

This group of isomers is of interest because it comprises a wide variety of chemical classes. Spiropentane is a di-cyclic saturated compound.

[2] E. G. Bloom, F. L. Mohler, C. E. Wise, and E. J. Wells, J. Research NBS **43**, 65 (1949) RP2005.
[3] F. L. Mohler, E. G. Bloom, E. J. Wells, J. H. Lengel and C. E. Wise; J. Research NBS **42**, 369 (1949) RP1975.

There are two monoolefin cyclics, six diolefins, and one acetylene. It happens that the spectrum of spiropentane is very much like that of the acetylene, 1-pentyne, except for the large $C_2H_5^+$ peak in the latter compound. There are no obvious similarities between compounds of the same chemical class. On the other hand there are several striking characteristics of the spectra as a group; notably the high probability of ionization with loss of one H atom, relatively large peaks at $C_4H_5^+$, at $C_3H_3^+$, or $C_3H_4^+$, and at $C_2H_3^+$. It is evident that the mass spectrum depends markedly on the number of H atoms but not on the chemical unsaturation of the compound. In the ionization and dissociation process there is isomerization, which modifies the original molecular structure. Somewhat similar generalizations can be made concerning the C_4H_6 butadienes and butynes.[4]

Each compound of the group has distinctive characteristics in the mass spectrum to aid in its identification in chemical analysis. The relative height of the $C_5H_8^+$ and $C_5H_7^+$ peaks distinguishes many of the compounds.

[4] F. L. Mohler, J. Wash. Acad. Sci. **38**, 193 (1948).

WASHINGTON, July 25, 1949.

U. S. Department of Commerce
National Bureau of Standards

Research Paper RP2046
Volume 43, December 1949

Part of the Journal of Research of the National Bureau of Standards

A Note on the Numerical Integration of Differential Equations[1]

By W. E. Milne[2]

An integration method for ordinary differential equations is developed, in which the approximation formulae contain derivatives of higher order than those contained in the differential equation itself. The method is particularly useful for linear differential equations. Numerical examples are given for Bessel's differential equation.

I. Introduction

The object of this note is to present a method for the numerical integration of ordinary differential equations that appears to possess rather outstanding advantages when applied to certain types of equations. The equations to which the method most readily applies are those for which it is possible to obtain, in comparatively simple form, expressions for two additional derivatives. That is, for an equation of n-th order

$$y^{(n)}=f(x,y,y',\ldots,y^{(n-1)}),$$

we obtain by differentiation expressions for $y^{(n+1)}$ and $y^{(n+2)}$. If these expressions are not so involved as to make the labor of substitution prohibitive, then the method here proposed is applicable.

The advantages claimed for the process are:

(1) The start of the integration is accomplished by the same formulas that are used in the regular routine of the process, so that no special formulas or procedures are required in order to get the computation underway.

(2) Each step of the integration makes use of only two lines of the computation, whereas a method employing differences and having a comparable degree of accuracy would require five lines in the computation.

(3) A change in the length of step for step-by-step integration is often necessary as the integration proceeds. Such a change can be more readily made in this process than where five-line formulas of integration are employed.

(4) The coefficients occurring in the formulas are simpler than those in comparable five-line quadrature formulas, so that the machine calculation is not at all complicated.

The most obvious disadvantage of the process is that it requires the calculation of two additional derivatives at each step, and the labor of substitution in certain instances may be excessive. In such cases this method is not recommended. On the other hand, for equations of simple analytical form, and particularly for linear differential equations, it should prove valuable.

II. Derivation of Formulas

Let x_0 and x_1, where $x_1-x_0=h$, be two values of the independent variable x, and let y_0, y_0', etc., $y_1 y_1'$ etc., be the corresponding values of y, y', ... Assuming that y has a continuous derivative of order 7 we may express y, y', y'', and y''' by Taylor's series with remainder term, as follows:

$$y_1=y_0+hy_0'+\frac{h^2y_0''}{2!}+\frac{h^3y_0^{(3)}}{3!}+\frac{h^4y_0^{(4)}}{4!}+\frac{h^5y_0^{(5)}}{5!}+\frac{h^6y_0^{(6)}}{6!}+R_1, \tag{1}$$

$$hy_1'=hy_0'+h^2y_0''+\frac{h^3y_0^{(3)}}{2!}+\frac{h^4y_0^{(4)}}{3!}+\frac{h^5y_0^{(5)}}{4!}+\frac{h^6y_0^{(6)}}{5!}+R_2, \tag{2}$$

$$h^2y_1''=h^2y_0''+h^3y_0^{(3)}+\frac{h^4y_0^{(4)}}{2!}+\frac{h^5y_0^{(5)}}{3!}+\frac{h^6y_0^{(6)}}{4!}+R_3, \tag{3}$$

[1] The preparation of this paper was sponsored (in part) by the Office of Naval Research.

[2] Mathematics Department, Oregon State College.

$$h^3y_1'''=h^3y_0''+h^4y_0^{(4)}+\frac{h^5y_0^{(5)}}{2!}+\frac{h^6y_0^{(6)}}{3!}+R_4, \tag{4}$$

$$y_2=y_0+2hy_0'+\frac{4h^2y_0''}{2!}+\frac{8h^3y_0'''}{3!}+\frac{16h^4y_0^{(4)}}{4!}+\frac{32h^5y_0^{(5)}}{5!}+\frac{64h^6y_0^{(6)}}{6!}+R_5. \tag{5}$$

From the four equations (1, 2, 3, and 4), the three quantities $y_0^{(4)}$, $y_0^{(5)}$, and $y_0^{(6)}$ may be eliminated, and the resulting equation can be rearranged so as to give

$$y_1-y_0=\frac{h}{2}(y_1'+y_0')-\frac{h^2}{10}(y_1''-y_0'')+\frac{h^3}{120}(y_1'''+y_0''')+R_6. \tag{6}$$

It may be shown by a separate investigation[3] that

$$R_6=\frac{-h^7y^{(7)}(s)}{100{,}800},$$

in which $x_0<s<x_1$.

In a similar manner from eq 1 to 5 we may derive

$$y_2-2y_1+y_0=7h(y_1'-y_0')-3h^2(y_1''+y_0'')+\frac{h^3}{12}(11y_1'''-5y_0''')+\frac{210h^7y^{(7)}(s)}{100{,}800}, \tag{7}$$

with s in the interval $x_0<s<x_2$. These are the required formulas.

III. Application to Equations of First Order

Let the given differential equation be

$$y'=f(x,y). \tag{8}$$

Differentiation gives

$$y''=f_x(x,y)+f_y(x,y)y', \tag{9}$$

and

$$y'''=f_{xx}(x,y)+2f_{xy}(x,y)y'+f_{yy}(x,y)y'^2+f_y(x,y)y''. \tag{10}$$

Let the given initial values be x_0, y_0. Then from eq 8, 9, and 10 in succession we obtain y_0', y_0'', y_0''', giving the first line of the computation

$$x_0 \quad y_0 \quad y_0' \quad y_0'' \quad y_0'''.$$

To proceed we assume a trial value for y_1. A fairly good trial value is provided by

$$y_1=y_0+hy_0'+\frac{h^2y_0}{2!}+\frac{h^3y_0'''}{3!}.$$

Next with x_1, and the trial value y_1, we obtain trial values for y_1', y_1'', y_1''' from eq 8, 9, and 10 and have the trial line for x_1:

$$x_1 \quad y_1 \quad y_1' \quad y_1'' \quad y_1'''.$$

Now using eq 6 we secure an improved value of y_1, compute y_1', y_1'', y_1''', from eq 8, 9, and 10, recalculate y_1 by 2, (eq 6), and repeat this sequence of steps until no change occurs in the value obtained for y_1. This is taken as correct, and we have two lines of the computation:

$$x_0 \quad y_0 \quad y_0' \quad y_0'' \quad y_0''',$$

$$x_1 \quad y_1 \quad y_1' \quad y_1'' \quad y_1'''.$$

We are now in a position to use formula 7 in order to calculate a trial value for y_2. Then trial values of y_2', y_2'', y_2''' are obtained from eq 8, 9, and 10, and we leave the trial line:

$$x_2 \quad y_2 \quad y_2' \quad y_2'' \quad y_2'''.$$

Formula 6 (with subscripts advanced by 1) gives an improved value for y_2. If the "improved" value of y_2 is different from the "trial" value of y_2, it will be necessary to recompute y_2', y_2'', y_2''' and apply eq 6 again, repeating these steps until no further change occurs. At this stage we have completed three lines of the computation:

$$x_0 \quad y_0 \quad y_0' \quad y_0'' \quad y_0''',$$

$$x_1 \quad y_1 \quad y_1' \quad y_1'' \quad y_1''',$$

$$x_2 \quad y_2 \quad y_2' \quad y_2'' \quad y_2'''.$$

Subsequent lines of the calculation are obtained by exactly the same steps as were used to get y_2.

IV. Discussion of the Process

This completes the description of the process for the case of equations of the first order. Some comments of a practical nature are, however, pertinent.

(1) Obviously, the error in y at any step due to the use of the approximate formula 6 is bounded by the quantity

$$E=\frac{h^7M}{100{,}800}, \tag{11}$$

[3] W. E. Milne, The remainder in linear methods of approximation, J. Research NBS 43, 501 (1949) RP2042.

in which $M=\max|y^{(7)}|$ in the interval covered by the step. Supposing for the moment that M is a known constant, we see that the above equation connects the magnitude of the error E with the length of the step-interval h.

If, for example, the problem in question requires that y be obtained accurately to a specified number of decimal places, eq 11 enables us to select an appropriate value of h that will secure this accuracy. On the other hand, if we have already decided on the value of h, eq 11 will tell us how many decimals in the result may be regarded as correct.

(2) Actually, M is rarely constant from step to step, and moreover the value of M is unknown since it is ordinarily utterly impractical to calculate the value of the seventh derivative of y at each step. However, a crude estimate (which actually proves to be sufficiently satisfactory) may be made as follows: Assume that the calculation has been performed correctly to the nth step so that we have the correct values of the line

$$x_n \quad y_n \quad y_n' \quad y_n'' \quad y_n''',$$

a trial value $\overline{y}_{n+1}$ is obtained by eq 7. A final value of y_{n+1} is obtained by eq 6, repeated if necessary. Now the error of $\overline{y}_{n+1}$ is

$$\frac{210h^7y^{(7)}(s)}{100{,}800},$$

whereas that of y_{n+1} is

$$-\frac{h^7y^{(7)}(s')}{100{,}800}+e,$$

e being the error produced in y_{n+1} by the errors in y_{n+1}', y_{n+1}'', y_{n+1}''', these latter being due to the error of y_{n+1}. In actual practice, if the process is rapidly enough convergent for practical use, the error e must be much smaller than the error in $\overline{y}_{n+1}$. Hence, we may neglect e. Then

$$\overline{y}_{n+1}-y_{n+1}=\frac{210h^7y^{(7)}(s)}{100{,}800}+\frac{h^7y^{(7)}(s')}{100{,}800}.$$

If we ignore the fact that $y^{(7)}(s)$ and $y^{(7)}(s')$ are not exactly the same, we may add the terms on the right, divide by 211, and obtain

$$\text{Error of } y_{n+1}=-\frac{h^7y^{(7)}(s)}{100{,}800}=\frac{y_{n+1}-\overline{y}_{n+1}}{211}.$$

Although the foregoing reasoning seems very crude, the final formula

$$\text{Error of } y_{n+1}=\frac{y_{n+1}-\overline{y}_{n+1}}{211},$$

proves to be not only simple in application but actually quite reliable in determining how many significant figures of the result can be trusted.

(3). At each step of the computation the quantity $c_n=y_n-\overline{y}_n$ should be recorded in a separate column. This column of c's is used for several purposes.

(a) As long as the c's vary regularly and have significant figures only in the last two places retained, we proceed with the computation in reasonable confidence that all is well.

(b) A sudden fluctuation in the c's suggests that a computational mistake has been made, and the lines involved should be rechecked.

(c) If the c's increase to the point of affecting the last three places retained, then either the interval, h, should be shortened, or one less place should be retained.

(d) The necessity for recomputing y_{n+1}', y_{n+1}'', y_{n+1}''' can frequently be obviated by estimating c_{n+1} from the known values c_{n-2}, c_{n-1}, c_n and adding it to the trial value $\overline{y}_{n+1}$ *before* computing y_{n+1}', y_{n+1}'', y_{n+1}'''. If the estimate is sufficiently accurate, no recomputation is required.

(4). The foregoing discussion applies only after the computation is under way and does not give any clue to the accuracy of y_1. We would, of course, like to decide on the value of h and on the number of decimal places before starting the computation. This requires that we calculate $y_0^{(7)}$ from the differential equation and the initial values.

V. Equations of Higher Order

The modifications required to apply the process to equations of second or higher order are slight. In the case of an equation of second order, for example, the routine (after the start has been made) is as follows:

Predict y_2' by eq 7 modified as follows:

$$y_2'-2y_1'+y_0'=7h(y_1''-y_0'')-3h^2(y_1'''+y_0''')+\frac{h^3}{12}(11y_1^{(4)}-5y_0^{(4)}).$$

Predict y_2 by eq 7. Calculate y_2'', y_2''', $y_2^{(4)}$ from the differential equations and the equations obtained by differentiation.

Correct y_2' by

$$y_2'-y_1'=\frac{h}{2}(y_2''+y_1'')-\frac{h^2}{10}(y_2'''-y_1''')+\frac{h^3}{130}(y_2^{(4)}+y_1^{(4)}).$$

Correct y_2 by

$$y_2-y_1=\frac{h}{2}(y_2'+y_1')-\frac{h^2}{10}(y_2''-y_1'')+\frac{h^3}{130}(y_2'''+y_1''').$$

VI. Illustrative Examples

The foregoing method is applied to the second order differential equation

$$xy''+y'+xy=0,$$

with conditions $y=1$, $y'=0$ at $x=0$.

Example 1, below, gives the solution by another method using $h=0.1$. Example 2 uses the present method with $h=0.5$. A comparison of the computation time is given. Example 3 uses the present method with $h=0.1$.

It appears that in example 2 the error of y is about 2 in sixth place, whereas in example 3 the error is occasionally 1 in the tenth place.

A comparison of example 1 and example 2 shows that the new method obtained the value of $J_0(3)$ in only six steps (and more accurately) than the simple method based on Simpson's Rule could secure in 30 steps. Although the labor of substitution per step is much greater for the new method, the reduction in number of required steps more than offsets this extra work, as is shown by a comparison of required times.

Example 3 provides further evidence of the power of the new method. Anyone with experience in numerical solution of differential equations will recognize that to solve Bessel's equation to 10 decimal places in the neighborhood of the orign with step-intervals of length 0.1 requires a pretty accurate method of solution.

EXAMPLE 1.

Differential equation: $x\frac{d^2y}{dx^2}+\frac{dy}{dx}+xy=0$

Computation formulas

Predictor: $y'_{n+1}=y'_{n-3}+h\left[4y''_{n-1}+8/3\,\delta^2y''_{n-1}\right]$.

Corrector: $y'_{n+1}=y'_{n-1}+h\left[2y''_n+1/3\,\delta^2y''_n\right]$.

Derivatives: $y''=-\frac{1}{x}\,y'-y$.

Time: 2¼ hr; $h=0.1$

x	y	y'	y''	$\frac{1}{3}\delta^2y'$	$\frac{1}{3}\delta^2y''$	c	c'	True values	
								y	y'
0.2	[a]0.990025	[a]−0.099501	−0.492520	.....	.....	...	...	.....	.....
.3	[a].977626	[a]−.148319	−.483229	0.000370	0.001203	...	...	.....	.....
.4	[a].960398	[a]−.196027	−.470330	.000489	.001166	...	...	.....	.....
.5	[a].938470	[a]−.242268	−.453934	.000603	.001122	...	...	.....	.....
.6	.912005	−.286702 (0)	−.434168	.000714	.001065	0	2	0.912005	−0.286701
.7	.881201	−.328995	−.411208	.000815	.001004	0	0	.881201	−.328996
.8	.846288	−.368843 (2)	−.385234	.000914	.000930	0	1	.846287	−.368842
.9	.807524	−.405949 (8)	−.356470	.001001	.000853	0	1	.807524	−.405950
1.0	.765198	−.440052	−.325146	.001085	.000764	0	0	.765198	−.440051
1.1	.719622	−.470802 (1)	−.291529	.001154	.000674	0	1	.719622	−.470802
1.2	[b].671133 (5)	−.498290	−.255891	.001219	.000574	2	0	.671133	−.498289
1.3	.620086	−.522023 (1)	−.218530	.001269	.000473	0	2	.620086	−.522023
1.4	.566855 (7)	−.541949	−.179749	.001313	.000366	2	0	.566855	−.541948
1.5	.511828	−.557936	−.139871	.001342	.000259	0	0	.511828	−.557937
1.6	.455402 (4)	−.569897	−.099216	.001364	.000146	2	0	.455402	−.569896
1.7	.397985	−.577765 (4)	−.058123	.001372	+.000037	0	1	.397985	−.577765
1.8	.339986 (7)	−.581518 (9)	−.016920	.001371	−.000077	1	−1	.339986	−.581517
1.9	.281819 (20)	−.581157 (6)	+.024053	.001357	−.000184	1	1	.281819	−.581157
2.0	.223890 (2)	−.576726 (7)	.064473	.001334	−.000295	2	−1	.223891	−.576725
2.1	.166607 (8)	−.568292 (1)	.104008	.001298	−.000398	1	+1	.166607	−.568292
2.2	.110361 (3)	−.555964 (5)	.142350	.001255	−.000502	2	−1	.110362	−.555963
2.3	.055540 (1)	−.539872	.179187	.001198	−.000595	1	0	.055540	−.539873
2.4	.002506 (8)	−.520186 (8)	.214238	.001136	−.000689	2	−2	+.002508	−.520185
2.5	−.048384 (3)	−.497093	.247221	.001060	−.000771	+1	0	−.048384	−.497094
2.6	−.096807 (5)	−.470819 (20)	.277891	.000982	−.000852	+2	−1	−.096805	−.470818
2.7	−.142450 (49)	−.441600	.306006	.000890	−.000919	+1	0	−.142449	−.441601
2.8	−.185038 (6)	−.409710 (1)	.331363	.000798	−.000984	+2	−1	−.185036	−.409709
2.9	−.224312	−.375426	353769	.000694	−.001034	0	0	−.224312	−.375427
3.0	−.260054 (3)	−.339060 (1)	.373074	.....	.....	+1	−1	−.260052	−.339059

[a] Starting values given.

[b] In the column for y and y' appear the corrected values. The digits of the predicted values when different from the corrected are shown in parentheses.

Example 2.

Differential equation: $x\frac{d^2y}{dx^2}+\frac{dy}{dx}+xy=0$

Computation formulas

Predictor: $$y'_{n+1}=2y'_n-y'_{n-1}+7h(y''_n-y''_{n-1})-3h^2(y'''_n+y'''_{n-1})+\frac{h^3}{12}(11y^{IV}_n-5y^{IV}_{n-1})$$

$$y_{n+1}=2y_n-y_{n-1}+7h(y'_n-y'_{n-1})-3h^2(y''_n+y''_{n-1})+\frac{h^3}{12}(11y'''_n-5y'''_{n-1})$$

Corrector: $$y'_{n+1}=y'_n+\frac{h}{2}(y''_{n+1}+y''_n)-\frac{h^2}{10}(y'''_{n+1}-y'''_n)+\frac{h^3}{120}(y^{IV}_{n+1}+y^{IV}_n)$$

$$y_{n+1}=y_n+\frac{h}{2}(y'_{n+1}+y'_n)-\frac{h^2}{10}(y''_{n+1}-y''_n)+\frac{h^3}{120}(y'''_{n+1}+y'''_n)$$

Derivatives: $$y''=\frac{1}{x}y'-y$$

$$y'''=\frac{2}{x}y''-y'-\frac{1}{x}y$$

$$y^{IV}=-\frac{3}{x}y'''-y''-\frac{2}{x}y'$$

Time: 1½ hr; $h=0.5$

x	y	y'	y''	y'''	y^{IV}	c	c'	True values	
								y	y'
0	[a]1.	[a]0	−0.5	0	0.375	...	...	.....	.....
0.5	0.938470	[a]−0.242268	−.453934	0.181064	.336622	...	...	.....	.....
1.0	[b].765195 (9)	−.440047 (63)	−.325148	.325148	.229798	4	−16	0.765198	−0.440051
1.5	.511826 (31)	−.557934 (5)	−.139870	.403210	.077382	5	−1	.511828	−.557937
2.0	.223889 (2)	−.576721 (18)	+.064472	.400304	−.088207	−7	+3	.223891	−.576725
2.5	−.048382 (6)	−.497090 (1)	.247218	.318968	−.231948	−4	−6	−.048384	−.497094
3.0	−.260053 (47)	−.339057 (48)	.373066	.177021	−.324043	6	+3	−.260052	−.339059

[a] Starting values given.
[b] In the column for y and y' appear the corrected values. The digits of the predicted values when different from the corrected are shown in parentheses.

Example 3.

Differential equation: $x\frac{d^2y}{dx^2}+\frac{dy}{dx}+xy=0$.

Computation formulas: (Same as Example 2.).

Computation, $h=0.1$.

y		y'	y''	y'''	y^{IV}	c	c'	True values	
								y	y'
0.5	[a]1.	[a]0	−0.5	0	0.375	...	...	.....	.....
.1	[a]0.99750 15621	[a]−0.04993 75260	−.49812 63017	0.03744 79394	.37343 86390	...	...	.....	.....
.2	.99002 49723	−.09950 08326 (7)	−.49252 08093	.07458 40641	.36876 81738	−0	−1	0.2 0.99002 49722	−0.09950 08326
.3	.97762 62466	−.14831 88162 (6)	−.48323 01926	.11109 92782	.36102 95182	0	−4	.3 .97762 62465	−.14831 88163
.4	.96039 82267	−.19602 65779 (81)	−.47033 17820	.14668 99212	.35029 02625	0	−2	.4 .96039 82267	−.19602 65780
.5	[b].93846 98073 (2)	−.24226 84576 (9)	−.45393 28921	.18106 04114	.33664 42541	−1	−3	.5 .93846 98072	−.24226 84577
.6	.91200 48639 (5)	−.28670 09880 (1)	−.43416 98836	.21392 58273	.32021 07071	−1	−1	.6 .91200 48635	−.28670 09881
.7	.88120 08887	−.32899 57415 (6)	−.41120 69723	.24501 43928	.30113 31217	0	−1	.7 .88120 08886	−.32899 57415
.8	.84628 73528 (7)	−.36884 20461 (2)	−.38523 47952	.27406 98431	.27957 79688	−1	−1	.8 .84628 73528	−.36884 20461
.9	.80752 37982 (0)	−.40594 95461 (2)	−.35646 87470	.30085 36525	.25573 33411	−2	−1	.9 .80752 37981	−.40594 95461
1.0	.76519 76866 (0)	−.44005 05858 (9)	−.32514 71008	.32514 71008	.22880 69709	−6	−1	1.0 .76519 76866	−.44005 05857

[a] Starting values given.
[b] In the column for y and y' appear the corrected values. The digits of the predicted values when different from the corrected are shown in parentheses.

Los Angeles, June 17, 1949.

U. S. Department of Commerce
National Bureau of Standards

Research Paper RP2047
Volume 43, December 1949

Part of the Journal of Research of the National Bureau of Standards

Measurement of the Disintegration Rate of Sodium^{22} by the Coincidence Method[1]

By J. L. Herson

A coincidence method of measuring the absolute disintegration rate (total strength) of sodium^{22} sources is described.

Prevention of false coincidences and the separation of the total gamma counts observed in the basic measurements into nuclear and annihilation radiation incident to the positron emission is accomplished by magnetic deflection and a series of supplementary measurements in which a platinum-cylinder Geiger-Müller gamma counter is used. A copper cylinder gamma counter was used in the basic measurements.

The radioactive preparation was an aqueous solution of NaCl of 1 milligram per milliliter concentration and with a ratio of radioactive $Na^{22}Cl$ to carrier (stable) NaCl of the order of 1 to 10^{10}. The disintegration rate of the test source (0.8 milliliter of this solution) was found to be 2.15×10^4 disintegrations per second with a conservatively estimated accuracy of ±5 percent. Of the total gamma counts, 70 percent was of nuclear origin; whereas 30 percent were due to annihilation radiation.

The efficiency of the platinum counter relative to that of the copper counter in detecting annihilation radiation (0.51 Mev) was 2.9. Their detecting efficiencies for nuclear gamma radiation (1.3 Mev) were nearly alike.

I. Introduction

The absolute disintegration rate of a radioactive preparation can be readily determined by the coincidence method if the disintegration scheme is known to be simple. Thus, if the isotope in question emits one beta followed by one gamma ray, observations are made of the beta, gamma, and beta-gamma coincidence rates and the absolute disintegration rate determined without reference to the efficiencies of the detectors or the geometry of the arrangement, from the relation

$$N=\frac{B\times G}{C}, \qquad (1)$$

where

B=beta counting rate;
G=gamma counting rate;
C=beta-gamma coincidence rate.

In the case of positron emitters, the application of the coincidence method presents two difficulties.

a. False coincidences result from the positrons registered by the beta counter and the associated annihilation radiation registered by the gamma counter.
b. The gamma counter responds to nuclear gamma rays as well as to the annihilation radiation; and there is no simple way of ascertaining what fraction of the total counts is due to the nuclear gamma rays alone.

Sodium^{22} is a positron emitter and exhibits a simple disintegration scheme: 0.6 Mev positron followed by a 1.3 Mev gamma ray. To circumvent the above mentioned difficulties, a somewhat more elaborate coincidence method first employed by Leibnitz[2] was used.

[1] This work was done with the assistance of the Atomic Energy Commission.

[2] Z. f. Phys. **122**, 233 (1944).

859368—49——3

II. Source and Experimental Arrangement

The radioactive sodium used in these measurements was produced in a cyclotron by the reaction Mg (d, α) and received here in the form of magnesium uranyl acetate. It was converted to NaCl by using a process developed by J. W. Irvine of MIT. The source was prepared by four successive depositions of 200 μl of the NaCl solution on paraffin coated cellophane.

The experimental arrangement is shown schematically in figure 1. The source and the two counters were placed between the pole pieces of an electromagnet. A lead block was placed between the two counters. With this arrangement the counted positrons follow a semicircular path, and the annihilation radiation produced in and near the beta counter is prevented from reaching the gamma counter and registering false coincidences. The magnetic field used throughout these measurements was about 300 gausses.

III. Procedure

As in the standard coincidence method, measurements were first made of the positron, gamma, and coincidence rates (B, G_1, and C_1) with the application of the usual corrections for background, accidentals, and cosmic coincidences. Following these principal measurements a series of supplementary tests was made as follows:

An aluminum cover about 1/32 in. thick was placed over the source and the gamma counting rate again observed. Although the counter now registered the same number of nuclear gamma's as in the previous test, additional annihilation quanta were produced by the interaction of the positrons with the aluminum, and the total counting rate increased to a new value (G_2).

The copper-cylinder gamma counter used in the preceding measurements was then replaced with a platinum-cylinder gamma counter of the same dimensions, the aluminum cover was removed, and the coincidence rate (C_2) again measured. The platinum counter is known to have a different detecting efficiency characteristic as a function of gamma-ray energy, the efficiency being particularly higher for low energy gamma rays. Since the annihilation radiation did not contribute to the observed coincidences (C_1 and C_2), the ratio of the coincidence rates is also the ratio of the efficiencies of the respective counters in detecting the nuclear gamma radiation. We designate the ratio as $m=C_2/C_1$.

The gamma counting rate of the platinum-cylinder gamma counter was then measured; first without any cover over the source (G_3) and then with an aluminum cover placed over the source (G_4). As in the case of the similar measurement with the copper-cylinder counter, G_4 was greater than G_3 due to the additional annihilation radiation.

The increase in the gamma count could conceivably be produced partially by the Compton-effect photons, but this increase, if present, will be small and has been neglected.

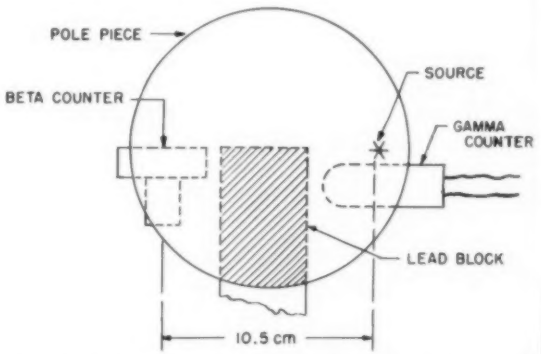

FIGURE 1. *Experimental arrangement for measuring the disintegration rate of* Na^{22}.

IV. Interpretation of Experimental Data

To derive the desired information from the experimental data, the following quantities are introduced:

y, counting rate due to nuclear gamma rays only in the determination of G_1.

x, counting rate due to annihilation radiation only in the determination of G_1.

n, the ratio of the annihilation counts in the measurement of G_2 (using aluminum cover) to the annihilation counts in the measurement of G_1 (without aluminum cover).

l, relative efficiency for detecting annihilation quanta of the platinum gamma counter with respect to the copper counter.

The following four equations relate these four quantities to the measurements data

$$\left.\begin{aligned} G_1 &= y + x \\ G_2 &= y + nx \\ G_3 &= my + lx \\ G_4 &= my + nlx \end{aligned}\right\} \qquad (2)$$

These equations can be solved, and it is the value of y rather than G_1 that is used in eq 1 in computing the absolute strength of the source.

V. Numerical Values

The following numerical results were obtained in our measurements

B, 2,067/min.

C_1, 1.98/min.

C_2, 1.93/min.

$m = \frac{C_2}{C_1}$, 0.97

G_1, 1,766/min.

G_2, 1,903/min.

G_3, 2,751 min.

G_4, 3,152/min.

The set of equations then yielded:

$y = 1{,}236$/min.

$x = 530$/min.

$l = 2.9$

$n = 1.26$

Using the value of y in place of G in eq 1, the disintegration rate of the test source (800 μl)

$$N = \frac{2{,}067 \times 1{,}236}{1.98 \times 60} = 2.15 \times 10^3 \text{ disintegration/sec.}$$

$$= 0.0215 \text{ rd.}$$

A sample taken from the same preparation was later measured by an independent method of positron counting and comparison with a known standard. Both results were in agreement to within less than 1 percent.

It is interesting to note that of the total gamma counts observed in the main test only 70 percent was due to nuclear gamma rays, and the remaining was due to annihilation radiation. Without any correction derived from the supplementary measurements, a 43-percent error would have been incurred. The value of l (2.9) is significant, showing that for gamma rays of 0.5 Mev. the platinum counter is 2.9 times more efficient than the copper counter, whereas their efficiencies do not differ for 1.3-Mev gamma rays.

It is a pleasure to acknowledge the cooperation of H. Seliger, who made the confirming independent measurement and of A. Schwebel, who performed the preliminary chemical processing of the preparation.

Washington, July 17, 1949.

U. S. Department of Commerce
National Bureau of Standards

Research Paper RP2048
Volume 43, December 1949

Part of the Journal of Research of the National Bureau of Standards

Submicroscopic Structure of Cellulose from Nitrogen Sorption Measurements[1]

By Charles M. Hunt, Raymond L. Blaine, and John W. Rowen

When cotton linters were soaked in cold 10-percent sodium hydroxide, washed, and neutralized, and transferred successively to methyl alcohol and benzene, and carefully dried at reduced pressure, a surface area as high as 71.3 square meters per gram was obtained by the Brunauer, Emmett, Teller technique. Previous areas for untreated cotton were all below 1 square meter per gram. Linters carried through the above steps after soaking in water instead of alkali had an area as high as 47.3 square meters per gram. When the alkali-treated sample was conditioned in water vapor to 3.3 percent gain in weight, the surface decreased to 31.6 square meters per gram; further conditioning to an 11.0-percent gain in weight decreased the surface to 2.1 square meters per gram.

The isotherms of the treated samples showed strong hysteresis, whereas the isotherms of untreated cotton showed little or no hysteresis.

Calculations of pore size distribution by the method of Wheeler and Shull indicated these materials have rather narrow distributions, the alkali-treated material having a maximum at a pore radius of about 20 Angstroms and the water-soaked material a maximum at about 16 Angstroms.

I. Introduction

The view that native and regenerated cellulose fibers contain longitudinal submicroscopic channels, or that such a structure can be produced by imbibition of water has been suggested from a number of lines of evidence as, for example, X-ray and ultramicroscopic studies of fibers in which metals have been deposited from solution [1, 2, 3].[2] A review of this subject is presented by Frey-Wyssling [20] and Hock and Mark [4a]. The existence of channels in wet cellophane has been suggested to explain its use as a semipermeable membrane, and Valko [4b] has reviewed the measurement of pore diameters in this material by different methods and cites values, most of which lay between 40 and 60 A. The observation of Collins [5, 6] that cotton and rayon fibers swell laterally but very little longitudinally upon imbibing water indicates that some sort of lateral separation of the chains occurs in the swelling process.

Previous work in this laboratory showed that the surface area of a cotton sample was 0.72 m^2/g when based on the sorption of nitrogen at liquid nitrogen temperatures and calculated by the Brunauer, Emmett, Teller equation [16]. When this equation was applied to the data for the sorption of water at 25° C by the same cotton, a specific surface of 108 m^2/g was obtained. From this it was evident that water had access to regions within the fiber unavailable to nitrogen. Shaw and coworkers made a similar kind of observation when they compared the water and nitrogen absorption of certain proteins [7] and sodium pectate [8]. However Assaf, Haas, and Purves [9, 10] reported that cotton linters soaked in sodium hydroxide and carried through a solvent exchange procedure had a calculated area as large as 64.7 m^2/g available to nitrogen. Thus it appears that regions within the fiber ordinarily available only to water were made available to nitrogen.

The experiments reported here were undertaken to study the structure of expanded cellulose by low-temperature nitrogen sorption, because measurements of this type on other adsorbents have

[1] This paper will also appear in the January 1950 issue of the Textile Research Journal.

[2] Figures in brackets indicate the literature references at the end of this paper.

been found to have real significance. Cotton linters were carried through the procedure of Assaf, Haas, and Purves and nitrogen adsorption-desorption isotherms were obtained. Pore size distributions were calculated from the desorption data as has been done for certain silica gels [11, 12] and other materials [13c]. The effect of adding water vapor to the expanded material was observed, and an experiment was carried out to see if high nitrogen sorption could be obtained with cotton linters presoaked with water instead of alkali.

II. Experimental Part

The sample of cotton linters used in this work was furnished by the Hercules Powder Co. through the courtesy of H. M. Spurlin and Peter Van Wyck. It was designated as 05843 Grade 27LV Cotton Seed Hull Shavings Pulp. According to descriptive material furnished by the company, chemical cotton of this type is digested with dilute alkali and bleached. The sample had a reported [3] viscosity of 608 sec in 2.5 g/100 ml concentration in ACS cuprammonium solvent, corresponding to an intrinsic viscosity of about 9 and a degree of polymerization of about 1,800. The material was used without further purification. The methyl alcohol and benzene used in the solvent exchange described in this study were dried by distillation from sodium.

The control sample of cotton linters (sample *A*) received no treatment. Sample *B* was put through the procedure described by Assaf, Haas, and Purves [9], neutralizing the sample after removing most of the alkali. No preliminary dewaxing was performed, as the material wet readily with water. After drying in vacuum, the sample was stored several weeks over a drying agent and paraffin before use. The paraffin was used as an absorbent for desorbed benzene vapor. Sample *C* was prepared by soaking 5 g of cotton linters for 3 hr in water at room temperature. The sample was then pressed to remove excess water and transferred to ½ l of absolute methyl alcohol. After 30 min the sample was pressed and transferred to a second portion of methanol. The process was repeated once more with methyl alcohol and twice with benzene. The sample was vacuum dried by intermittent evacuation to a pressure of about 25 mm Hg and stored over a drying agent and paraffin. This procedure is similar to that of Assaf, Haas, and Purves, but the preliminary swelling was done with water alone at room temperature instead of 10-percent sodium hydroxide in an ice bath.

Five to seven g of samples *A*, *B*, and *C* were quickly transferred from the desiccator and sealed into glass holders. A glass plug was placed on top of each sample and this permitted the sealing flame to be applied 2 to 3 in. from the cotton without unduly increasing dead space. The tips of the holders were drawn out so that they could be easily broken off and resealed. Samples *A* and *C* were outgassed overnight at room temperature, or longer if necessary, to obtain a vacuum of 10^{-6} mm Hg, and nitrogen adsorption-desorption isotherms were obtained. Nitrogen adsorption-desorption measurements were made on sample *B*, both after outgassing at liquid nitrogen temperature (determinations 1, 2, and 3), and after outgassing at room temperature (determination 4), in order to see if large differences were obtained. Sample *B* was then conditioned at 20- to 25-percent relative humidity. Conditioning was accomplished by passing nitrogen through sulfuric acid of proper concentration, glass wool, and finally through the sample. Passage through the sample was achieved by breaking the tip of the holder, and after constant weight was attained the tip was resealed. The sample was outgassed under liquid nitrogen to retain the water that had been added, and nitrogen adsorption-desorption measurements were made (determinations 5 and 6). The process was repeated after conditioning the sample at 70- to 75-percent relative humidity (determinations 7 and 8). The sample was then dried by passing nitrogen, dried with magnesium perchlorate, through the sample. Nitrogen adsorption-desorption measurements were made after outgassing at room temperature. This provided a means of seeing if any of the nitrogen sorptive capacity of the sample lost by hydration could be regained by removal of the water (determinations 9 and 10).

Nitrogen adsorption measurements were made with an apparatus similar to that described by Emmett [14]. The saturation vapor pressure of the nitrogen at the temperature of the liquid nitrogen bath was determined by a vapor pressure thermometer, using the purified nitrogen employed for the adsorption experiment. A correction for the nonideality of nitrogen was calculated, assuming the volume of nitrogen in the dead space at

[3] Private communication from Peter Van Wyck.

760 mm Hg pressure was 5 percent greater than that calculated from the ideal gas laws, and that the percentage deviation varied linearly with pressure, being negligible at very low partial pressures.

Pressure-volume measurements covering a range of p/p_0 from less than 0.1 to above 0.9 were made, where p is the pressure of nitrogen above the sample and p_0 is the vapor pressure of liquid nitrogen at the same temperature. Each adsorption-desorption isotherm required 2 or 3 days to complete. Apparently longer times were required to reach equilibrium on the steeper portions of the curves than the flatter portions. Final readings were recorded when two pressure readings taken 10 min apart did not differ by more than 0.1 mm Hg. Pressure readings obtained in this way usually agreed within 1 or 2 percent with readings obtained when the sample was left overnight, the drift being in the direction of slightly greater nitrogen adsorption in adsorption measurements and slightly less nitrogen adsorption in desorption measurements.

III. Nitrogen Sorption Isotherms

The volumes of nitrogen adsorbed per gram of sample are given in table 1, and typical isotherms are shown in figures 1 and 2. The untreated cotton linters (fig. 2 curve *A*) adsorbed much less nitrogen than the other samples and had a type II isotherm [13a]. That is, the curve gave no indication of leveling off up to the highest partial pressure measured. No hysteresis was observed within the limits of experimental error. The adsorption of nitrogen by untreated cotton is conceived as a multilayer adsorption process in which capillary condensation plays little or no part.

The cotton swollen with alkali and subjected to solvent exchange (fig. 1 curve *B*) and the cotton swollen with water and given solvent exchange (fig. 2 curve *C*) had what appeared to be type IV isotherms [13*a*]. Strong hysteresis was observed with inflection points in the desorption curves at partial pressures of 0.49 and 0.47, respectively.

When sample *B* was conditioned to a 3.3 percent gain in weight at a relative humidity of 20 to 25 percent, the isotherm (fig. 1 curve *B'*) also appeared to be type IV with strong hysteresis. The sorptive capacity was smaller, however. When sample *B* was further conditioned at 70 to 75 percent relative humidity to a weight 11.0 percent greater than the weight of the original sample, the form of the isotherm changed completely (fig. 1 curve *B''*). It was more like a type II curve, up

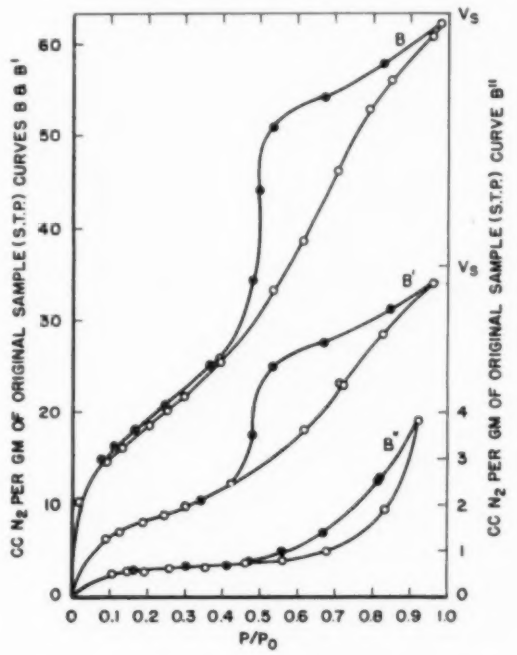

FIGURE 1. *Nitrogen adsorption-desorption isotherms.*

B, Alkali swelled, solvent exchanged cotton linters (determination 4); B', B conditioned at 20- to 25-percent relative humidity (determination 5); B'', B' conditioned at 70- to 75-percent relative humidity (determination 8). ●, desorption; ○, adsorption.

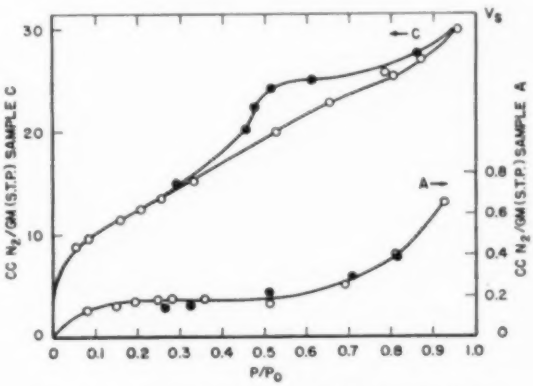

FIGURE 2. *Nitrogen adsorption-desorption isotherms.*

A, Control cotton linters (determination 1); C, water swelled, solvent exchanged cotton linters (determination 2). ●, Desorption; ○, adsorption.

TABLE 1. *Nitrogen sorbed by cotton linters*

Sample A—control				Sample B														Sample C			
Determination 1[a]		Determination 2		Determination 1		Determination 2		Determination 3		Determination 4[b]		Determination 5[c]		Determination 6		Determination 7		Determination 8[d]		Determination 9		Determination 10		Determination 1		Determination 2[e]	
p/p_0	ml N_2 per gram	p/p_0	ml N_2 per gram	p/p_0	ml N_2 per gram	p/p_0	ml N_2 per gram	p/p_0	ml N_2 per gram	p/p_0	ml N_2 per gram	p/p_0	ml N_2 per gram	p/p_0	ml N_2 per gram	p/p_0	ml N_2 per gram	p/p_0	ml N_2 per gram	p/p_0	ml N_2 per gram	p/p_0	ml N_2 per gram	p/p_0	ml N_2 per gram
Adsorption		Adsorption		Adsorption		Adsorption		Adsorption		Adsorption		Adsorption		Adsorption		Adsorption		Adsorption		Adsorption		Adsorption		Adsorption	
0.081	0.14	0.075	0.11	0.006	7.0	0.090	14.2	0.024	10.5	0.018	10.3	0.079	6.4	0.066	6.7	0.113	0.52	0.107	0.48	0.114	0.51	0.128	0.52	0.027	7.8	0.055	8.8
.152	.15	.138	.13	.029	11.6	.131	15.7	.091	11.1	.090	14.7	.126	7.1	.125	7.1	.154	.56	.146	.53	.150	.54	.175	.55	.037	7.7	.084	9.7
.194	.17	.185	.13	.038	12.3	.251	19.5	.120	15.1	.131	16.2	.190	8.1	.155	7.5	.202	.60	.191	.54	.204	.56	.182	.55	.120	10.3	.159	11.5
.249	.19	.228	.13	.076	14.2	.287	20.8	.149	16.1	.203	18.6	.245	8.9	.213	8.4	.257	.63	.261	.62	.267	.61	.227	.60	.192	12.0	.207	12.5
.283	.19	.280	.14	.109	15.5	.362	23.6	.177	16.9	.250	20.2	.302	9.8	.261	9.1	.312	.65	.355	.64	.363	.64	.259	.61	.269	13.8	.256	13.6
.360	.19	.346	.11	.144	17.3	.436	26.8	.239	18.9	.294	21.8	.419	12.0					.463	.72	.471	.72			.316	14.9	.293	15.4
.516	.17	.430	.19	.178	17.9	.519	31.0	.274	20.2	.389	25.6	.616	18.1					.562	.79	.596	.84					.325	20.0
.692	.25	.568	.17	.209	19.0	.589	35.6	.347	22.8	.387	25.9	.718	23.0					.678	.97	.747	1.23					.654	22.8
.813	.41	.672	.19	.240	20.0	.641	39.2	.422	25.9	.531	33.3	.716	23.1					.832	1.30	.855	2.16					.806	25.4
.928	.66	.780	.22	.274	21.3	.702	45.5	.506	30.2	.611	38.8	.826	28.5					.923	3.81	.942	4.31					.786	25.8
		.931	.47	.320	23.0	.827	53.6	.573	34.5	.701	46.4	.959	34.0													.872	27.1
Desorption		Desorption				.878	55.9	.636	39.5	.783	53.0															.958	30.9
0.813	0.38	0.732	0.20			.987	61.1	.632	39.8	.844	56.2	Desorption						Desorption		Desorption				Desorption			
.709	.30	.607	.18	Desorption				.715	46.6	.954	61.0	0.842	31.2					0.819	2.59	0.843	2.90			0.862	27.6
.515	.21	.498	.14	0.804	56.0	Desorption		.819	54.0	.974	62.3	.665	27.6					.813	2.54	.847	2.92			.613	25.1
.327	.18	.381	.18	.686	53.4	0.804	56.0	.833	54.5	Desorption		.541	25.0					.667	1.38	.715	1.68			.515	24.3
.266	.17	.313	.17	.554	50.3	.686	53.4	.942	59.3			.478	17.6					.555	0.96	.598	1.05			.475	22.4
		.271	.18	.495	42.9	.554	50.3	.976	61.3	0.823	58.0	.340	10.5					.469	.74					.455	20.3
		.239	.20	.442	28.0	.495	42.9	Desorption		.665	54.3							.413	.68					.291	15.1
		.195	.16	.308	22.1	.442	28.0			.527	51.0							.304	.65						
				.277	21.0	.308	22.1	0.812	56.7	.491	44.2							.193	.57						
				.206	18.6	.277	21.0	.789	56.1	.493	44.0														
				.156	17.0	.206	18.6	.656	53.1	.475	34.3														
				.136	16.4	.156	17.0	.522	49.9	.393	25.2														
						.136	16.4	.508	49.5	.245	20.9														
								.491	46.5	.163	18.1														
								.496	46.1	.109	16.3														
								.475	33.3	.074	15.0														
								.434	28.1																
								.399	24.6																
								.243	20.4																
								.161	17.7																
								.107	16.6																
								.072	13.7																
								.070	13.7																

[a] Plotted in figure 2 as curve A.
[b] Plotted in figure 1 as curve B.
[c] Plotted in figure 1 as curve B'.
[d] Plotted in figure 1 as curve B''.
[e] Plotted in figure 2 as curve C.

to the highest partial pressure measured, and showed measurable hysteresis with both branches convex to the pressure axis.

When sample B was redried after conditioning at 70 to 75 percent relative humidity an isotherm identical with curve B'' in figure 1 was obtained.

IV. Surface Areas

The volume of nitrogen required to cover the adsorbate with a unimolecular layer was determined from nitrogen adsorption data between p/p_0 values of 0.05 and 0.3 by methods already described [13b, 14, 15]. Surface areas were calculated from this volume assuming each nitrogen molecule to cover an area of 16.2 A^2. The values are summarized in table 2. Each value in the table represents a single determination, and they are listed in the order in which they were made.

TABLE 2. *Summary of surface area determinations*

	Determination No.	Specific surface, square meters per gram of sample
Sample A, control, outgassed at room temperature	1	0.6
	2	.5
Sample B, NaOH and solvent exchange, and outgassed at liquid nitrogen temperature	1	71.3
	2	68.2
	3	67.7
Outgassed at room temperature	4	70.4
Sample B, conditioned at 20 to 25% RH, and outgassed at liquid nitrogen temperature	5	31.6
	6	30.8
Sample B, conditioned at 70 to 75% RH, and outgassed at liquid nitrogen temperature	7	2.1
	8	2.0
Sample B, redried and outgassed at room temperature	9	2.0
	10	2.1
Sample C, solvent exchange only, and outgassed at room temperature	1	47.3
	2	46.5

The area of 0.5 to 0.6 m^2/g for untreated cotton linters is comparable with 0.72 m^2/g previously obtained in this laboratory for a cotton yarn [16]. This is slightly larger than the value of 0.16 m^2/g reported by Howell and Jackson [17] from microscopic measurements. This suggests that there may be a few accessible surface irregularities and pores, but nitrogen does not penetrate the untreated cotton fiber to any great extent.

However, when the linters were given the treatment of Assaf, Haas, and Purves a large surface was obtained, such as they reported. Successive additions of water to the sample greatly decreased the surface available to nitrogen, and when the water was removed the surface remained at the same low value. The sensitivity of surface area to small amounts of water indicates that refinements aimed at the complete removal and rigorous exclusion of water would lead to higher surface areas than those given in table 1.

The collapse of expanded cellulose upon wetting and drying suggests that the expanded material is in an unstable state. Recent unpublished work of P. H. Hermans [4] indicates that the expanded cellulose has an X-ray diffraction pattern that is somewhat different from that of native cellulose (cellulose I). Since expanded cellulose tends to revert to cellulose I upon wetting, it appears that the water molecules assist the cellulose in the expanded state in getting over a special energy barrier. Water probably facilitates lateral and transverse ordering through the formation of hydrogen bonds. It is believed that this ability of the cellulose molecule to become linked with other cellulose molecules by means of intermolecular hydrogen bonding is responsible for many of the physical properties of cellulose, such as insolubility and strength.

Swelling with water followed by solvent exchange from methyl alcohol to benzene without prior alkali treatment also produced a large increase in the calculated surface area of the cotton linters. Thus, although 10 percent sodium hydroxide undoubtedly produced structural changes in the cotton fiber, the use of alkali was not necessary to make comparatively large regions within the fiber available to nitrogen. A paper by Kistler is of interest in this connection [18]. He prepared aerogels from a large number of inorganic and organic materials by substituting a swelling liquid within the gel by a liquid that could be evaporated above its critical temperature in an autoclave. Thus, it was possible to replace the liquid in the structure by a gas without allowing the surface of the liquid to "recede within the gel." Kistler states that this last condition is quite important. He prepared an aerogel from cellophane by extracting the wet material with ether, followed by propane. The propane was removed in an autoclave at 115° C.

The procedure employed here differed in at least one important respect from that of Kistler in that the final liquid was benzene, which was removed at room temperature. However the

[4] Communication through H. Mark to one of the authors.

853368—49——4

high sorptive capacity for nitrogen suggests the material had some of the properties of an aerogel. Apparently cotton linters possessed sufficient rigidity to retain much of the expanded structure even though the benzene-air interface was allowed to "recede within the gel". As already noted [10] water cannot be removed in this way without collapsing the expanded structure of cellulose.

It is to be noted in table 2 that a repeated surface area measurement on the expanded material is usually slightly lower than the preceding measurement. This again suggests that the expanded state is unstable.

V. Pore Size Distribution

Hysteresis in the sorption isotherms of samples *B* and *C* has suggested that capillary condensation plays a part in the process. Although it is possible to interpret hysteresis other than by capillary condensation, and modern statistical mechanical treatments of sorption do not explicitly interpret it in terms of capillary condensation [19], hysteresis in the isotherms of rigid solids has generally been attributed to this mechanism. Brunauer [13c] has reviewed much of the work on this subject. The postulation of channels in wet cellulose from lines of evidence previously mentioned suggested that pores might exist in cellulose from which water had been removed by solvent exchange.

Pore size distributions have been calculated by the method of Wheeler [21] and Shull [11] from the desorption isotherms plotted in figure 1, curves B and B′, and figure 2, curve C. These distributions have been plotted in figure 3.

The method is briefly outlined here. It corrects the capillary radii, as calculated by the Kelvin equation, for the thickness of the layer of gas laid down by multilayer adsorption. The pore size distribution is based upon integration of the equation:

$$V_s - V = \pi \int_R^\infty (r-t)^2 L(r)\,dr, \qquad (1)$$

where:

V_s is the volume of gas adsorbed at saturation pressure;

V is the volume of gas adsorbed at any given partial pressure;

r is the pore radius;

t is the thickness of gas laid down by multilayer adsorption;

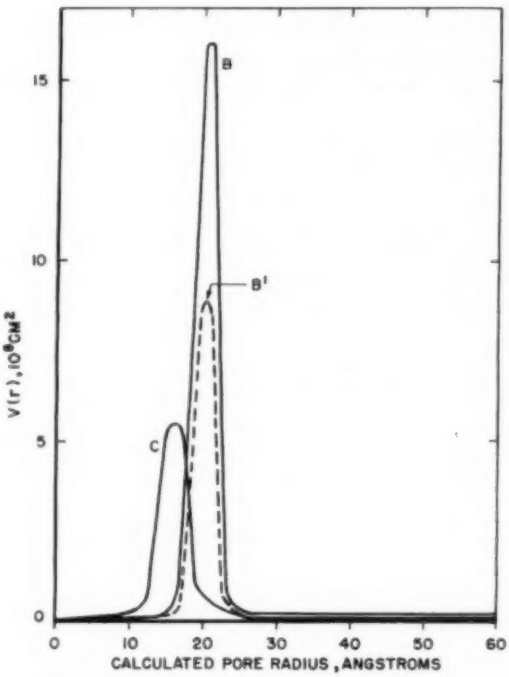

FIGURE 3. *Pore size distribution curves.*

B, Alkali swelled, solvent exchanged cotton linters (determination 4); B′, B conditioned at 20- to 25-percent relative humidity (determination 5); C, water swelled, solvent exchanged cotton linters (determination 2).

$L(r)\,dr$ is proportional to the total length of pores whose radii fall between r and $r+dr$;

R is the Kelvin radius corrected for multilayer adsorption and is given by the expression:

$$R = t - \frac{2\sigma v}{R_g T \ln p/p_0}, \qquad (2)$$

in which:

σ is the surface energy of the adsorbate at the temperature of adsorption, T;

v is the molar volume of the adsorbate in the liquid state;

R_g is the gas constant in ergs/mole/degree;

p/p_0 is the relative pressure.

Equation 1 is integrated by assuming $L(r)$ is either a Maxwellian distribution,

$$L(r) = A_0 r_0 e^{-r/r_0}, \qquad (3a)$$

or a Gaussian distribution,

$$L(r) = A_1 e^{-\frac{B_1}{r_1}(r-r_1)^2}, \qquad (3b)$$

or the sum of a Maxwellian and a Gaussian distribution,

$$L(r) = A_0 r_0 e^{-r/r_0} + A_1 e^{-\frac{B_1}{r_1}(r-r_1)^2}. \qquad (3c)$$

A_0 and A_1 are constants, and r_0, r_1, and B_1 are parameters.

By way of illustration, when the equation for a Maxwellian distribution [13a] is substituted in eq 1 and the integration carried out, the expression

$$V_s - V = A_0 r_0^4 M(R, r_0), \qquad (4)$$

is obtained, where $M(R, r_0)$ is a function of R, r_0, and contains t, the multilayer thickness. Shull has calculated this function for a number of values of R and r_0 and prepared a family of standard inverted isotherms by plotting $M(R, r_0)$ on the logarithmic scale of semilog paper against R. Experimental $V_s - V$ values are similarly plotted on a logarithmic scale against R, and the curve matched with the standard isotherms to find one giving the closest fit. This gives the parameters of the standard distribution most closely approximating the experimental distribution, and the constant A_0 may be obtained by substituting values of r_0, $M(R, r_0)$, and $V_s - V$ in eq 4. The procedure is similar for a Gaussian distribution, and entails a few more steps for the sum of a Maxwellian and a Gaussian distribution, but involves curve matching in each case. The total volume of gas sorbed in pores with radii between r and $r+dr$ is $V(r)dr$, and this volume distribution function is given by

$$V(r) = \pi r^2 L(r).$$

Certain assumptions have been made in applying this method. First is the basic assumption of the method itself that the sorption process takes place in circular pores whose radii may be calculated from the Kelvin equation, corrected for multilayer adsorption. It has also been assumed that Vs, the volume of nitrogen required to condense and exactly fill the pores may be obtained by extrapolating the isotherm to saturation pressure, and it has been assumed that the adsorbent undergoes no important dimensional changes during sorption.

Sample B (fig. 3, curve B) is shown as having most of the nitrogen sorbed within a rather narrow distribution of pore radii with a maximum volume at a pore radius of 20A. When the sample was conditioned at 20- to 25-percent relative humidity (fig. 3, curve B′), the position of the maximum remained about the same. The mechanism by which addition of water to expanded cotton reduced subsequent capacity for nitrogen is not clear at present. It is difficult to visualize a uniform multilayer process by which water could be deposited in pores without decreasing pore radius. If it is assumed that a certain fraction of the entire pore length in the sample was completely destroyed by water while the remainder was left intact, pore volume could be decreased without changing pore radius. The volume of water added was nearly large enough to account for the decreased pore volume if it merely took up space and exerted no specific action in the collapse of the structure. Eleven percent of water was more than enough to account for the pore volume of the original sample on this basis, which suggests additional swelling of the expanded cotton took place upon conditioning at 70- to 75-percent relative humidity.

When the desorption measurements on solvent exchanged cotton (fig. 3, curve C′) were analyzed by the Wheeler-Shull method, a slightly broader distribution of pore radii with a maximum at 16A was obtained.

No curves are shown for the control sample or the cotton conditioned at 70- to 75- percent relative humidity. This is because of the difficulty in estimating Vs for a type II curve. For a true multilayer adsorption process on a plane surface, Vs should approach infinity, and a pore volume calculation would have no physical significance.

VI. Summary

A sample of cotton linters swollen with strong alkali and given a solvent exchange treatment was found to have a large surface area available to nitrogen. This confirms the observation of Assaf, Haas, and Purves. The shape of the adsorption and desorption isotherms were found to be more like type IV than type II, and they showed strong hysteresis. Pore size distributions, calculated by the method of Wheeler and Shull, showed most of the nitrogen absorbed in pores having radii of about 20 A.

Addition of about 3.3-percent moisture to the expanded cotton reduced the surface area greatly without noticeably changing the type of isotherm or pore radius. Addition of about 11.0-percent moisture destroyed nearly all of the internal

surface, and the isotherm more closely resembled that of untreated cotton, but a slight hysteresis remained.

Cotton swollen with water only and given solvent exchange also had a much larger surface than untreated cotton. The isotherm was more nearly type IV, and most of the nitrogen was adsorbed in pores having calculated radii of about 16 A.

VII. References

[1] A. Frey-Wyssling, Protoplasma **27,** 372 (1937).
[2] A. Frey-Wyssling, Protoplasma **27,** 563 (1937).
[3] O. Kratky and F. Schossberger, Z. Physik. Chem. B**39,** 145 (1938).
[4] Cellulose and cellulose derivatives, ed. Emil Ott (Interscience Publishers, Inc., New York, N. Y., 1943) a, Charles W. Hock and H. Mark, pp. 346 to 351; b, E. I. Valko, pp. 415 to 419.
[5] G. E. Collins, J. Textile Inst. **21,** T311 (1930).
[6] G. E. Collins, J. Textile Inst. **30,** P46 (1939).
[7] T. M. Shaw, J. Chem. Phys. **12,** 391 (1944).
[8] K. J. Palmer, T. M. Shaw, and M. Ballantyne, J. Polymer Sci. **2,** 318 (1947).
[9] A. G. Assaf, R. H. Haas, and C. B. Purves, J. Am. Chem. Soc. **66,** 59 (1944).
[10] A. G. Assaf, R. H. Haas, and C. B. Purves, J. Am. Chem. Soc. **66,** 66 (1944).
[11] C. G. Shull, J. Am. Chem. Soc. **70,** 1405 (1948).
[12] C. G. Shull, P. B. Elkin, and L. C. Roess, J. Am. Chem. Soc. **70,** 1410 (1948).
[13] Stephen Brunauer, The adsorption of gases and vapors (Princeton Univ. Press, 1945). a, p. 150; b, p. 155; c, Chapter XI.
[14] P. H. Emmett, A new method for measuring the surface areas of finely divided materials and for determining the size of particles. Symposium on New Methods for Particle Size Determination in the Subsieve Range ASTM 1941, p. 95 to 105.
[15] S. Brunauer, P. H. Emmett, and E. Teller, J. Am. Chem. Soc. **60,** 309 (1938).
[16] J. W. Rowen and R. L. Blaine, Ind. Eng. Chem. **39,** 1659 (1947).
[17] R. Howell and A. Jackson, J. Chem. Soc. p. 979 to 982 (1937).
[18] S. S. Kistler, J. Phys. Chem. **36,** 52 (1932).
[19] Terrel L. Hill, J. Chem. Phys. **15,** 767 (1947).
[20] A. Frey-Wyssling, Kolloid Z. **85,** 148 (1938).
[21] A. Wheeler, Presentation at Catalysis Symposia, Gibson Island, AAAS Conferences (June 1945 and June 1946).

Washington, July 14, 1949.

U. S. Department of Commerce
National Bureau of Standards

Research Paper RP2049
Volume 43, December 1949

Part of the Journal of Research of the National Bureau of Standards

Vapor Pressures and Boiling Points of Sixty API-NBS Hydrocarbons[1]

By Alphonse F. Forziati,[2] William R. Norris, and Frederick D. Rossini

Measurements of vapor pressures and boiling points, over the range 48 to 780 millimeters of mercury, and above about 11° C, were made on 60 purified hydrocarbons. The apparatus consisted of an electrically heated boiler, a vapor space with a vertical reentrant tube containing a platinum thermometer having a resistance of 25 ohms, and a condenser. Measurements of the temperature of the liquid-vapor equilibrium were made at 20 fixed pressures maintained automatically. The values of the fixed pressures were determined by calibration of the apparatus with water using the vapor pressure-temperature tables prepared at this Bureau.

The experimental data on the hydrocarbons were correlated, the method of least squares being used, with the three-constant Antoine equation for vapor pressures, $\log P = A - B/(C+t)$ or $t = B/(A - \log P) - C$. Experimental data, together with the values of the three constants of the Antoine equation applicable over the range of measurement, are reported for 60 API–NBS hydrocarbons, including 17 paraffins, 14 alkylcyclopentanes, 8 alkylcyclohexanes, and 21 alkylbenzenes.

I. Introduction

This investigation is part of the systematic program of determining physical properties of highly purified hydrocarbons being prepared in the cooperative program of the American Petroleum Institute and the National Bureau of Standards. Measurements of vapor pressures and boiling points were made over the range 48 to 780 mm Hg, and above about 11° C, on 60 hydrocarbons of the API-NBS series. This paper gives the experimental data, and results of the correlation with the Antoine equation, for 17 paraffin, 14 alkylcyclopentane, 8 alkylcyclohexane, and 21 alkylbenzene hydrocarbons.

II. Apparatus and Procedure

The apparatus and procedure employed in this investigation were essentially similar to those already described [1].[3] The modifications consisted of increasing the thermometric sensitivity from 1.4 to 3.3 mm of scale deflection per 0.001° C; installing a new condenser and reflux regulator patterned after one previously described [2]; blending the heat of a reentrant 50-watt heater with that of the external heater, wrapped around the boiler, to minimize bumping at low pressures; and connecting a high-pressure nitrogen cylinder, with suitable reducing values and drying train, to the inlet of the ballast tank. The nitrogen cylinder obviated the use of a pressure pump for measurements above 1 atmosphere and permitted boiling without contact with oxygen.

III. Determination of Pressures

The values of the pressures produced by the apparatus, when controlled at the 20 fixed contacts, were determined from periodic measurements of the temperature of the liquid-vapor equilibrium made with water in the apparatus. The changes in these values were substantially the same as those previously reported [1]. The vapor pressure of water at 1-deg. intervals from 35° to 103° C was taken from table 2 of Osborne and Meyers [3], together with unpublished small revisions of

[1] This investigation was performed at the National Bureau of Standards as part of the work of the American Petroleum Institute Research Project 6 on the "Analysis, Purification, and Properties of Hydrocarbons."

[2] Research Associate on the American Petroleum Institute Research Project 6 at the National Bureau of Standards.

[3] Figures in brackets indicate the literature references at the end of this paper.

these values by Meyers, Stimson, and Cragoe [4]. From these values, several values were interpolated (by Lagrangian five point curvilinear interpolation) at 0.1-deg. intervals in the neighborhood of the temperature of the liquid-vapor equilibrium for water at each of the 20 fixed pressures. The final calculation of the pressure at each observed temperature was made by linear interpolation within the 0.1-deg. intervals.

IV. Source and Purity of Compounds

The compounds whose vapor pressures were measured in the present investigation were samples from the API–NBS series of highly purified hydrocarbons, which are being prepared through a cooperative undertaking of the American Petroleum Institute and the National Bureau of Standards. The description of the compounds is given in a preceding report [5], with the purification and determination of purity and freezing points of these compounds described in references [6, 7, 8, 9, 10]. It is believed that in each case the impurity was of such nature and present in such small amounts that the properties measured were not affected beyond the indicated limits of uncertainty.

V. Experimental Data on 60 API-NBS Hydrocarbons

In table 1 are given the experimental data on the temperatures and pressures of the liquid-vapor equilibrium for 17 paraffin, 14 alkylcyclopentane, 8 alkylcyclohexane, and 21 alkylbenzene hydrocarbons.

TABLE 1. *Experimental data for 60 hydrocarbons on the temperatures and pressures of the liquid-vapor equilibrium*

t	P	t	P	t	P	t	P	t	P
n-Heptane		2-Methylhexane		3-Methylhexane		3-Ethylpentane		2,2-Dimethylpentane	
°C	*mm* Hg	°C	*mm* Hg	°C	*mm* Hg	°C	*mm* Hg	°C	*mm* Hg
99.322	780.20	90.936	780.13	92.737	780.13	94.367	780.12	.....	.....
98.813	768.63	90.430	768.58	92.229	768.58	93.856	768.58	80.074	780.13
98.237	755.75	89.860	755.62	91.655	755.61	93.277	755.61	79.573	768.58
97.728	744.49	89.357	744.40	91.148	744.40	92.771	744.39	79.005	755.61
97.180	732.53	88.814	732.46	90.602	732.46	92.238	732.46	78.508	744.39
92.078	628.32	83.769	628.24	85.529	628.24	87.119	628.23	77.970	732.46
84.856	501.15	76.628	501.07	78.347	501.07	.....	.....	72.908	628.23
78.202	402.93	70.051	402.84	71.732	402.84	73.242	402.84	65.895	501.07
71.966	325.42	63.889	325.31	65.533	325.41	.....	.....	59.384	402.84
65.916	262.13	57.913	262.04	59.509	262.04	60.962	262.03	53.287	325.30
60.902	217.54	52.960	217.44	54.535	217.43	55.954	217.43	47.378	262.03
55.442	176.26	47.579	176.15	49.119	176.15	50.511	176.15	42.477	217.43
51.373	149.76	43.549	149.67	45.068	149.66	46.423	149.66	37.162	176.14
46.987	124.95	39.219	124.84	40.713	124.84	42.045	124.84	33.186	149.66
42.680	104.00	34.956	103.90	36.428	103.89	37.734	103.89	28.915	124.83
38.901	88.06	31.235	87.97	32.684	87.97	33.971	87.97	24.708	103.89
36.105	77.65	28.459	77.55	29.911	77.55	31.179	77.55	21.032	87.97
33.108	67.60	25.518	67.51	26.932	67.50	28.182	67.50	18.312	77.54
29.813	57.88	22.269	57.77	23.662	57.77	24.930	57.76	15.395	67.50
26.039	48.19	18.528	48.08	19.915	48.08	21.126	48.07	12.188	57.76
2,3-Dimethylpentane		2,4-Dimethylpentane		3,3-Dimethylpentane		2,2,3-Trimethylbutane		*n*-Nonane	
90.678	780.12	81.374	780.12	86.962	780.12	81.772	780.07	151.786	780.13
90.167	768.58	80.874	768.58	86.447	768.57	81.262	768.54	151.222	768.57
89.588	755.60	80.308	755.60	85.866	755.60	80.682	755.50	150.579	755.57
89.080	744.39	79.813	744.39	85.355	744.38	80.174	744.32	150.017	744.37
88.531	732.46	79.277	732.46	84.803	732.45	79.627	732.41	149.409	732.45
83.429	628.23	74.297	628.23	79.672	628.23	74.523	628.17	143.751	628.22
76.209	501.07	67.251	501.07	72.411	501.06	67.308	501.01	135.741	501.05
69.562	402.83	60.764	402.83	65.727	402.83	60.668	402.77	128.357	402.81
63.333	325.30	54.688	325.30	59.466	325.30	54.445	325.22	121.433	325.27
57.295	262.03	48.801	262.03	53.396	262.02	48.422	261.95	114.712	262.00
52.290	217.42	43.919	217.42	48.365	217.42	43.424	217.34	109.136	217.40

TABLE 1. *Experimental data for 60 hydrocarbons on the temperatures and pressures of the liquid-vapor equilibrium*—Con.

t	*P*	*t*	*P*	*t*	*P*	*t*	*P*	*t*	*P*
2,3-Dimethylpentane		2,4-Dimethylpentane		3,3-Dimethylpentane		2,3,3-Trimethylbutane		*n*-Nonane	
°C	*mm* Hg	°C	*mm* Hg	°C	*mm* Hg	°C	*mm* Hg	°C	*mm* Hg
46.849	176.14	38.623	176.14	42.904	176.14	38.012	176.06	103.072	176.11
42.786	149.65	34.661	149.65	38.824	149.65	33.960	149.58	98.545	149.63
38.407	124.83	30.399	124.83	34.432	124.83	29.599	124.75	93.661	124.80
34.100	103.88	26.213	103.88	30.109	103.88	25.313	103.81	88.864	103.86
30.342	87.96	22.540	87.96	.....	.....	21.571	87.90	84.658	87.94
27.563	77.54	19.823	77.54	23.545	77.54	18.804	77.47	81.548	77.52
24.575	67.49	16.911	67.49	20.547	67.49	15.833	67.43	78.219	67.47
21.293	57.76	13.714	57.76	17.252	57.75	12.555	57.68	74.546	57.73
17.523	48.07	.....	.....	13.484	48.06	.....	.....	70.343	48.04
2,2,5-Trimethylhexane		2,4,4-Trimethylhexane		3,3-Diethylpentane		2,2,3,3-Tetramethylpentane		2,2,3,4-Tetramethylpentane	
125.050	780.12	131.636	780.11	147.194	780.10	141.295	780.16	134.021	780.14
124.497	768.58	131.070	768.57	146.606	768.57	140.713	768.61	133.446	768.60
123.868	755.57	130.429	755.57	145.942	755.56	140.051	755.65	132.798	755.62
123.321	744.37	129.869	744.37	145.356	744.36	139.471	744.43	132.227	744.41
122.731	732.45	129.260	732.45	144.725	732.44	138.844	732.49	131.611	732.48
117.225	628.22	.....	.....	138.802	628.21	133.015	628.26	125.886	628.25
109.434	501.05	115.621	501.05	130.558	501.04	124.767	501.10	117.787	501.08
102.256	402.81	108.264	402.81	122.903	402.80	117.168	402.86	110.331	402.85
95.539	325.27	101.368	325.27	115.727	325.26	110.054	325.33	103.343	325.31
.....	.....	.....	.....	.....	.....	103.154	262.06	96.574	262.04
85.624	217.39	89.149	217.39	103.002	217.38	97.450	217.46	90.965	217.43
77.756	176.11	83.123	176.10	96.737	176.10	91.242	176.17	84.871	176.15
73.381	149.62	78.631	149.62	92.048	149.62	86.602	149.68	80.311	149.66
68.655	124.80	73.786	124.79	87.000	124.79	81.609	124.86	75.418	124.84
.....	.....	69.023	103.85	82.043	103.84	76.705	103.91	70.587	103.89
59.973	87.94	64.862	87.93	77.699	87.93	72.414	87.99	66.381	87.97
56.988	77.51	61.776	77.51	74.484	77.50	69.236	77.57	63.202	77.55
53.743	67.46	58.467	67.46	71.026	67.46	65.828	67.52	59.913	67.50
50.208	57.72	54.826	57.72	67.240	57.71	62.087	57.79	56.243	57.76
46.141	48.03	50.648	48.02	62.882	48.02	57.834	48.10	52.028	48.07
2,2,4,4-Tetramethylpentane		2,3,3,4-Tetramethylpentane		Ethylcyclopentane		1,1-Dimethylcyclopentane		cis-1,2-Dimethylcyclopentane	
123.267	780.16	142.571	780.10	104.382	780.00	88.736	779.99	100.446	780.00
122.709	768.61	141.987	768.57	103.855	768.50	88.227	768.49	99.922	768.49
122.072	755.65	141.326	755.56	103.264	755.60	87.647	755.59	99.329	755.60
121.510	744.43	140.746	744.36	102.739	744.39	87.137	744.40	98.806	744.40
120.906	732.49	140.120	732.44	102.173	732.40	86.585	732.40	98.244	732.40
115.289	628.27	134.294	628.20	96.910	628.21	81.470	628.20	93.005	628.21
107.342	501.10	126.053	501.04	89.453	500.98	74.228	500.99	85.589	500.99
100.031	402.86	118.461	402.80	82.588	402.71	67.558	402.72	78.755	402.71
93.183	325.33	111.345	325.26	76.143	325.17	61.312	325.17	72.358	325.17
86.549	262.06	.....	.....	69.909	261.88	.....	.....	66.155	261.88
81.052	217.45	98.732	217.38	64.739	217.36	50.257	217.36	61.012	217.36
75.085	176.17	.....	.....	59.114	176.08	44.815	176.08	55.426	176.08
70.625	149.68	87.881	149.61	54.908	149.60	40.744	149.60	51.253	149.60
65.828	124.86	82.872	124.78	50.386	124.81	36.361	124.81	46.770	124.81
61.117	103.91	77.960	103.84	45.935	103.80	32.030	103.81	42.346	103.80
56.991	87.99	73.670	87.93	42.040	87.93	28.300	87.92	38.482	87.93
53.944	77.56	70.491	77.50	39.165	77.46	25.476	77.47	35.616	77.46
50.671	67.52	67.037	67.45	36.058	67.42	22.527	67.43	32.555	67.42
47.079	57.78	63.320	57.71	32.673	57.72	19.202	57.72	29.195	57.72
42.956	48.09	59.010	48.02	28.778	48.11	15.498	48.12	25.347	48.11

TABLE 1. *Experimental data for 60 hydrocarbons on the temperatures and pressures of the liquid-vapor equilibrium*—Con.

t	*P*	*t*	*P*	*t*	*P*	*t*	*P*	*t*	*P*
trans-1,2-Dimethylcyclopentane		*cis*-1,3-Dimetyhlcyclopentane		*trans*-1,3-Dimethylcyclopentane		*n*-Propylcyclopentane		Isopropylcyclopentane	
°*C*	*mm* Hg	°*C*	*mm* Hg	°*C*	*mm* Hg	°*C*	*mm* Hg	°*C*	*mm* Hg
92.769	780.01	92.628	780.50	91.670	780.01	131.917	780.08	127.394	780.08
92.255	768.90	92.115	768.63	91.156	768.50	131.379	768.55	126.836	768.55
91.673	755.61	91.533	755.74	90.575	755.61	130.731	755.53	126.201	755.53
91.100	744.40	91.018	744.49	90.082	744.40	130.176	744.34	125.643	744.34
90.608	732.40	90.465	732.53			129.579	732.42	125.044	732.42
85.493	628.22	85.315	628.32	84.368	628.22	124.015	628.19	119.450	628.19
78.181	500.99	78.030	501.15	77.092	500.99	116.132	501.03	111.532	501.03
71.496	402.71	71.323	402.93	70.388	402.71	108.877	402.79	104.235	402.79
65.178	325.17	65.039	325.41	64.105	325.18	102.068	325.25	97.396	325.25
59.094	261.88	58.949	262.13	58.029	261.88			90.769	261.98
54.047	217.36	53.902	217.54	52.985	217.36	89.990	217.37	85.265	217.37
48.564	176.08	48.422	176.26	47.510	176.08	84.039	176.09	79.275	176.08
44.460	149.60	44.323	149.76	43.417	149.60	79.591	149.61	74.827	149.60
40.055	124.81	39.912	124.95	39.010	124.81	74.794	124.78	70.012	124.77
35.719	103.80	35.582	104.00	34.685	103.80	70.088	103.83	65.296	103.83
31.934	87.93	31.784	88.06	30.906	87.93	65.966	87.92	61.122	87.92
29.113	77.46	28.970	77.64	28.089	77.46	62.911	77.49	58.088	77.49
26.113	67.42	25.977	67.60	25.081	67.42	59.628	67.45	54.798	67.45
				21.782	57.72	56.030	57.70	51.183	57.70
				18.005	48.11	51.875	48.01	47.033	48.01
1-Methyl-1-ethylcyclopentane		1-Methyl-*cis*-2-ethylcyclopentane		1,1,2-Trimethylcyclopentane		1,1,3-Trimethylcyclopentane		*cis*, *cis*, *trans*-1,2,4-Trimethylcyclopentane	
122.484	780.04	129.021	780.09	114.686	780.04	105.830	780.03	117.680	780.00
121.933	768.52	128.463	768.55	114.138	768.52	105.292	768.52	117.140	768.49
121.307	755.64	127.832	755.54	113.517	755.64	104.688	755.63	116.518	755.60
120.752	744.41	127.281	744.34	112.971	744.42	104.148	744.42	115.969	744.40
120.159	732.41	126.684	732.43	112.381	732.42	103.572	732.42	115.378	732.41
114.622	628.24	121.105	628.19	106.900	628.24	98.197	628.23	109.887	628.21
106.833	501.00	113.205	501.03	99.144	501.00	90.594	501.00	102.109	500.99
99.559	402.71	105.929	402.79	91.992	402.71	83.585	402.71	94.942	402.72
92.783	325.18	99.105	325.25	85.302	325.18	77.023	325.18	88.224	325.17
86.232	261.87	92.490	261.98			70.674	261.88	81.725	261.89
80.796	217.37	87.011	217.38	73.455	217.37	65.411	217.37	76.327	217.36
74.898	176.09	81.070	176.09	67.615	176.09			70.477	176.08
70.476	149.61	76.582	149.61	63.251	149.61	55.423	149.61	66.100	149.60
65.724	124.81	71.702	124.78	58.502	124.82	50.828	124.82	61.380	124.82
61.049	103.80	67.070	103.84	53.962	103.81	46.308	103.81	56.756	103.81
56.967	87.94	62.935	87.93	49.920	87.94	42.361	87.94	52.704	87.93
53.937	77.46	59.862	77.50	46.937	77.46	39.432	77.46	49.701	77.47
50.691	67.41	56.539	67.45	43.728	67.41	36.299	67.41	46.426	67.43
47.137	57.71	52.975	57.71	40.224	57.72	32.881	57.72	42.972	57.72
43.056	48.10	48.846	48.02	36.207	48.10	28.944	48.11	38.907	48.12
cis, *trans*, *cis*-1,2,4-Trimethylcyclopentane		1,1-Dimethylcyclohexane		*n*-Propylcyclohexane		Isopropylcyclohexane		1,1,3-Trimethylcyclohexane	
110.229	780.01	120.520	780.05	157.756	780.09	155.602	780.14	137.636	780.05
109.680	768.50	119.959	768.52	157.166	768.55	155.009	768.59	137.058	768.55
109.082	755.60	119.327	755.65	156.494	755.53	154.334	755.63	136.401	755.52
108.541	744.41	118.768	744.42	155.904	744.34	153.747	744.41	135.824	744.34
107.962	732.41	118.168	732.42	155.269	732.42	153.109	732.47	135.203	732.42
102.571	628.22	112.575	628.24	149.347	628.19	147.177	628.25	129.411	628.18
94.940	500.99	104.658	501.00	140.965	501.03	138.782	501.08	121.220	501.02
87.906	402.72	97.361	402.70	133.245	402.79	131.051	402.85	113.678	402.78
81.310	325.18	90.497	325.18	126.004	325.24	123.806	325.32	106.606	325.23
74.929	261.89	83.925	261.87	118.982	261.97	116.782	262.04	99.762	261.96
69.641	217.36	78.447	217.37	113.165	217.37	110.953	217.44	94.080	217.35
63.892	176.08	72.496	176.09	106.842	176.08	104.612	176.16	87.915	176.07
59.599	149.60	68.047	149.61	102.111	149.60	99.887	149.67	82.305	149.59

TABLE 1. *Experimental data for 60 hydrocarbons on the temperatures and pressures of the liquid-vapor equilibrium*—Con.

t	P	t	P	t	P	t	P	t	P
cis, trans, cis-1,2,4-Trimethylcyclopentane		1,1-Dimethylcyclohexane		*n*-Propylcyclohexane		Isopropylcyclohexane		1,1,3-Trimethylcyclohexane	
°C	*mm* Hg	°C	*mm* Hg	°C	*mm* Hg	°C	*mm* Hg	°C	*mm* Hg
54.976	124.82	63.260	124.81	97.017	124.77	94.713	124.85	78.336	124.76
50.433	103.81	58.564	103.80	92.026	103.83	89.788	103.90	73.481	103.82
46.454	87.93	54.450	87.94	87.641	87.92	85.400	87.98	69.180	87.91
43.487	77.47	51.389	77.46	84.375	77.49	82.165	77.56	66.058	77.48
40.338	67.43	48.173	67.40	80.871	67.44	78.690	67.51	62.624	67.43
36.878	57.72	44.531	57.71	77.085	57.70	74.868	57.78	58.950	57.68
32.948	48.11	40.497	48.10	72.691	48.01	70.515	48.09	54.669	47.99
n-Butylcyclohexane		Isobutylcyclohexane		*sec*-Butylcyclohexane		*tert*-Butylcyclohexane		Benzene	
182.024	780.09	172.394	780.16	180.421	780.15	172.670	780.10	80.948	780.04
181.406	768.56	171.780	768.60	179.709	768.60	172.054	768.56	80.461	768.51
180.706	755.53	171.089	755.65	179.098	755.64	171.351	755.54	79.909	755.48
180.093	744.34	170.480	744.43	178.481	744.42	170.735	744.35	79.424	741.29
179.433	732.43	169.822	732.49	177.817	732.48	170.071	732.43	78.903	732.38
173.272	628.19	163.711	628.26	171.626	628.16	163.894	628.20	74.035	628.15
164.544	501.03	155.065	501.09	162.856	501.09	155.147	501.03	67.148	501.00
156.504	402.79	147.103	402.86	154.776	402.86	147.093	402.79	60.803	402.76
145.963	325.24	139.640	325.33	147.212	325.32	139.542	325.25	54.852	325.21
141.651	261.97	132.404	262.05	139.861	262.05	132.228	261.98	49.084	261.95
135.579	217.36	126.405	217.45	133.786	217.45	126.159	217.37	44.294	217.34
128.988	176.08	119.887	176.17	127.163	176.16	119.573	176.08	39.095	176.06
124.056	149.60	115.008	149.68	122.224	149.67	114.649	149.60	35.207	149.58
118.743	124.77	109.766	124.86	116.900	124.85	109.341	124.77	31.013	124.75
113.535	103.82	140.610	103.91	111.660	103.90	104.146	103.83	26.908	103.81
108.963	87.91	100.094	87.98	107.082	87.98	99.582	87.92	23.271	87.90
105.579	77.48	96.767	77.56	103.688	77.56	96.200	77.49	20.628	77.47
101.946	67.14	93.184	67.51	100.048	67.51	92.550	67.44	17.697	67.42
97.950	57.69	89.248	57.78	96.042	57.76	88.600	57.70	14.575	57.68
93.369	48.00	84.752	48.09	91.458	48.09	84.033	48.00	10.983	47.98
Methylbenzene		Ethylbenzene		1,2-Dimethylbenzene		1,3-Dimethylbenzene		1,4-Dimethylbenzene	
111.545	780.05	137.160	780.06	145.400	780.07	140.078	780.07	139.329	780.06
111.018	768.52	136.602	768.53	144.832	678.54	139.520	768.54	138.768	768.53
110.420	755.49	135.969	755.50	144.190	655.52	138.887	755.51	138.132	755.51
109.894	744.30	135.413	744.32	143.626	744.33	138.329	744.32	137.574	744.32
109.328	732.39	134.815	732.40	143.019	732.41	137.731	732.41	.....	.....
104.052	628.16	129.234	628.17	137.356	628.18	132.144	628.17	131.371	628.17
96.580	501.00	121.331	501.01	129.333	501.02	124.226	501.01	123.431	501.01
89.695	402.76	114.046	402.77	121.935	402.78	116.923	402.78	.....	.....
83.230	325.22	107.210	325.23	114.988	325.24	110.067	325.23	109.240	325.22
76.965	261.95	100.576	261.96	108.250	261.97	103.412	261.96	102.573	261.96
71.758	217.34	95.074	217.35	102.657	217.36	97.887	217.36	97.032	217.35
66.107	176.06	89.080	176.07	96.568	176.08	91.874	176.07	91.017	176.07
61.869	149.58	84.619	149.59	92.015	149.60	87.387	149.60	86.506	149.59
57.315	124.75	79.791	124.76	87.101	124.77	81.527	124.76	81.658	124.76
52.848	103.81	75.054	103.81	82.285	103.83	77.778	103.82	76.865	103.82
48.894	87.90	70.891	87.91	78.048	87.92	73.601	87.91	72.684	87.91
45.997	77.47	67.827	77.48	74.916	77.49	70.506	77.48	69.605	77.48
.....	.....	64.510	67.43	71.548	67.44	67.157	67.44	66.280	67.43
39.437	57.68	60.887	57.68	67.852	57.70	63.518	57.69	62.619	57.68
35.504	47.99	56.989	47.99	63.608	48.01	59.335	48.00	58.419	47.99
n-Propylbenzene		Isopropylbenzene		1-Methyl-2-ethylbenzene		1-Methyl-3-ethylbenzene		1-Methyl-4-ethylbenzene	
160.239	780.09	153.40	780.09	166.174	779.94	162.316	779.94	163.008	779.95
159.654	768.55	152.82	768.55	165.591	768.46	161.735	768.46	162.424	768.46
158.991	755.54	152.17	755.54	164.925	755.53	161.080	755.54	161.761	755.55
158.408	744.35	151.59	744.34	164.337	744.38	160.498	744.38	161.179	744.39
157.779	732.43	150.97	732.43	163.706	732.39	159.871	732.39	160.548	732.39

TABLE 1. *Experimental data for 60 hydrocarbons on the temperatures and pressures of the liquid-vapor equilibrium*—Con.

t	*P*	*t*	*P*	*t*	*P*	*t*	*P*	*t*	*P*
n-Propylbenzene		Isopropylbenzene		1-Methyl-2-ethylbenzene		1-Methyl-3-ethylbenzene		1-Methyl-4-ethylbenzene	
°*C*	*mm* Hg	°*C*	*mm* Hg	°*C*	*mm* Hg	°*C*	*mm* Hg	°*C*	*mm* Hg
151.921	628.20	145.19	628.19	157.825	628.17	154.053	628.17	154.684	628.18
143.625	501.03	137.01	501.03	149.482	500.98	145.795	500.98	146.368	500.98
135.972	402.80	129.46	402.79	141.792	402.73	138.178	402.73	138.701	402.73
128.794	325.26	122.38	325.25	134.570	325.16	131.027	325.16	131.499	325.16
.....	.....	115.52	261.98	127.574	261.92	124.082	261.92	.....	.....
116.060	217.38	109.82	217.37	121.762	217.35	118.338	217.35	118.727	217.35
109.781	176.09	103.64	176.09	115.436	176.06	112.074	176.06	112.422	176.07
105.085	149.61	99.00	149.61	110.711	149.59	107.383	149.59	107.710	149.59
100.020	124.78	94.01	124.78	105.598	124.82	102.326	124.82	102.619	124.82
95.049	103.84	89.11	103.83	100.584	103.81	97.368	103.81	97.630	103.81
90.688	87.93	84.82	87.92	96.200	87.91	93.022	87.91	93.252	87.91
87.457	77.50	81.64	77.49	92.949	77.43	89.793	77.47	89.998	77.47
83.983	67.45	78.23	67.45	89.448	67.45	86.283	67.45	86.523	67.45
80.181	57.71	74.47	57.70	85.618	57.73	82.525	57.73	82.701	57.43
75.818	48.02	70.16	48.01	81.146	48.13	78.105	48.13	78.306	48.13
1,2,3-Trimethylbenzene		1,2,4-Trimethylbenzene		1,3,5-Trimethylbenzene		*n*-Butylbenzene		Isobutylbenzene	
177.126	779.95	170.377	779.96	165.725	779.97	184.329	779.98	173.814	779.99
176.527	768.46	169.788	768.47	165.146	768.47	183.725	768.48	173.209	768.49
175.852	755.55	169.121	755.55	164.489	755.56	183.036	755.57	172.526	755.59
175.252	744.34	168.534	744.39	163.911	744.39	182.429	744.40	171.920	744.41
174.606	732.39	167.896	732.39	163.289	732.39	181.767	732.40	171.270	732.41
168.614	628.18	161.991	628.18	157.477	628.19	175.666	628.20	165.217	628.21
160.106	500.98	153.603	500.98	149.228	500.98	167.011	500.99	156.632	500.99
152.290	402.72	145.867	402.72	141.618	402.72	159.032	402.73	148.724	402.73
144.882	325.16	138.599	325.16	134.464	325.17	151.541	325.17	141.301	325.17
137.737	261.91	131.556	261.91	.....	.....	.....	.....	134.112	261.91
131.800	217.35	125.694	217.35	121.765	217.36	138.300	217.36	128.149	217.36
125.333	176.07	119.328	176.07	115.489	176.07	.....	.....	121.659	176.07
120.504	149.59	114.572	149.59	110.789	149.59	129.797	149.60	116.808	149.60
115.287	124.81	109.418	124.81	105.716	124.82	124.506	124.82	111.582	124.82
110.157	103.81	104.369	103.81	100.747	103.81	119.322	103.81	106.450	103.81
105.663	87.91	99.940	87.91	96.386	87.92	114.762	87.92	101.946	87.92
102.336	77.47	96.670	77.47	93.131	77.47	111.403	77.47	98.620	77.47
98.770	67.45	93.155	67.44	89.662	67.44	107.778	67.44	95.026	67.44
94.826	57.73	89.259	57.73	85.857	57.73	103.814	57.73	91.118	57.73
90.332	48.13	84.804	48.13	81.488	48.12	99.233	48.12	86.637	48.12
sec-Butylbenzene		*tert*-Butylbenzene		1,2-Diethylbenzene		1,3-Diethylbenzene		1,4-Diethylbenzene	
174.358	779.99	170.165	780.00	184.493	780.21	182.162	780.20	184.821	780.20
173.754	768.49	169.565	768.50	183.885	768.64	181.558	768.64	184.212	768.63
173.068	755.59	168.886	755.59	183.197	755.75	180.877	755.74	183.524	755.73
172.468	744.40	168.287	744.41	182.580	744.50	180.275	744.49	182.916	744.49
171.820	732.41	167.646	732.41	181.936	732.54	179.628	732.53	182.260	732.53
165.768	628.21	161.649	628.21	175.853	628.32	173.595	628.31	176.164	628.31
157.194	500.99	153.149	500.99	167.235	501.16	165.050	501.15	167.530	501.14
149.288	402.73	145.315	402.72	159.200	402.93	157.169	402.92	159.566	402.92
141.867	325.17	137.908	325.18	151.832	325.42	149.777	325.41	152.086	325.40
134.683	261.90	.....	.....	144.566	262.13	142.597	262.12	144.823	262.12
128.715	217.36	124.936	217.36	138.560	217.54	136.638	217.53	138.811	217.53
122.232	176.08	118.524	176.08	132.059	176.26	130.157	176.25	132.256	176.24
117.387	149.60	113.720	149.60	127.171	149.76	125.393	149.75	127.360	149.75
112.151	124.82	108.546	124.82	121.906	124.95	120.082	124.94	122.043	124.94
107.089	103.81	103.471	103.81	116.728	104.00	114.946	103.98	116.893	103.98
102.523	87.92	99.017	87.92	112.191	88.05	110.436	88.04	112.339	88.04
99.179	77.47	95.715	77.50	108.822	77.64	107.096	77.63	108.962	77.63
95.620	67.43	92.194	67.43	105.223	67.59	103.524	67.58	105.353	67.58
91.684	57.72	88.312	57.72	101.263	57.88	99.573	57.86	101.370	57.86
87.118	48.12	83.877	48.20	96.729	48.19	95.092	48.18	96.817	48.17

VI. Correlation of the Data With the Antoine Equation

The method of correlation has been described previously [1]. The values of the three constants of the Antoine equation for vapor pressures, obtained from the data in table 1, are given in table 2, together with the ranges of pressure and temperature over which the experimental data were obtained (and over which, therefore, the resulting equation for each compound is applicable without loss of accuracy). The values of the boiling point and the pressure coefficient of the boiling point at 760.00 mm Hg, calculated from the Antoine equation, are also given.

The last column of table 2 gives, for each compound, the root-mean-square value, ρ, of the ratios of the deviations of the observed points from the Antoine equation to the expected standard deviations. The expected deviations were calculated on the basis of standard deviations (of a single value) of ± 0.003 deg C in the temperature and ± 0.06 to ± 0.11 mm Hg in the pressure, for the lowest and highest pressures, respectively. The values of ρ for the 60 compounds vary from 0.24 to 1.75, whereas the over-all value of ρ, computed for the total of 1,169 points on 60 compounds, is 0.56.

TABLE 2. *Summary of the results of the correlation of the experimental data with the Antoine equation for vapor pressures, for 60 API-NBS hydrocarbons*

Compound	Formula	Constants of the Antoine equation $\log_{10} P = A - B/(C+t)$, or $t = B/(A - \log_{10} P) - C$ (P in mm Hg; t in °C)			Normal boiling point at 760 mm Hg	Pressure coefficient, dt/dP, at 760 mm Hg	Range of measurement		Measure of precisions
		A	B	C			Pressure	Temperature	ρ
PARAFFINS									
					°C	°C/mm Hg	mm Hg	°C	
n-Heptane	C_7H_{16}	6.90027	1266.871	216.757	98.427	0.04481	48 to 780	26.0 to 99.3	0.36
2-Methylhexane	C_7H_{16}	6.87319	1236.026	219.545	90.052	.04431	48 to 780	18.5 to 90.9	.43
3-Methylhexane	C_7H_{16}	6.86764	1240.196	219.223	91.850	.04459	48 to 780	19.9 to 92.7	.38
3-Ethylpentane	C_7H_{16}	6.87565	1251.827	219.887	93.475	.04482	48 to 780	21.1 to 94.4	.61
2,2-Dimethylpentane	C_7H_{16}	6.81479	1190.033	223.303	79.197	.04394	58 to 780	12.2 to 80.1	.29
2,3-Dimethylpentane	C_7H_{16}	6.85382	1238.017	221.823	89.784	.04482	48 to 780	17.5 to 90.7	.33
2,4-Dimethylpentane	C_7H_{16}	6.82621	1192.041	221.634	80.500	.04376	58 to 780	13.7 to 81.4	.40
3,3-Dimethylpentane	C_7H_{16}	6.82998	1228.693	225.316	86.064	.04509	48 to 780	13.5 to 87.0	.28
2,2,3-Trimethylbutane	C_7H_{16}	6.79230	1200.563	226.050	80.882	.04484	58 to 780	12.6 to 81.8	.33
n-Nonane	C_9H_{20}	6.93513	1428.811	201.619	150.798	.04967	48 to 780	70.3 to 151.8	.24
2,2,5-Trimethylhexane	C_9H_{20}	6.83532	1324.049	210.737	124.084	.04838	48 to 780	46.1 to 125.0	.39
2,4,4-Trimethylhexane	C_9H_{20}	6.85164	1368.723	214.047	130.648	.04960	48 to 780	50.6 to 131.6	.55
3,3-Diethylpentane	C_9H_{20}	6.89262	1451.245	215.575	146.168	.05109	48 to 780	62.9 to 147.2	.43
2,2,3,3-Tetramethylpentane	C_9H_{20}	6.82876	1397.483	213.703	140.274	.05124	48 to 780	57.8 to 141.3	.36
2,2,3,4-Tetramethylpentane	C_9H_{20}	6.83173	1374.042	214.762	133.016	.05030	48 to 780	52.0 to 134.0	.43
2,2,4,4-Tetramethylpentane	C_9H_{20}	6.79711	1325.183	216.093	122.284	.04937	48 to 780	43.0 to 123.3	.37
2,3,3,4-Tetramethylpentane	C_9H_{20}	6.85961	1417.473	214.705	141.551	.04223	48 to 780	59.0 to 142.6	.49
ALKYLCYCLOPENTANES									
Ethylcyclopentane	C_7H_{14}	6.88709	1298.599	220.675	103.466	0.04623	48 to 780	28.8 to 104.4	0.52
1,1-Dimethylcyclopentane	C_7H_{14}	6.81725	1219.474	221.946	87.846	.04497	48 to 780	15.5 to 88.7	.59
cis-1,2-Dimethylcyclopentane	C_7H_{14}	6.85008	1269.140	220.209	99.532	.04693	48 to 780	25.3 to 100.4	.39
trans-1,2-Dimethylcyclopentane	C_7H_{14}	6.84422	1242.708	221.686	91.869	.04521	67 to 780	26.1 to 92.8	.75
cis-1,3-Dimethylcyclopentane	C_7H_{14}	6.88817	1240.023	221.621	91.725	.04525	67 to 780	26.0 to 92.6	.30
trans-1,3-Dimethylcyclopentane	C_7H_{14}	6.83715	1237.456	222.005	90.773	.04518	48 to 780	18.0 to 91.7	.51
n-Propylcyclopentane	C_8H_{16}	6.90392	1384.386	213.159	130.949	.04888	48 to 780	51.9 to 131.9	.74
Isopropylcyclopentane	C_8H_{16}	6.88623	1379.415	217.969	126.419	.04913	48 to 780	47.0 to 127.4	.55
1-Methyl-1-ethylcyclopentane	C_8H_{16}	6.87149	1355.287	218.092	121.522	.04893	48 to 780	43.1 to 122.5	1.75
1-Methyl-*cis*-2-ethylcyclopentane	C_8H_{16}	6.90562	1388.307	216.888	128.050	.04897	48 to 780	48.8 to 129.0	0.25
1,1,2-Trimethylcyclopentane	C_8H_{16}	6.82306	1309.618	218.557	113.729	.04818	48 to 780	36.2 to 114.7	.46
1,1,3-Trimethylcyclopentane	C_8H_{16}	6.80948	1275.908	219.899	104.893	.04724	48 to 780	28.9 to 105.8	.40
cis-cis-trans-1,2,4-Trimethylcyclopentane	C_8H_{16}	6.85448	1333.894	218.952	116.731	.04827	48 to 780	38.9 to 117.7	.71
cis, trans, cis-1,2,4-Trimethylcyclopentane	C_8H_{16}	6.84971	1306.153	219.808	109.280	.04738	48 to 780	32.9 to 110.2	.38

TABLE 2. *Summary of the results of the correlation of the experimental data with the Antoine equation for vapor pressures, for 60 API-NBS hydrocarbons*—Continued

Compound	Formula	Constants of the Antoine equation $\log_{10} P = A - B/(C+t)$, or $t = B/(A - \log_{10} P) - C$ (P in mm Hg; t in °C)			Normal boiling point at 760 mm Hg	Pressure coefficient, dt/dP, at 760 mm Hg	Range of measurement		Measure of precision
		A	B	C			Pressure	Temperature	σ
ALKYLCYCLOHEXANES									
					°C	°C/mm Hg	mm Hg	°C	
1,1-Dimethylcyclohexane	C_8H_{16}	6.80225	1323.861	218.073	119.543	0.04920	48 to 780	40.5 to 120.5	1.25
n-Propylcyclohexane	C_9H_{18}	6.88866	1461.715	207.980	156.724	.05280	48 to 780	72.7 to 157.8	0.59
Isopropylcyclohexane	C_9H_{18}	6.87257	1452.816	209.391	154.563	.05210	48 to 780	70.5 to 155.6	.30
1,1,3-Trimethylcyclohexane	C_9H_{18}	6.83705	1393.299	215.551	136.626	.05089	48 to 780	54.7 to 137.6	.60
n-Butylcyclohexane	$C_{10}H_{20}$	6.91261	1539.449	200.880	180.947	.05412	48 to 780	93.4 to 182.0	.30
Isobutylcyclohexane	$C_{10}H_{20}$	6.86703	1492.402	203.085	171.321	.05367	48 to 780	84.8 to 172.4	.32
sec-Butylcyclohexane	$C_{10}H_{20}$	6.88907	1529.373	202.220	179.335	.05440	48 to 780	91.4 to 180.4	.59
tert-Butylcyclohexane	$C_{10}H_{20}$	6.85449	1700.118	205.923	171.591	.05429	48 to 780	84.0 to 172.7	.45
ALKYLBENZENES									
Benzene	C_6H_6	6.91210	1214.645	221.205	80.099	0.04271	48 to 780	10.9 to 80.9	0.82
Methylbenzene	C_7H_8	6.95508	1345.087	219.516	110.626	.04630	48 to 780	35.5 to 111.5	.54
Ethylbenzene	C_8H_{10}	6.95904	1425.464	213.345	136.186	.04898	48 to 780	56.7 to 137.2	.56
1,2-Dimethylbenzene	C_8H_{10}	6.99891	1474.679	213.686	144.411	.04969	48 to 780	63.6 to 145.4	.43
1,3-Dimethylbenzene	C_8H_{10}	7.00849	1461.925	215.073	139.104	.04903	48 to 780	59.3 to 140.1	.40
1,4-Dimethylbenzene	C_8H_{10}	6.99184	1454.328	215.411	138.351	.04917	48 to 780	58.4 to 139.3	.46
n-Propylbenzene	C_9H_{12}	6.95094	1490.903	207.100	159.218	.05143	48 to 780	75.8 to 160.2	.43
Isopropylbenzene	C_9H_{12}	6.93958	1462.717	207.993	152.392	.05074	48 to 780	70.2 to 153.4	.39
1-Methyl-2-ethylbenzene	C_9H_{12}	7.00314	1535.374	207.300	165.153	.05163	48 to 780	81.1 to 166.2	1.18
1-Methyl-3-ethylbenzene	C_9H_{12}	7.01582	1529.184	208.509	161.305	.05111	48 to 780	78.1 to 162.3	1.12
1-Methyl-4-ethylbenzene	C_9H_{12}	6.99801	1527.113	208.921	161.989	.05148	48 to 780	78.3 to 163.0	0.68
1,2,3-Trimethylbenzene	C_9H_{12}	7.04082	1593.958	207.078	176.084	.05263	48 to 780	90.3 to 177.1	.66
1,2,4-Trimethylbenzene	C_9H_{12}	7.04383	1573.267	208.564	169.351	.05187	48 to 780	84.8 to 170.4	.83
1,3,5-Trimethylbenzene	C_9H_{12}	7.07437	1569.622	209.578	164.716	.05100	48 to 780	81.5 to 165.7	.53
n-Butylbenzene	$C_{10}H_{14}$	6.98518	1577.965	201.378	183.270	.05358	48 to 780	96.2 to 184.3	1.38
Isobutylbenzene	$C_{10}H_{14}$	6.93033	1526.384	204.171	172.759	.05319	48 to 780	86.6 to 173.8	0.34
sec-Butylbenzene	$C_{10}H_{14}$	6.95097	1540.174	205.101	173.305	.05313	48 to 780	87.1 to 174.4	1.03
tert-Butylbenzene	$C_{10}H_{14}$	6.92050	1504.572	203.328	169.119	.05269	48 to 780	83.9 to 170.2	0.73
1,2-Diethylbenzene	$C_{10}H_{14}$	6.99016	1577.894	200.554	183.423	.05340	48 to 780	96.7 to 184.5	.43
1,3-Diethylbenzene	$C_{10}H_{14}$	7.00601	1576.261	201.004	181.102	.05283	48 to 780	95.1 to 182.2	.49
1,4-Diethylbenzene	$C_{10}H_{14}$	7.00054	1589.273	202.019	183.752	.05351	48 to 780	96.8 to 184.8	.62

VII. Discussion

The vapor pressures of different samples of 15 of the above hydrocarbons have been previously measured in this laboratory [1]. Table 3 gives, for each of these 15 hydrocarbons, the calculated difference in pressure for a low, intermediate, and high temperature and the calculated difference in temperature for a low (50 mm Hg), intermediate (250 mm Hg), and high (760 mm Hg) pressure, in the range of measurement. Omitting two compounds, *n*-propylcyclopentane and *n*-propylcyclohexane, of which the previous samples contained a significantly greater amount of impurity, the average differences in temperature and in pressure at each of the three levels are seen to be quite satisfactory.

TABLE 3. *Comparison of the data obtained on 15 compounds in this and the previous investigation [1]*

Compound	Temperature	Calculated difference in pressure	Pressure	Calculated difference in temperature
	°C	*mm Hg*	*mm Hg*	°C
n-Heptane	98.427	−0.05	760	0.002
	64.624	.01	270	−.001
	26.811	−.01	50	.002
2,2-Dimethylpentane	79.197	.10	760	−.005
	46.127	.02	270	−.002
	9.315	−.01	50	.002
3,3-Dimethylpentane	86.064	.11	760	−.004
	52.113	.07	270	−.008
	14.296	.07	50	−.029
n-Nonane	150.798	−.04	760	.002
	113.292	.03	270	−.004
	71.255	−.02	50	.013
n-Propylcyclopentane	130.949	−.26	760	.012
	94.074	.05	270	−.006
	52.816	.09	50	−.039
Isopropylcyclopentane	126.419	−.08	760	.005
	89.367	.04	270	−.006
	47.955	.06	50	−.028
n-Propylcyclohexane	156.724	−.24	760	.013
	117.507	−.08	250	.010
	73.667	.02	50	−.007
Benzene	80.099	.07	760	−.003
	47.869	.05	270	−.006
	11.792	.11	50	−.046
Methylbenzene	110.626	−.07	760	.003
	75.644	−.01	270	.001
	36.393	.01	50	−.005
Ethylbenzene	136.186	.02	760	.000
	99.181	.02	250	−.006
	57.652	.07	50	−.031
1,2-Dimethylbenzene	144.411	.05	760	−.002
	106.828	.02	270	−.004
	64.558	.01	50	−.003
1,3-Dimethylbenzene	139.104	−.03	760	.002
	102.030	.06	270	−.006
	60.267	.06	50	−.027
1,4-Dimethylbenzene	138.351	−.08	760	.003
	101.167	−.02	270	.002
	59.360	.03	50	−.011
n-Propylbenzene	159.218	−.06	760	.003
	120.368	−.03	270	.003
	76.786	.00	50	.005
Isopropylbenzene	152.392	.02	760	.000
	114.075	−.01	250	.002
	71.119	.04	50	−.020

Average	For temperature corresponding to—	Calculated difference in pressure	at—	Calculated difference in temperature
Average	760 mm	0.060	760 mm	0.0026
	250 mm	.030	250 mm	.0039
	50 mm	.038	50 mm	.0171

In the previous report [1], it was pointed out that some correlation exists between the values of the constants B and C of the Antoine equation and the number of carbon atoms in the normal alkyl side chain for the members of several normal alkyl series of hydrocarbons, as normal paraffins, normal alkylcyclopentanes, normal alkylcyclohexanes, and normal alkylbenzenes. For the previous correlation, values for ethylcyclopentane, *n*-butylcyclohexane, and *n*-butylbenzene were not available. The values of the B and C constants for these three compounds obtained from the present investigation are found to be in good accord with those previously reported for the neighboring members of these series [1].

Acknowledgment is made to Corinne R. DeCelles and Ruth C. MacKay for assistance in making the calculations reported in this paper.

VIII. References

[1] C. B. Willingham, W. J. Taylor, J. M. Pignocco, and F. D. Rossini, J. Research NBS **35,** 219 (1945) RP1670.

[2] C. B. Willingham and F. D. Rossini, J. Research NBS **33,** 85 (1944) RP1615.

[3] N. S. Osborne and C. H. Meyers, J. Research NBS **13,** 1 (1934) RP691.

[4] C. H. Meyers, H. F. Stimson, and C. S. Cragoe, National Bureau of Standards; private communication.

[5] A. F. Forziati and F. D. Rossini, J. Research NBS **43,** (1949) RP2039.

[6] A. R. Glasgow, Jr., E. T. Murphy, C. B. Willingham, and F. D. Rossini, J. Research NBS **37,** 141 (1946) RP1734.

[7] A. J. Streiff, E. T. Murphy, V. A. Sedlak, C. B. Willingham, and F. D. Rossini, J. Research NBS **37,** 331 (1946) RP1752.

[8] A. J. Streiff, E. T. Murphy, J. C. Cahill, H. F. Flanagan, V. A. Sedlak, C. B. Willingham, and F. D. Rossini, J. Research NBS **38,** 53 (1947) RP1760.

[9] A. J. Streiff, E. T. Murphy, J. C. Zimmerman, L. F. Soule, V. A. Sedlak, C. B. Willingham, and F. D. Rossini, J. Research NBS **39,** 321 (1947) RP1833.

[10] A. J. Streiff, J. C. Zimmerman, L. F. Soule, M. T. Butt, V. A. Sedlak, C. B. Willingham, and F. D. Rossini, J. Research NBS **41,** 323 (1948) RP1929.

WASHINGTON, June 3, 1949.

U. S. Department of Commerce
National Bureau of Standards

Research Paper RP2050
Volume 43, December 1949

Part of the Journal of Research of the National Bureau of Standards

Bond of Concrete Reinforcing Bars

By Arthur P. Clark [1]

The tests reported were made to compare the resistance to slip in concrete (bond) of deformed bars when tested in beams and companion pull-out specimens, to secure information on the effects of size of bar, the type of deformations on the bars, and the strength of concrete on the bond. The bars were cast in a horizontal position in all test specimens. The variables were depth of concrete under the bar, length of embedment of the bar in the concrete, strength of concrete, and diameter of bar. Slip of the bar was measured at the loaded and free ends. Three tests were made each with 2 in. of concrete under the bar, with 15 in. of concrete under the bar, and with 8-, 12-, and 16-in. embedments.

Bond strengths for the beams and the pull-out specimens were affected similarly by changes in the geometry of the bars and the bond test specimens. They were greater when the bars were near the bottom than when they were near the top of the specimens as cast. The highest bond strengths were obtained with bars having deformations conforming to suggested requirements for maximum spacing and minimum height and providing ratios of shearing to bearing areas less than 10, usually less than 6.

I. Introduction

The tests reported in this paper were made at the National Bureau of Standards under a Research Fellowship for the Committee on Reinforced Concrete Research of the American Iron and Steel Institute. This Committee consists of a representative from each of the principal producers of concrete reinforcing bars.

The primary purpose of the tests was to determine the bond value of concrete reinforcing bars when tested in beam specimens in accordance with the "Proposed test procedure to determine relative bond value of reinforcing bars" of Committee 208, Bond Stress, of the American Concrete Institute.[2] Additional objectives were to determine the correlation between the results of the beam and the pull-out tests made at the same time and under identical conditions, to secure information as to the influence of size of bar and strength of concrete on bond, and to test the experimental designs of deformations by member companies in their efforts to produce bars having bond resistance approaching the maximum consistent with economical commercial production.

II. Materials

1. Reinforcing Bars

The bars in this series of tests were nominally ½ in. round, ⅞ in. round, and 1⅛ in. square in size. The areas of the bars and details of the deformations are given in table 1. All ⅞-in. bars, except bar No. 16, and one ½-in. bar (No. 15) are illustrated in figure 1. Bar No. 16 was the same as bar No. 11 except for the height of deformations. The bars nominally 1⅛ in. in size, with two exceptions described below, were round in cross section with areas equal to 1⅛ in. square bars. Bars Nos. 2 and 18 were square in cross section and of a type similar to the ⅞ in. round bar No. 2.

With the exception of the plain bar (No. 9), all bars were deformed and were similar in type to those included in a series of tests previously reported,[3] but some had improved deformations. The plain bar and one unimproved deformed bar (No. 2) of a type heretofore in general use were

[1] Research Associate at the National Bureau of Standards, representing the American Iron & Steel Institute.

[2] Proposed test procedure to determine relative bond value of reinforcing bars, J. Am. Concrete Inst. **41**, 273 (Feb. 1945).

[3] A. P. Clark Comparative bond efficiency of deformed concrete reinforcing bars, J. Research NBS **37**, 399 (1946) RP1755.

included in these tests for the purpose of comparison.

TABLE 1. *Detail dimensions of bars*

Bars			Deformations				
Size	No.	Area	Spacing	Average height	Bearing area	Shearing area	Ratio of shearing to bearing area
in.		*in.²*	*in.*	*in.*	*in.²/in.*	*in.²/in.*	
½	2	0.200	1.234	0.018	0.013	0.835	64.2
½	5	.200	0.371	.018	.139	1.225	8.7
½	6	.198	.368	.027	.100	1.160	11.6
½	8	.200	.250	.031	.191	1.149	6.0
½	11	.196	.269	.028	.217	1.382	6.4
½	13	.202	.443	.030	.094	1.306	13.9
½	15	.200	.206	.041	.245	0.795	3.2
⅞	1	.603	.671	.056	.148	1.792	12.1
⅞	2	.599	1.412	.032	.040	1.621	40.1
⅞	3	.591	0.667	.060	.185	2.063	11.2
⅞	4	.599	.656	.050	.177	2.085	11.8
⅞	5	.599	.581	.057	.232	2.313	10.0
⅞	6	.606	.606	.058	.248	2.629	10.6
⅞	7	.610	.375	.033	.161	2.208	13.8
⅞	8	.610	.380	.050	.355	2.100	5.9
⅞	*9	.597	.....	.....	.....	.....	.....
⅞	10	.578	.398	.047	.276	1.981	7.2
⅞	11	.615	.368	.045	.305	1.930	6.3
⅞	12	.605	.296	.040	.327	1.867	5.7
⅞	13	.594	.702	.070	.242	2.460	10.2
⅞	14	.605	.434	.062	.359	1.956	5.5
⅞	17	.594	.633	.054	.207	2.234	10.8
1⅛	2	1.268	1.735	.034	.069	3.281	47.6
1⅛	5	1.245	0.921	.074	.282	3.500	12.4
1⅛	6	1.210	.944	.063	.283	3.139	11.9
1⅛	8	1.268	.544	.072	.522	3.373	6.5
1⅛	11	1.269	.525	.052	.385	3.298	8.6
1⅛	13	1.254	1.115	.078	.416	5.281	12.7
1⅛	15	1.278	0.517	.083	.479	2.906	6.1
1⅛	16	1.274	.475	.071	.589	2.888	4.9
1⅛	18	1.269	1.255	.036	.084	2.737	32.7

* Plain, no deformations.

2. Concrete

Concrete was machine mixed and rodded when placed in the molds. One brand of cement, from the same mill, which met the current ASTM Standard Specification for portland cement of type 1 was used throughout.

Coarse aggregate was Potomac River gravel ranging in size from No. 4 to 1 in. The fine aggregate was Potomac River sand described in the previous series (see footnote 2). There were three concretes of different mixes, which are hereafter referred to as 6,000-, 3,500-, and 2,000-lb concretes. The first concrete proportioned by weight in the ratio 1:1.4:2.0 with water-cement ratio of 5.15 gal per sack gave an average compressive strength for 6- by 12-in. cylinders at 28 days of 6,030 lb/in.² and an average slump of 5.5 in. The second concrete proportioned 1:2.91:4.04 with 8.7 gal of water per sack averaged 3,570 lb/in.² with a slump of 4.8 in. The third concrete proportioned 1:3.97:5.15 with 11.77 gal of water per sack averaged 1,840 lb/in.² with a slump of 4.5 in.

III. Description of Test Specimens

Beam specimens were 8 by 18 in. in cross section and 78 in. in over-all length. Two notches 6 in. long and 3 in. high near each end exposed the reinforcing bar. Half of the specimens were cast with the bar held 2 in. from the bottom of the mold and the other half with the bar held 2 in. from the top. The molds were of steel and fabricated in accordance with the details given in the report of the ACI Committee 208 (see footnote 2).

Pull-out specimens were 8 by 9 in. in cross section and 8, 12, and 16 in. in length. Two specimens were cast with the bars in a horizontal position, in a mold 18 in. in depth with one bar held near the bottom and one near the top comparable to the positions in the beams. At the end of 2 days, the block was removed from the mold and separated into two specimens. The molds were made of heavy steel sections and sealed to prevent leakage.

IV. Testing Procedure

The beams were tested in a 600,000-lb capacity hydraulic testing machine on supports 72 in. apart, the supports being a roller at one end and a spherical bearing unit at the other end. A beam in position for test with gages attached is shown in figure 2. The load was applied through a steel loading beam with a roller at one load point and a spherical bearing unit at the other load point. The load points were adjusted at 8, 12 and 16 in. from the supports. The distances of the load points from the supports thus corresponded to the three lengths of embedment of the bar. The load points in each case were directly over the outer edges of the 6-in. notches, which exposed the bar. In these notches two yokes were clamped into drilled contact points on 5-in. centers on each side of the bar. Dial gages attached to the yokes permitted measurement of the strain in the bar. The gage on the reaction side of the notch bore on a steel angle clip attached with a screw to the

concrete at the edge of the notch; this gage measured the slip of the bar directly under the load (loaded end slip). Dial gages at each end of the beam, held in position by steel yokes, clamped to the concrete, measured the slip at the end (free end slip) of the bar. Deflection at the center of the beam was measured by a dial gage supported by an aluminum bar, whose ends were attached to the sides of the beam over the supports; this gage bore on an angle clip attached with a screw to the concrete. The specimens that were cast with the bar held 2 in. from the top were turned upside down in testing. The beams were removed from the mold 5 days after casting and kept moist until tested at the age of 28 to 30 days.

Pull-out specimens were tested in a 60,000-lb capacity universal hydraulic testing machine. The specimen, shown in figure 3, was seated on a rubber cushion on two segments of a 2-in. base plate attached to a spherical bearing block. Slip of the bar was measured with 0.0001-in. micrometer dial gages and estimated to 0.00005 in. At the loaded end two dial gages were held by a steel bar attached to the bottom face of the specimen by bolts secured into inserts cast in the specimen. The gages were in contact with a steel yoke fastened to the reinforcing bar 1 in. below the surface of the concrete. The support bar for the gages and the yoke were free to move in the recess in the base plate. The average of the two gage readings indicated the amount of movement of the point on the reinforcing bar at which the yoke was attached with reference to the lower face of the concrete. To give the slip at the face of the concrete (slip at loaded end), the gage readings were corrected for the elongation of the reinforcing bar in the 1-in. distance between the point of attachment of the yoke and the face of the concrete.

The slip at the free end was read directly from the gage mounted on a support, seated in plaster, on the top of the specimen with the point of the dial resting on the planed end of the bar.

With the ⅞-in. bars, 18 beam and 18 pull-out tests were made for each type of bar, three each with the bar in the bottom and top positions and with 8-, 12-, and 16-in. embedments. With ½-in. and 1⅛-in. bars, 12 tests each were made, three each in the bottom and top positions and with 8- and 12-in. embedments for the ½-in. and with 12- and 16-in. embedments for the 1⅛-in. bar.

V. Results and Discussions

Beams generally failed in bond, although with the longer embedments diagonal tension failure combined with bond failure occurred with some specimens. The pull-out specimens failed by splitting of the concrete in all cases except with the plain bar.

The relation of bond stress to slip of bar as shown by the curves and the comparative charts is based in all cases, unless otherwise shown, on the average results for all tests and all lengths of embedment of the bar and for 3,500-lb concrete.

The bond-slip relation of ⅞-in. bars in beams, as measured at the loaded and free ends and for bottom and top cast bars, is shown in figures 4, 5, 6, and 7. The deflection at the center of beams with bottom cast bars for increasing loads for each of the three embedments of the bar is shown in figures 8, 9, and 10. Typical crack patterns after failure of the beam are shown in figures 11 and 12. The bond-slip relation of ⅞-in. bars in pull-outs, for loaded and free ends and for bottom and top cast bars, is shown in figures 13, 14, 15, and 16.

Authorities considering the allowable unit stresses for bond to be permitted in design have used, by applying a suitable factor of safety, the average of bond stresses developed in tests at a slip of 0.01 in. at the loaded end and 0.005 in. at the free end. Figure 17 represents the bond stresses at loaded end slip of 0.01 in. and free end slip of 0.005 in. and the average of two as determined by beam and pull-out tests of ⅞-in. bottom and top cast bars.

The average performance of a bar through a range of slip values was used to obtain a comparison of bond developed in beam specimens with that in pull-out specimens cast at the same time. The bond stresses for slips of 0.0005, 0.001, 0.002, 0.003, 0.004, 0.005, 0.0075, and 0.01 in. at the loaded end were totaled for each and divided by the number of slip values to give an average value. Slips of 0.00005, 0.0001, 0.0005, and 0.001 in. were used in a similar manner for free end comparison. The results for loaded end and free end slips, on the basis outlined above for all ⅞-in. bars tested in both beam and pull-out specimens, shown in figure 18, indicated that the pull-out tests fairly represent the relative bonding efficiency of the bars. In table 2 the average values,

as above, at the loaded end for each embedment of the bar as developed in pull-outs is listed and in table 3 the same information as developed in beams. Figure 19 gives a comparison of all bars in the series as tested in pull-outs for slips at the loaded end. Although the results for loaded and free end slips of top cast bars and free end slips of bottom cast bars were not as consistent as the results for loaded end slips of bottom cast bars, the load-slip relations were of similar form and show a consistent pattern for all tests in both types of specimens.

TABLE 2. *Average bond stress of pull-outs for slips of 0.0005, 0.001, 0.002, 0.003, 0.004, 0.005, 0.0075, and 0.01 in. at the loaded end*

Bar No.	Bond stress, lb/in.²							
	⅞-in. Bottom cast				⅞-in. Top cast			
	Embedment				Embedment			
	8 in.	12 in.	16 in.	Avg.	8 in.	12 in.	16 in.	Avg.
1	435	274	222	310	257	147	151	185
2	350	291	223	288	161	104	102	122
3	426	301	224	317	224	154	172	183
4	456	351	235	347	308	175	172	218
5	498	330	236	355	258	254	153	222
6	407	357	220	328	305	223	159	228
7	445	337	258	347	208	227	201	212
8	543	390	291	408	437	289	210	312
9	325	176	168	223	138	84	97	106
10	525	360	260	392	313	176	196	228
11	531	392	278	394	399	282	233	305
13	428	354	252	338	219	269	129	206
14	480	358	272	370	438	361	264	354
17	436	295	221	318	378	195	159	244
	1½-in. Bottom cast				1½-in. Top cast			
2	319	231	...	275	211	106	...	158
5	426	282	...	354	344	169	...	256
6	458	286	...	372	201	206	...	204
8	496	304	...	400	320	314	...	317
11	409	312	...	360	418	274	...	346
13	391	247	...	319	150	120	...	135
15	475	342	...	408	466	309	...	387
	1⅞-in. Bottom cast				1⅞-in. Top cast			
2	...	268	192	230	...	194	144	169
5	...	336	264	300	...	226	192	209
6	...	177	237	207	...	177	190	184
8	...	392	280	336	...	304	278	291
13	...	299	261	275	...	242	133	188
15	...	388	279	334	...	348	264	306
16	...	365	262	313	...	277	247	262
18	...	321	198	260	...	193	170	181

TABLE 3. *Average bond stress in beams for slips of 0.0005, 0.001, 0.002, 0.003, 0.004, 0.005, 0.0075 and 0.01 in. at the loaded end*

Bar No.	Bond stress, lb/in.²							
	⅞-in. Bottom cast				⅞-in. Top cast			
	Embedment				Embedment			
	8 in.	12 in.	16 in.	Avg.	8 in.	12 in.	16 in.	Avg.
1	424	336	242	334	226	182	160	189
2	272	244	205	240	114	97	98	103
3	431	359	250	347	215	192	143	183
4	435	344	282	354	203	217	183	201
5	460	350	287	366	177	220	212	203
6	431	345	258	345	208	193	166	189
7	454	361	259	358	171	152	158	160
8	561	412	292	422	379	207	208	265
9	228	188	194	203	...	...	...	...
11	571	416	325	437	259	251	233	248
	½-in. Bottom cast				½-in. Top cast			
2	191	217	...	204	73	79	...	76
6	403	277	...	340	202	196	...	199
	1⅛-in. Bottom cast				1⅛-in. Top cast			
2	...	213	195	204	...	161	151	156
6	...	361	287	324	...	201	191	196

The bond-slip relation of the ½-in. and 1⅛-in. bars in pull-outs for loaded and free ends and bottom and top cast bars is shown in figures 20 to 27. The ½-in. bars were round, whereas the 1⅛-in. bars were round in section with areas equal to that of a 1⅛ in. square, except bar No. 2, which was a 1⅛ in. square.

Results of tests of ½-, ⅞-, and 1⅛-in. bars of type No. 6 are shown by the bond slip curves of figures 28, 29, 30, and 31 for loaded and free ends, bottom and top cast and beam and pull-out specimens.

Pull-out tests of ½- and 1⅛-in. bars of type No. 6 in three concrete strengths are shown by the curves of figures 32, 33, 34, and 35.

The Committee on Reinforced Concrete Research of the American Iron and Steel Institute after a study of the results of the first series of bond tests (see footnote 3) sponsored the "Tentative specification for minimum requirements for the deformations of deformed steel bars for concrete reinforcement" ASTM Designation: A305–49. "Data from the present series of tests indicated two desirable revisions" of the above Tentative

specifications; one changing the maximum average spacing of the deformations to seven-tenths of the nominal size of the bar, and the other changing the minimum height of deformations to $4\frac{1}{2}$ percent of the nominal size for $\frac{5}{8}$-in. bars and to 5 percent for bars $\frac{3}{4}$ in. and larger. "The Tentative Specification, including the revisions, has now been adopted as a standard ASTM designation A305–49."

The following bars met the requirements of ASTM A305–49: $\frac{7}{8}$-in. bars 5, 6, 8, 10, 11, and 14; $\frac{1}{2}$-in. bars 8, 11, 14, and 15; $1\frac{1}{8}$-in. bars 8, 14, 15, and 16.

VI. Summary

Bond tests were conducted on both beam and pull-out specimens in which the bars were cast in a horizontal position. The specimens provided three lengths of embedment and two different depths of concrete under the bars. Slip of the bar was measured at both the loaded and the free end.

The results of the tests with both types of specimens were as consistent as expected for bond tests. The least consistent data were those pertaining to the slips at the free ends of the bars and for the bars cast in the top position.

The correlation between the results of the beam and the pull-out tests was such as to indicate that pull-out tests can give reliable estimates of the bonding efficiency of deformed reinforcing bars. Although the data obtained from the two types of specimens did not always rate the bars in the same order, the differences in ratings were usually too small to be of practical significance; moreover, the relations between load and slip were of similar form and the general behavior of the bars was similar in the two types of tests. The plain bar gave the least bond; the old type of deformed bar gave a somewhat higher bond and the rest of the bars gave still higher values, with those meeting ASTM Specification A305–49 showing the highest bond.

The ratings of the bars were based upon the average performances for a range of slips at both the loaded and free ends, for either two or three lengths of embedment and with 2 or 15 in. of concrete beneath the bar as cast. The deformations of the bars that had the highest values of bond had bearing areas equal to or greater than the bearing area provided under ASTM A305–49 limitations of maximum spacing, minimum height and length of deformations, and the ratio of the shearing areas to bearing areas were less than 10. These results confirmed the previous observation that for good bond a maximum ratio of the shearing to bearing areas of 5 or 6 is desirable provided requirements of A305-49 are met.

The bond strengths obtained with bars conforming to the proposed specifications were much greater than those developed by bars in common use at the time Committee 318 on Standard Building Codes of the American Concrete Institure determined the allowable bond stresses of the building code requirements for reinforced concrete. The superior performance of the bars of improved types was most marked when the conditions were least favorable for obtaining a strong bond, that is, with the bars in top position in the beams as cast.

Albert E. Holbrook, Research Associate, was in charge of much of the laboratory procedure and the reduction of the very extensive data developed in these tests. Timothy Miles, Jr., laboratory assistant, carried out the laboratory work with ingenuity and care. Acknowledgement is made and appreciation expressed for the willing cooperation and very helpful advice and assistance of the Bureau staff.

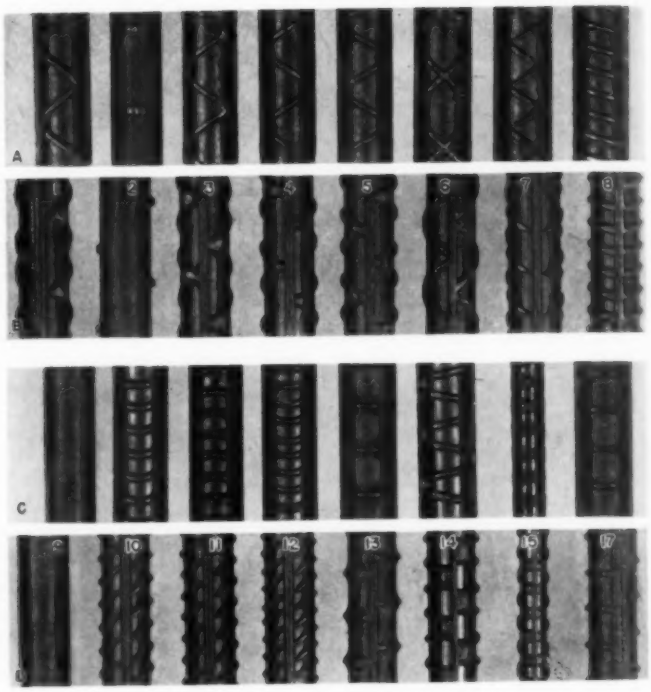

FIGURE 1. *Types of bars tested.*

A, Front view; B, side view of A; C, front view; D, side view of C.

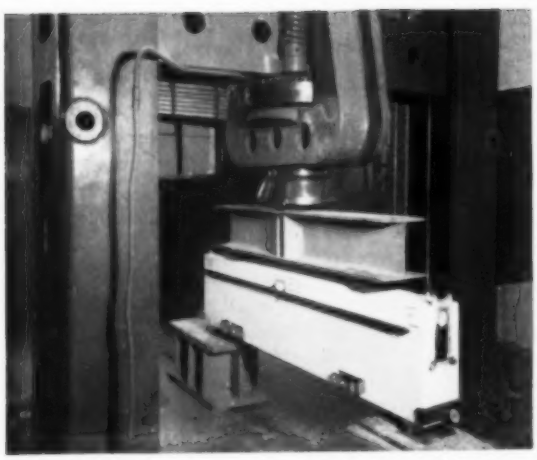

FIGURE 2. *Beam specimen in testing machine.*

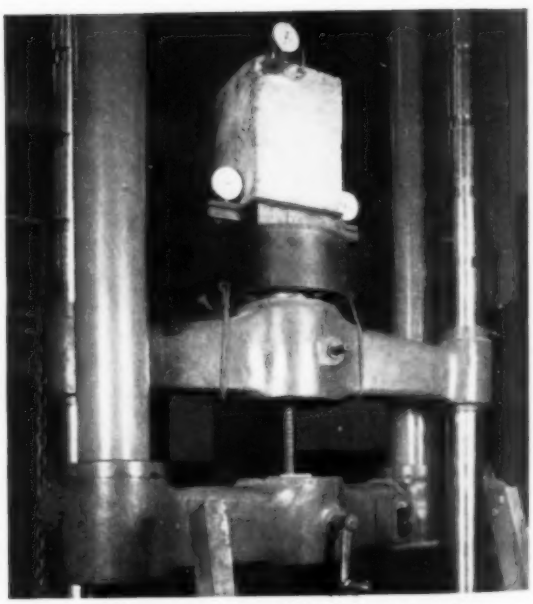

FIGURE 3. *Pull-out specimen in testing machine.*

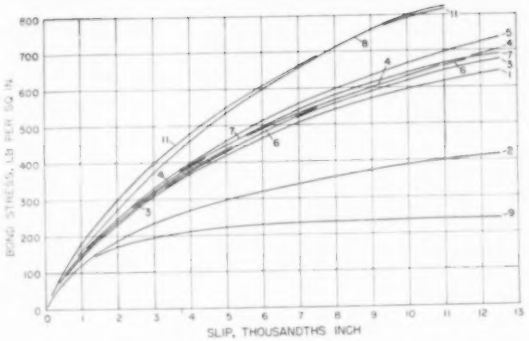

FIGURE 4. *Bond-slip curves for ⅞-in. bottom bars in beams.*

Slip measured at loaded end.

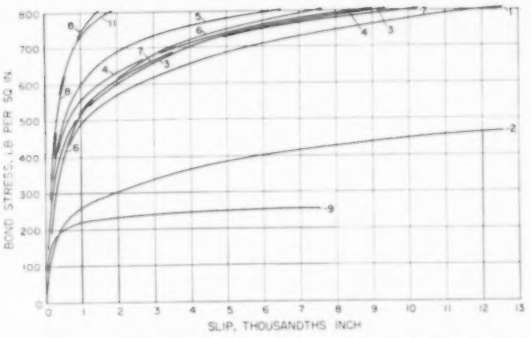

FIGURE 5. *Bond-slip curves for ⅞-in. bottom bars in beams*

Slip measured at free end.

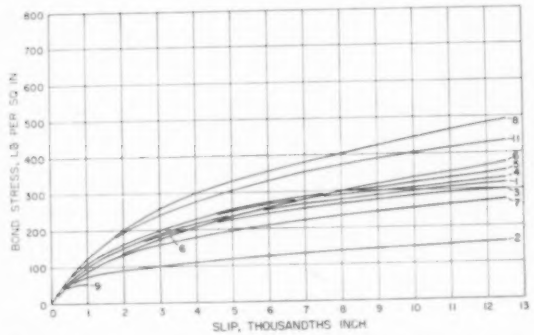

FIGURE 6. *Bond-slip curves for ⅞-in. top bars in beams.*

Slip measured at loaded end.

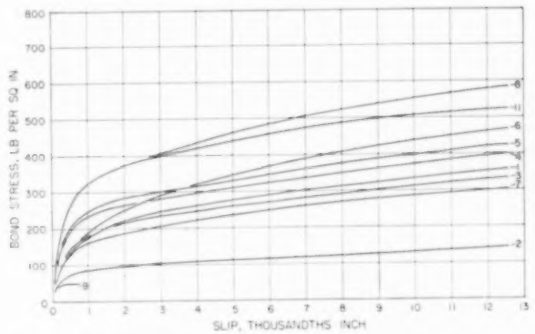

FIGURE 7. *Bond-slip curves for ⅞-in. top bars in beams.*

Slip measured at free end.

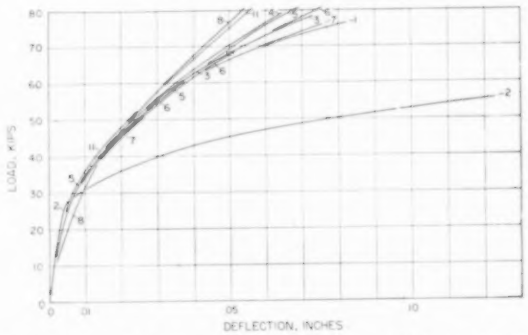

FIGURE 8. *Deflection curves for beams with ⅞-in. bottom bars.*

Embedded 8 in.

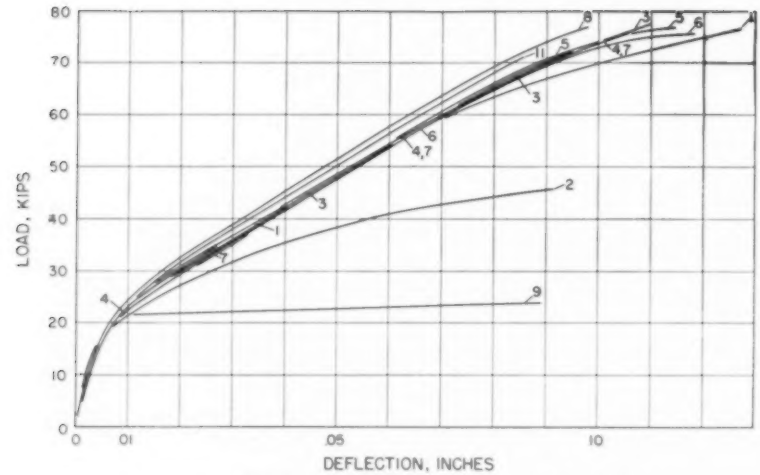

FIGURE 9. *Deflection curves for beams with $\frac{7}{8}$-in. bottom bars.*

Embedded 12 in.

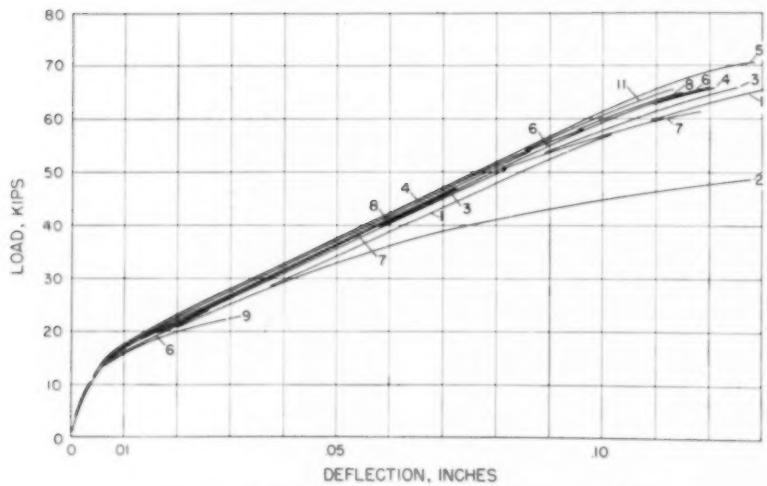

FIGURE 10. *Deflection curves for beams with $\frac{7}{8}$-in. bottom bars.*

Embedded 16 in.

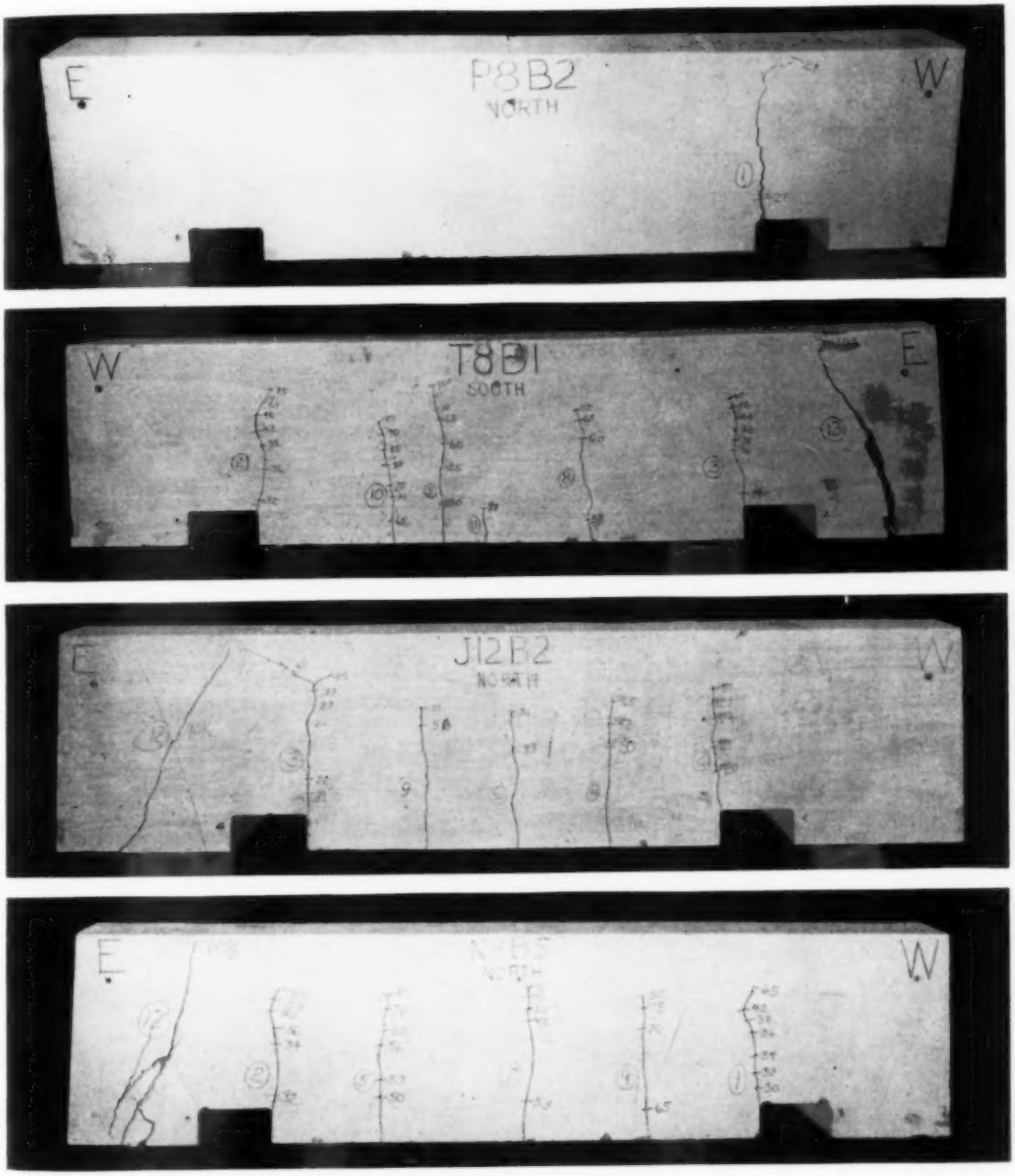

FIGURE 11. *Typical beam cracks at failure.*

FIGURE 12. *Typical beam cracks at failure.*

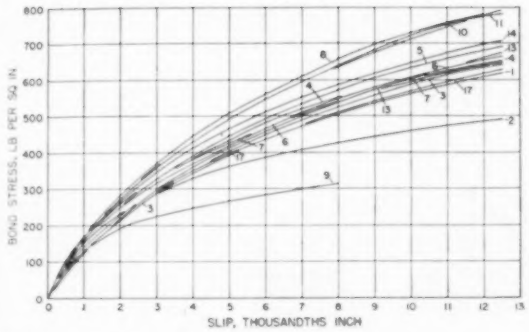

FIGURE 13. *Bond-slip curves for ⅞-in. bottom bars in pull-outs.*

Slip measured at loaded end.

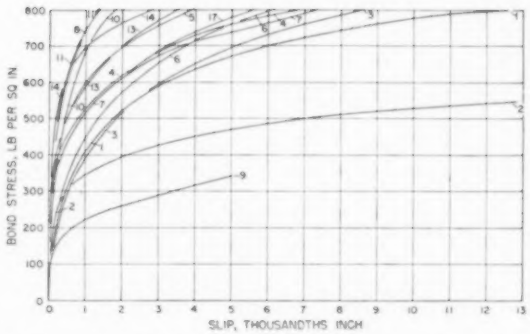

FIGURE 14. *Bond-slip curves for ⅞-in. bottom bars in pull-outs.*

Slip measured at free end.

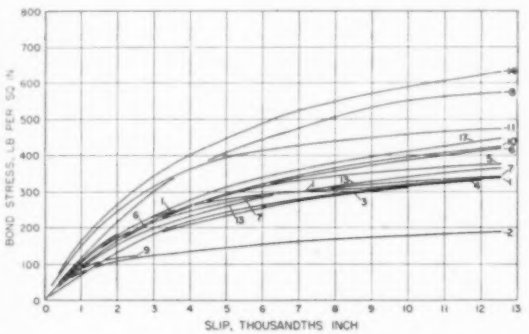

FIGURE 15. *Bond-slip curves for ⅞-in. top bars in pull-outs.*

Slip measured at loaded end.

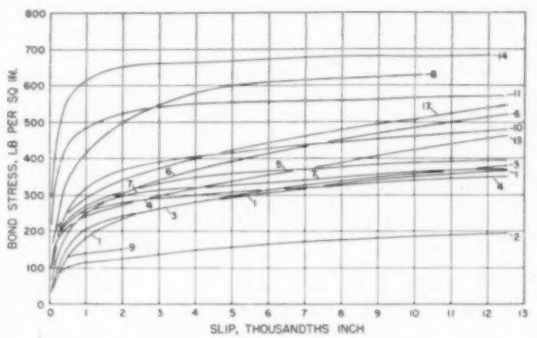

FIGURE 16. *Bond-slip curves for ⅞-in. top bars in pull-outs.*

Slip measured at free end.

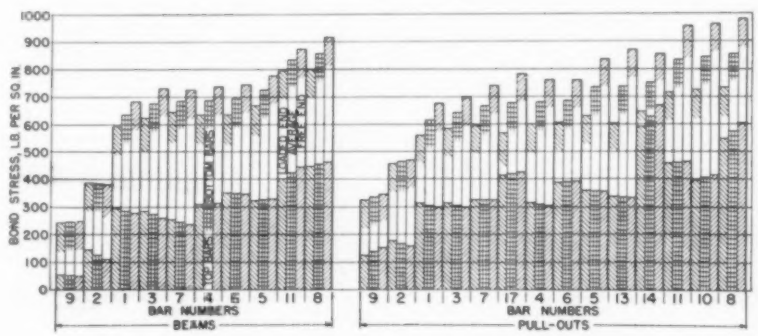
BOND STRESS, LB PER SQ IN
TOP BARS
BOTTOM BARS
LOADED END
FREE END
9 2 1 3 7 4 6 5 11 8
BAR NUMBERS
BEAMS
9 2 1 3 7 17 4 6 5 13 14 11 10 8
BAR NUMBERS
PULL-OUTS

FIGURE 17. *Bond stress for each ⅞-in. bar.*

At loaded end slip of 0.01 in., free end slip of 0.005 in., and average of the two for bottom and top bars in beams and pull-outs.

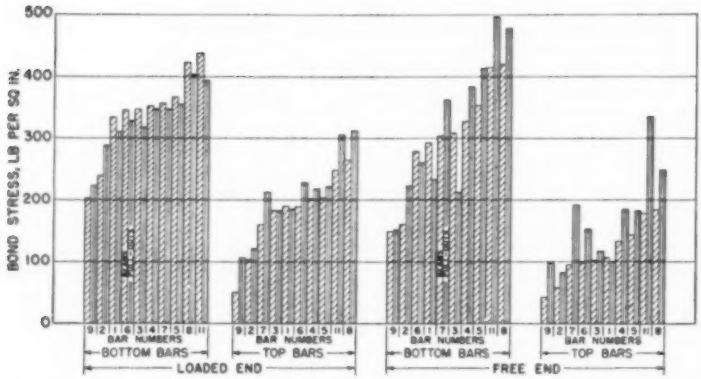

FIGURE 18. *Comparison of beam and pull-out tests of each ⅞-in. bar in bottom and top positions based on the average of bond stresses at slips of 0.0005, 0.001, 0.002, 0.003, 0.004, 0.005, 0.0075, and 0.01-in. measured at loaded end and the average at slips of 0.00005, 0.0001, 0.005, and 0.001-in. measured at free end.*

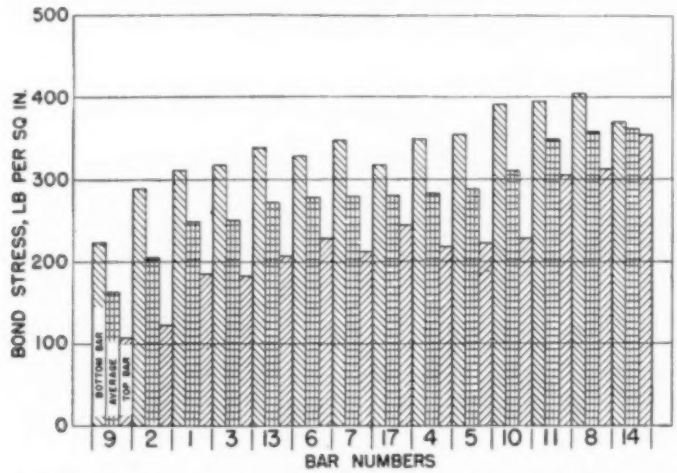

FIGURE 19. *Average of the bond stresses at slips of 0.0005, 0.001, 0.002, 0.003, 0.004, 0.005, 0.0075, and 0.01-in. measured at loaded end for each ⅞-in. bar in bottom and top positions in pull-outs.*

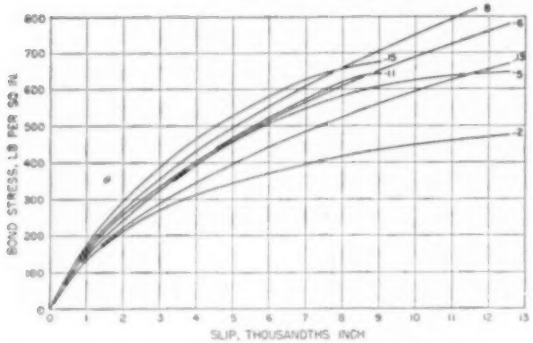

FIGURE 20. *Bond-slip curves for ½-in. bottom bars in pull-outs.*

Slip measured at loaded end.

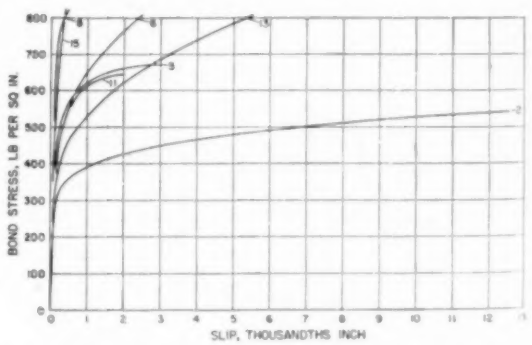

FIGURE 21. *Bond-slip curves for ½-in. bottom bars in pull-outs.*

Slip measured at free end.

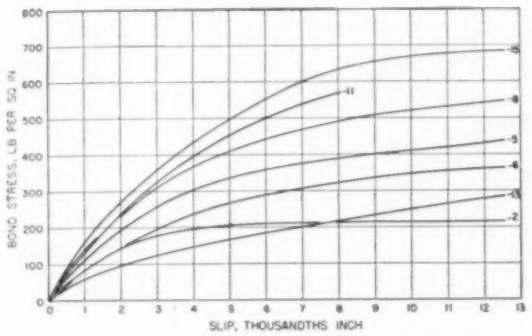

FIGURE 22. *Bond-slip curves for ½-in. top bars in pull-outs.*
Slip measured at loaded end.

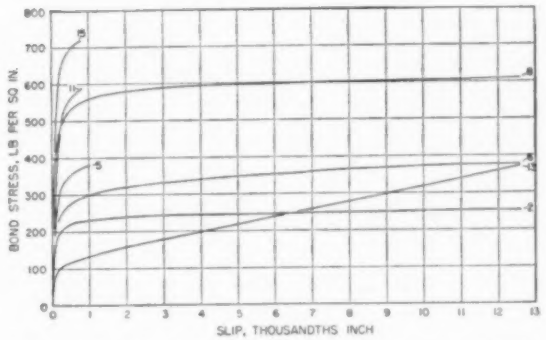

FIGURE 23. *Bond-slip curves for ½-in. top bars in pull-outs.*
Slip measured at free end.

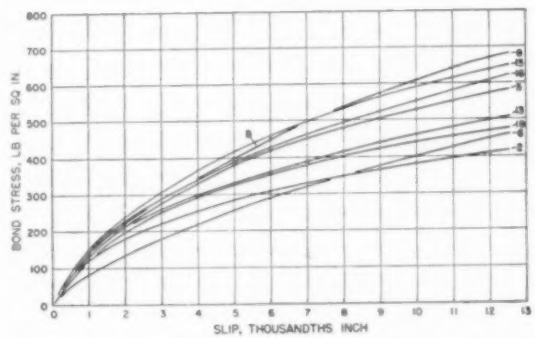

FIGURE 24. *Bond-slip curves for 1⅛-in. bottom bars in pull-outs.*
Slip measured at loaded end.

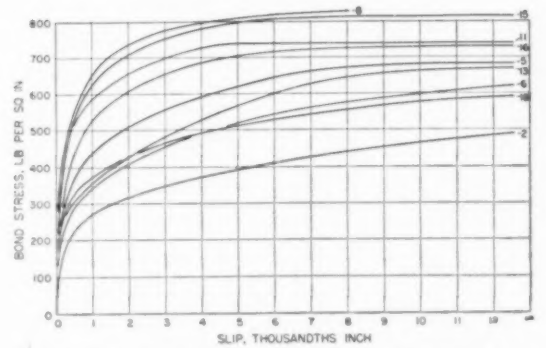

FIGURE 25. *Bond-slip curves for 1⅛-in. bottom bars in pull-outs.*
Slip measured at free end.

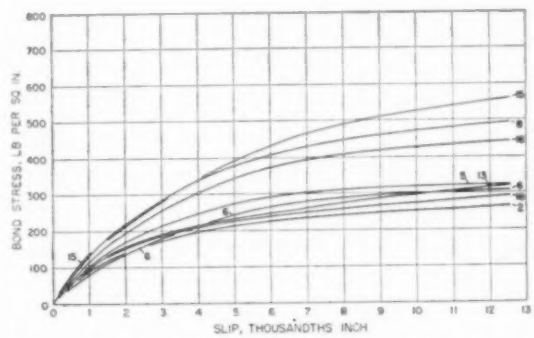

FIGURE 26. *Bond-slip curves for 1⅛-in. top bars in pull-outs.*
Slip measured at loaded end.

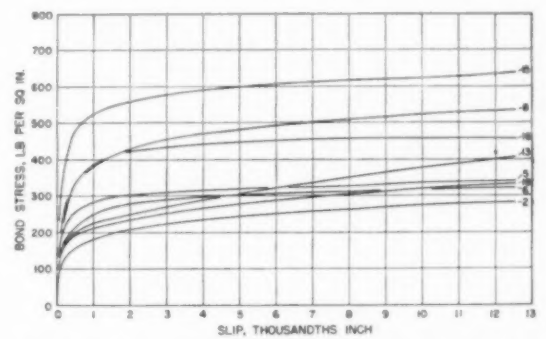

FIGURE 27. *Bond-slip curves for 1⅛-in. top bars in pull-outs.*
Slip measured at free end.

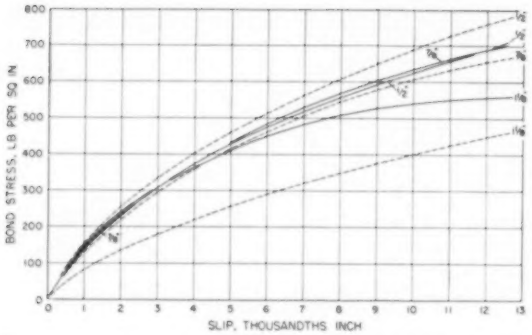

FIGURE 28. *Bond-slip curves for ½-, ⅞- and 1⅛-in. Bar No. 6 bottom cast in beams and pull-outs.*

Slip measured at loaded end. ....., Pull-outs; ——, beams.

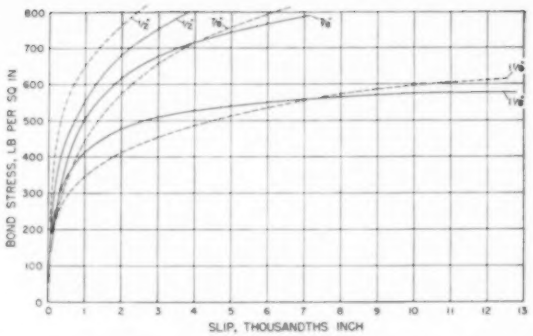

FIGURE 29. *Bond-slip curves for ½-, ⅞- and 1⅛-in. Bar No. 6 bottom cast in beams and pull-outs.*

Slip measured at free end. ....., Pull-outs; ——, beams.

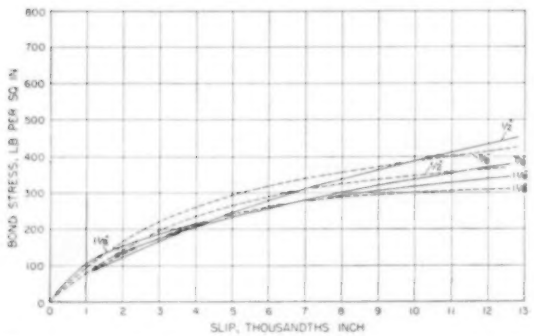

FIGURE 30. *Bond-slip curves for ½-, ⅞- and 1⅛-in. Bar No. 6 top cast in beams and pull-outs.*

Slip measured at loaded end. ....., Pull-outs; ——, beams.

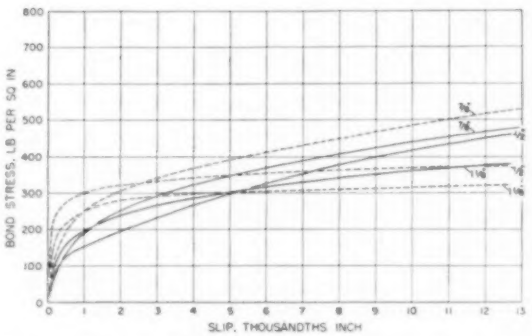

FIGURE 31. *Bond-slip curves for ½-, ⅞- and 1⅛-in. Bar No. 6 top cast in beams and pull-outs.*

Slip measured at free end. ....., Pull-outs; ——, beams.

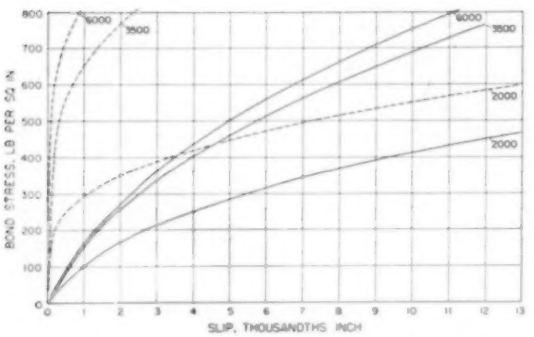

FIGURE 32. *Bond-slip curves for ½-in. Bar No. 6 in 2,000-3,500- and 6,000-lb strength concretes, bottom cast, in pull-outs.*

Slip measured at loaded and free ends. ....., Free end; ——, loaded end.

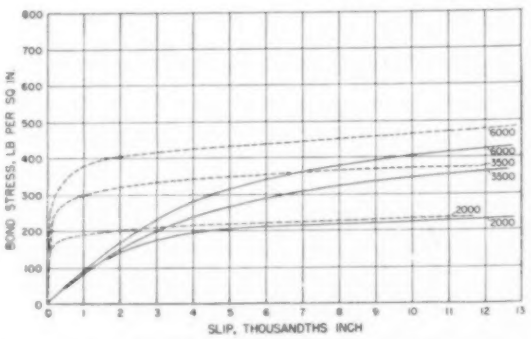

FIGURE 33. *Bond-slip curves for ½-in. Bar No. 6 in 2,000-3,500- and 6,000-lb strength concretes, top cast, in pull-outs.*

Slip measured at loaded and free ends. ....., Free end; ——, loaded end.

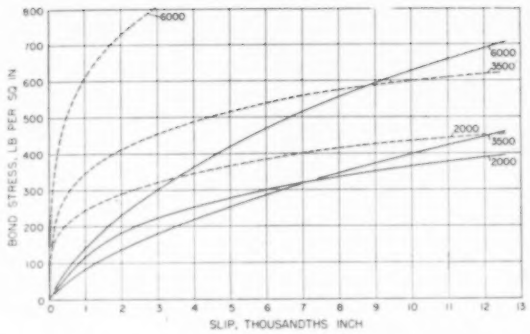

FIGURE 34. *Bond-slip curves for 1⅛-in. Bar No. 6 in 2,000- 3,500- and 6,000-lb strength concretes, bottom cast in pull-outs.*

Slip measured at loaded and free ends. ....., Free end; ——, loaded end.

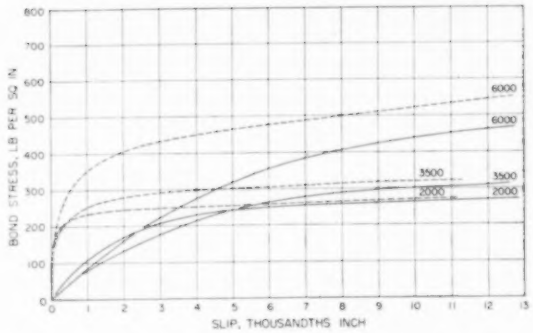

FIGURE 35. *Bond-slip curves for 1⅛-in. Bar No. 6 in 2,000-, 3,500- and 6,000-lb strength concretes, top cast, in pull-outs.*

Slip measured at loaded and free ends. ....., Free end; ——, loaded end.

WASHINGTON, August 16, 1949.

U. S. Department of Commerce
National Bureau of Standards

Research Paper RP2051
Volume 43, December 1949

Part of the Journal of Research of the National Bureau of Standards

Analysis of the Direct-Current Bolometer Bridge

By David M. Kerns

The behavior of a direct-current Wheatstone bridge with a nonlinear element (bolometer) in one arm, as used in the measurement of microwave power, is analyzed. Results of rather general applicability are obtained by ascribing arbitrary values to the resistances making up the bridge-network and by employing a resistance law of a general form for the bolometer element. Emphasis is placed upon the development of first-order theory in convenient form. General characteristics of the behavior of the type of network (and nonlinear element) under consideration are indicated. Results obtained include expression for the derivatives of galvanometer current with respect to radio-frequency power, ambient temperature, source-voltage, and source-resistance.

I. Introduction

Bolometers, consisting, for example, of bead thermistors or of fine platinum wires, have received wide use as microwave power measuring elements. In this application a bolometer is mounted in a wave-guide structure whose function is to enable the bolometer to absorb radio-frequency power from a source whose output is to be measured. The bolometer is also connected into a direct-current (or low-frequency alternating-current) network whose functions are to detect or measure changes in bolometer resistance and to supply bias power to the bolometer. Thus in this arrangement the total electrical power dissipated in the bolometer consists of bias power plus any radio-frequency power that may be present. An essential property of the bolometer is, of course, that its resistance, through the dependence of the resistance upon temperature, is determined in a given environment by the total electrical power dissipated in the bolometer. Thus radio-frequency power may be measured in terms of the change of resistance produced by the application of the power to be measured, or it may be measured by the change in bias power required to keep the resistance constant. These principles have been employed in various, more or less elaborate, arrangements;[1] technical details, however, are not needed for the purpose of this paper.

[1] See, for example, Technique of microwave measurements **11**, chapter 3, MIT Radiation Laboratory series (McGraw-Hill Book Co., New York, N. Y., 1947).

This paper is concerned with the analysis of the behavior of what is probably the simplest bolometer circuit-arrangement that is useful in power measurements by the methods outlined. This arrangement is the Wheatstone-bridge network shown in figure 1. The analysis of this network, however, is general: arbitrary values are ascribed to the resistances making up the network, and a resistance law of a general form is employed for the bolometer. Previously published analytical work on networks of the type considered (see footnote 1) is less general and in some respects less complete than that given here.

The point of view of this discussion, and the particular results derived, are perhaps especially appropriate in the planning and the analysis of precise experiments or measurements. Nevertheless, the treatment at the same time provides a basis for an understanding of some of the general characteristics of the behavior of the type of bolometer-bridge arrangement considered.

Although Wheatstone-bridge calculations can become tedious, it is found possible to put the calculations in a relatively convenient form and to obtain results in forms suited to numerical calculation. The notation and the methods used can be applied to the investigation of features of more specialized interest than those considered here. (A few identities that have been found of value in such investigations are given in the appendix.)

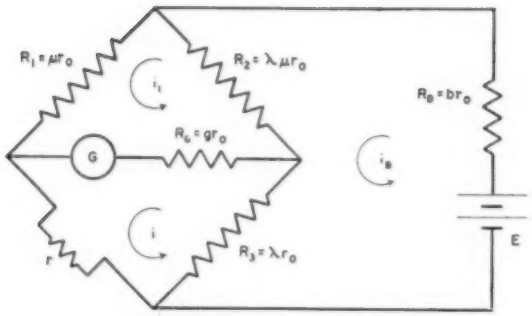

FIGURE 1. *Network and notation.*

II. Expressions for the Currents

The first task is to obtain convenient expressions for the currents in a Wheatstone-bridge network in which a bolometer of resistance r constitutes one arm. The bolometer is a nonlinear element; r is its direct-current resistance, defined by the equation $e=ri$, where i is the bolometer current, and e is the voltage across the bolometer terminals. In obtaining these first formulas, however, the value of r is assumed to be given, so that the nonlinear behavior of the bolometer does not at first come into consideration.

The network and the notation are illustrated in figure 1. R_1,R_2,R_3 are the respective resistances of three arms of the bridge, R_G is the resistance of the galvanometer branch, R_B is the resistance of the battery branch, and E is the battery voltage. Instead of employing these quantities directly as parameters of the network, it is of some convenience in numerical calculation and in the algebraic work to employ another set defined as follows. The bolometer resistance r_0 for which the bridge is balanced is given by

$$r_0R_2=R_1R_3. \tag{1}$$

It is convenient to introduce r_0 as an explicit parameter and to express R_1,R_2,R_3 in terms of r_0 and two ratios λ,μ by means of the equations

$$R_1=\mu r_0,\ R_2=\lambda\mu r_0,\ R_3=\lambda r_0. \tag{2}$$

Clearly these equations are such that (1) is automatically satisfied. The quantities R_B, R_G will also be expressed in terms of r_0 by letting

$$\left.\begin{aligned} R_B&=br_0,\\ R_G&=gr_0,\end{aligned}\right\} \tag{3}$$

where b, g are dimensionless parameters. The six quantities r_0, λ, μ, b, g, E will be regarded as the basic parameters of the network.

The system of equations for the mesh currents i_B,i_1,i (which are illustrated in fig. 1) may be written

$$\left.\begin{aligned} E/r_0&=(b+\lambda+\lambda\mu)i_B-\lambda\mu i_1-\lambda i,\\ 0&=-\lambda\mu i_B+(g+\mu+\mu\lambda)i_1-gi,\\ 0&=-\lambda i_B-gi_1+(g+\lambda+r/r_0)i.\end{aligned}\right\} \tag{4}$$

The determinant of this system is

$$D=\begin{vmatrix} b+\lambda+\lambda\mu & -\lambda\mu & -\lambda\\ -\lambda\mu & g+\mu+\mu\lambda & -g\\ -\lambda & -g & g+\lambda+r/r_0\end{vmatrix}. \tag{5}$$

Let M_B,M_1,M denote respectively the cofactors of the first, the second, and the third elements in the first row of (5). One may then write for the mesh currents and the galvanometer current

$$i_B=M_BE/(r_0D)=[(1+\lambda)g\mu+(r/r_0+\lambda)(g+\mu+\mu\lambda)]\,E/(r_0D), \tag{6}$$

$$i_1=M_1E/(r_0D)=(g+g\mu+\mu\lambda+\mu r/r_0)\lambda E/(r_0D), \tag{7}$$

$$i=ME/(r_0D)=(g+g\mu+\mu\lambda+\mu)\lambda E/(r_0D), \tag{8}$$

$$i_G=i-i_1=(1-r/r_0)\lambda\mu E/(r_0D). \tag{9}$$

When $r=r_0$—that is, when the bridge is balanced—the cofactors just defined are evidently related by

$$M=(M_1)_0=(M_B)_0\lambda/(1+\lambda), \tag{10}$$

so that

$$i_0=(i_1)_0=(i_B)_0\lambda/(1+\lambda), \tag{11}$$

where, by inspection of the network,

$$(i_B)_0=(E/r_0)\left[b+\lambda\,\frac{1+\mu}{1+\lambda}\right]^{-1}. \tag{12}$$

(The subscript zero will be used generally to denote quantities evaluated for $r=r_0$.)

It is advantageous to write the determinant D in the form

$$D=p+qr/r_0, \tag{13}$$

where p and q do not depend upon r. By comparing (12) and (6) it is easily found that

$$D_0=(g+g\mu+\mu+\mu\lambda)(b+b\lambda+\lambda+\lambda\mu). \quad (14)$$

To evaluate D for general values of r, both p and q must be known. The quantity q is the coefficient of r/r_0 in the expansion of the determinant (5):

$$q=(b+\lambda+\lambda\mu)(g+\mu+\mu\lambda)-(\lambda\mu)^2. \quad (15)$$

An expression for p is perhaps most easily obtained by noting that $D_0=p+q$ and calculating $p=D_0-q$. The result is

$$p=(g+g\mu+\mu\lambda)(b+b\lambda+\lambda\mu)-gb. \quad (16)$$

This expression may be verified, if desired, by expanding the determinant (5) with $r=0$, since D evaluated for $r=0$ is precisely p.

By Thévenin's theorem, the network into which the bolometer is connected may be represented by a suitable voltage E' and resistance R' in series. These quantities may be evaluated in a convenient form by using (13) and (8) to write

$$i=\frac{EM/q}{r_0p/q+r}.$$

But i is to be given by $E'/(R'+r)$; hence

$$E'=EM/q, \qquad R'=r_0p/q. \quad (17)$$

Since M,p,q, are independent of r, the quantities E',R' are also independent of r, as indeed they must be.

The expression (9) for galvanometer current may now be put in a useful form, which shows explicitly the dependence upon r, viz,

$$i_G=I\frac{r_0-r}{R'+r}, \quad (18)$$

where I is an abbreviation for $E\lambda\mu/(r_0q)$. As the final preliminary formula, the solution of this last equation for r is recorded:

$$r=r_0-(R'+r_0)\frac{i_G/I}{1+i_G/I}. \quad (19)$$

III. Introduction of a General Bolometer Law

The currents calculated in the preceding section are those that are obtained when the bolometer has the resistance r. To approach the essential problem of determining the bolometer resistance actually assumed under various operating conditions, some expression for the law of resistance of the bolometer must be introduced. It is both convenient and informative to employ a resistance law of a general form,

$$r=r(T,P), \quad (20)$$

where r is the direct-current resistance of the bolometer, T is the *ambient* temperature, and P is the electrical power dissipated in the bolometer. This electrical power is considered to be the sum of two terms,

$$P=P_{dc}+P_{rf}, \quad (21)$$

where P_{dc} and P_{rf} are respectively the direct-current power and the radio-frequency power dissipated in the bolometer. Equations 20 and 21 contain the assumption that direct-current power and radio-frequency power have precisely equivalent effects on the bolometer resistance. Thermal lag prevents the bolometer resistance from following rapid changes of either ambient temperature or electrical power; the law (20) is therefore to be understood as giving equilibrium values of r. It may be noted that, in particular, the respective resistance laws used for bead-thermistor and platinum-wire bolometers can be written in the form (20).

The behavior of a bolometer in the neighborhood of a given operating point (T,P) is characterized by two partial derivatives evaluated at that point. The basic equation is simply

$$dr=\left(\frac{\partial r}{\partial T}\right)_P dT+\left(\frac{\partial r}{\partial P}\right)_T dP. \quad (22)$$

If r is held constant, the resistance law $r=r(T,P)$ defines a relationship between T and P. From the rule for the differentiation of implicit functions (or, indeed, directly from the differential equation 22), one may write

$$\left(\frac{\partial P}{\partial T}\right)_r=-\left(\frac{\partial r}{\partial T}\right)_P\Big/\left(\frac{\partial r}{\partial P}\right)_T \quad (23)$$

Any two of the derivatives in this equation determine the third. In practice it is sometimes convenient to make use of this fact, determining $(\partial r/\partial T)_P$ by measuring the other two derivatives rather than by measuring it directly.

Upon introducing the notation

$$\left(\frac{\partial r}{\partial P}\right)_T=\gamma, \left(\frac{\partial P}{\partial T}\right)_r=-\frac{1}{c}, \tag{24}$$

the identity (23) may be written

$$\left(\frac{\partial r}{\partial T}\right)_P=\frac{\gamma}{c}, \tag{23'}$$

and the expression (22) for dr becomes (22')

$$dr=\gamma(dT/c+dP).$$

The important parameter γ, which is the rate of change of bolometer resistance with respect to electrical power at a given ambient temperature, is the "ohms-per-watt" coefficient characteristic of the bolometer. The differential coefficient $(\partial P/\partial T)_r$, as suggested by the notation chosen for it, is in many cases a constant to a good approximation. But it should be remembered that both γ and c are, in general, functions of T and P.

The resistance law (20) may be written in the form

$$P=P(T, r), \tag{25}$$

which represents (20) solved for P. For $r=r_0$, $P_{rf}=0$, and any fixed value of T, the bolometer current is i_0, where

$$r_0 i_0^2=P(T, r_0), \tag{26}$$

since $P=P_{dc}=r_0 i_0^2$. The current i_0 is also given by

$$i_0=E'/(R'+r_0),$$

where E', R', as defined in section II, represent the bridge into which the bolometer is connected. By eliminating i_0 between the last two equations, one obtains

$$E'/(E'+r_0)=\sqrt{P(T, r_0)/r_0}. \tag{27}$$

The process of balancing the bridge consists of adjusting the bridge-parameters involved so that (27) is in fact satisfied. The left-hand side of (27) may be written in a form that exhibits the parameters involved:

$$E'/(R'+r_0)=(\lambda E)[r_0(b+b\lambda+\lambda+\lambda\mu)]^{-1}.$$

In many cases λ and μ, as well as r_0, are preferably not varied; in these cases, b or E (or both) may be adjusted to obtain bridge-balance. The bolometer current i_0 obtained when the bridge is balanced (with $P_{rf}=0$) is often called the bias current.

The fundamental equations applying to the so-called balanced-bridge method of measuring radio-frequency power are very easily obtained. If the bridge is balanced with radio-frequency power present, the corresponding bolometer current satisfies

$$r_0 i^2=P(T, r_0)-P_{rf}. \tag{28}$$

On the other hand, (26) holds when the bridge is balanced with no radio-frequency power present. Equations 26 and 28 combined yield the equation

$$P_{rf}=r_0(i_0^2-i^2), \tag{29}$$

for the determination of P_{rf} in terms of r_0 and measured values of i and i_0. Granted the assumption of the form of the bolometer law itself, there remain two basic assumptions involved in (29). These are discussed briefly in the following two paragraphs.

Equation 29 involves the assumption that i_0 and i are measured under conditions of thermal equilibrium at the same ambient temperature T. If i_0 is measured at temperature T and i at temperature $T+dT$, eq 29 is replaced by the approximate equation

$$\left.\begin{aligned} P_{rf}&=r_0(i_0^2-i^2)+\left(\frac{\partial P}{\partial T}\right)_r dT \\ &=r_0(i_0^2-i^2)-dT/c. \end{aligned}\right\} \tag{30}$$

This equation is correct to the first order, provided that the somewhat unrealistic condition of thermal equilibrium at each of the two temperatures T and $T+dT$ is fulfilled.

The value of r_0, as a parameter of the bridge, can be made very precise. But the use of $r=r_0$ in 29 implies that the bridge is exactly balanced when the two currents are measured. The uncertainty in obtaining $r=r_0$ is determined largely by the useful sensitivity of the bridge with respect to unbalance. It is convenient to estimate the corresponding contribution to the uncertainty in P_{rf} directly (rather than by first finding the uncertainty in r) by means of an equation of the form

$$dP_{rf}=\frac{\partial P_{rf}}{\partial i_G}di_G, \tag{31}$$

with di_G placed equal to the smallest detectable change in galvanometer current. The quantity $(\partial i_G/\partial P_{rf})$, which is frequently called the "*rf* sensitivity," can be calculated by means of formulas to be derived later.

In the so-called unbalanced-bridge, or deflection method of measuring radio-frequency power, no adjustment of the initially balanced bridge is made when the radio-frequency power is applied, and the resulting value of galvanometer current is taken as a measure of the power. In this method the nonlinearity of the relationship of P_{rf} to i_G is naturally of some concern. For this reason an extension of 31 to include the quadratic term in i_G is given (section V).

In the treatment of nonlinear circuit elements, the nonlinear element is often described by a law written in the form

$$e=f(i). \tag{32}$$

Such a relationship—or rather a family of such relationships, with P_{rf}=constant, T=constant as parameters—is indeed defined by the bolometer resistance law in the form already adopted.

If an element having the e-i characteristic (32) is connected to a source consisting of a voltage E' and a resistance R' in series, the resulting current must simultaneously satisfy the two equations

$$\left.\begin{aligned} e&=f(i),\\ e&=E'-iR'. \end{aligned}\right\} \tag{33}$$

In other words, i must satisfy the equation

$$f(i)=E'-iR'.$$

Let E', R' receive increments dE', dR', respectively. Then the corresponding differential of i is given by

$$di=\frac{dE'-idR'}{R'+r_e}, \tag{34}$$

where r_e, denoting the derivative of f with respect to i, is the variational resistance (for slow variations) of the element. Thus with respect to small changes in E' and R', the nonlinear element behaves like an ohmic element of resistance r_e.

An expression for r_e may be derived from the resistance law in the original form (20). The equation

$$e-ir(T, P_{rf}+ei)=0, \tag{35}$$

which is obtained from (20) by substituting $r=e/i$ and $P_{dc}=ei$ in that equation, may be regarded as an identity in e or i for fixed values of T and P_{rf}, and thereby defines $e=f(i)$. The variational resistance is obtained from (35) as the derivative of an implicit function:

$$r_e=-\frac{\dfrac{\partial}{\partial i}\left[e-ir(T, P_{rf}+ei\right]}{\dfrac{\partial}{\partial e}\left[e-ir(T, P_{rf}+ei\right]}=-\frac{-r-i\epsilon\gamma}{1-i^2\gamma},$$

where $\gamma=(\partial r/\partial P)_T$ as previously defined. In a slightly modified form

$$r_e=r\,\frac{1+i^2\gamma}{1-i^2\gamma}. \tag{36}$$

This identity will be used to obtain an alternative form of one of the expressions to be derived in the next section.

IV. First-Order Theory

Since, so far as the bolometer is concerned, the bridge is completely represented by the equivalent E', R', the effects upon the bolometer of changes in any of the basic parameters characterizing the bridge in detail may be evaluated in terms of corresponding changes in E' and R'. Accordingly, in setting up the basic equation for a complete first-order theory, the quantities E', R', r, T, P_{rf} are selected as variables.

Equation 22′ may be written

$$dr=\gamma(dT/c+dP_{rf}+dP_{dc}),$$

where dP is separated into its parts dP_{rf}, dP_{dc}. Since P_{dc} is given in terms of E', R', r by $P_{dc}=rE'^2/(R'+r)^2$, the differential of P_{dc} is given by

$$dP_{dc}=\frac{2E'rdE'}{(R'+r)^2}+\frac{E'^2(R'-r)dr}{(R'+r)^3}-\frac{2E'^2rdR'}{(R'+r)^3},$$

which may be more conveniently written as

$$dP_{dc}=\eta i^2dr+2P_{dc}(dE'-idR')/E',$$

where, in addition to the obvious relation $i=E'/(R'+r)$, the notation

$$\eta=\frac{R'-r}{R'+r}$$

has been used. If this expression for dP_{dc} is substituted into the above expression for dr, one obtains upon solving for dr,

$$dr=\gamma_e[dT/c+dP_{rf}+2P_{dc}(dE'-idR')/E'], \quad (37)$$

where

$$\gamma_e=\frac{\gamma}{1-i^2\gamma\eta}. \quad (38)$$

Equation 37 serves as the basic equation for the first-order theory.

The role of the factor γ_e in (37) is significant. If E',R',T are held constant, equation 37 states that $dr=\gamma_e dP_{rf}$. Thus γ_e might be denoted by $(\partial r/\partial P_{rf})_T$ and is an effective ohms-per-watt coefficient, which depends not only upon the characteristics of the bolometer but also upon the network into which the bolometer is connected. γ_e, as a multipler in (37), includes the effect of the change in P_{dc} concomitant to a change in any one of the variables T,P_{rf},E',R'. The quantity η (which appears in the denominator of the expression (38) for γ_e) is in fact of the form of a reflection coefficient and is a measure of the mismatch between the equivalent source and its load.

Under certain conditions very large values for γ_e can be obtained. By inspection of the denominator of (38) it is apparent that $|\gamma_e|\to\infty$ if

$$\gamma\to\frac{1}{i^2\eta}=\frac{1}{i^2}\cdot\frac{R'+r}{R'-r}.$$

Comparing this expression with the relation (36), it is evident that this condition is equivalent to $r_v\to -R'$, as indeed might be expected. This fact is also apparent in another form for the expression for γ_e, which is obtained by using (36) to eliminate γ from (38). The result is

$$\gamma_e=\frac{R'+r}{2P_{dc}}\cdot\frac{r_v-r}{r_v+R'}. \quad (39)$$

Thus when r_v is negative (as it is for a bead thermistor under typical operating conditions), arbitrarily large values of γ_e can in principle be obtained by making $R'\to -r_v$. Unfortunately this fact is of somewhat limited usefulness in power measurement, because, as is evident from (37), the sensitivity of r to changes in all the other variables increases when the sensitivity to radio-frequency power—the desired sensitivity—is increased.

So far, this discussion has dealt essentially with changes produced in r. The sensitivity of the galvanometer current (which, rather than r, is the observed quantity) to changes in radio-frequency power, temperature, source-voltage (E), and source-resistance (R_B) will now be calculated. These sensitivities are perhaps most naturally denoted as partial derivatives, but neither the partial nor the total derivative notation is adequate to express their precise meanings. The selected independent variable, the dependent variables, and the quantities held constant must be noted in each case.

a. *RF power sensitivity, S_{rf}.* Consider first the sensitivity of galvanometer current to changes of radio-frequency power, with the temperature and all network parameters (including E) being held constant. Under these conditions the first-order change di_G in galvanometer current corresponding to a change dr in bolometer resistance is given by

$$di_G=\frac{\partial}{\partial r}\left(I\,\frac{r_0-r}{R'+r}\right)dr=-I\,\frac{R'+r_0}{(R'+r)^2}\,dr, \quad (40)$$

where the expression (18) for i_G is used. From (37) one finds

$$dr=\gamma_e dP_{rf},$$

since T,E',R' are here constants. Hence, letting $S_{rf}=\partial i_G/\partial P_{rf}$, one has the result

$$S_{rf}=-I\gamma_e\frac{R'+r_0}{(R'+r)^2}. \quad (41)$$

b. Temperature sensitivity, S_T. The definition of the temperature sensitivity differs from that for S_{rf} only in that T instead of P_{rf} is taken as the independent variable. Hence, from (37),

$$dr=\gamma_e dT/c.$$

Combining this with (40), and using the notation $S_T=\partial i_G/\partial T$, the result may be written

$$S_T=S_{rf}/c. \quad (42)$$

c. Sensitivity to source-voltage, S_E. The sensitivity of galvanometer current to changes in source-voltage E is calculated by considering E as the independent variable, all other circuit parameters, as well as T and P_{rf}, being held constant. In this case (40) must be replaced by the more general expression

$$di_G=\frac{i_G}{E}dE-I\frac{R'+r_0}{(R'+r)^2}dr, \qquad (40')$$

in which the additional term appears because (unless the bridge is initially balanced) i_G depends upon E directly, as well as indirectly through the dependence of r on E. From (37),

$$dr=2\gamma_e P_{dc}dE'/E'.$$

Since the network parameters are not varied, dE'/E' is equal to dE/E. It follows that

$$S_E=\frac{\partial i_G}{\partial E}=\frac{i_G}{E}-\frac{2\gamma_e P_{dc}I(R'+r_0)}{E(R'+r)^2}, \qquad (43)$$

where S_E is the desired sensitivity.

d. *Sensitivity to source-resistance*, S_B. The sensitivity of galvanometer current to changes in source-resistance is obtained by considering b as the independent variable, all other network parameters, as well as T and P_{rf}, being held constant. From the expression (18) for i_G it is apparent that the expression corresponding to (40), if written out, would have three terms, since q,R', and r depend upon b. Moreover dr is given by

$$dr=2\gamma_e P_{dc}(dE'-idR'),$$

wherein dE' and dR' are determined by the dependence of E' and R' upon b. (The dependence of E' and R' upon b is given explicitly by eq 15, 16, and 17. Although the calculations implied by these remarks can be carried out in fairly compact form, the result may be obtained by the following simpler method. If E and R_B are both varied, then di_G is given by

$$di_G=S_E dE+S_B dR_B,$$

where S_B denotes the sensitivity to be calculated. Now the bridge as a whole may be considered as a nonlinear element connected to the source consisting of E and R_B in series, and the principle expressed by (34) may be applied to this circuit:

$$di_B=\frac{dE-i_B dR_B}{R_B+F'(i_B)}.$$

In this expression i_B is battery-branch current (as defined in section II), and $F'(i_B)$ represents the variational resistance of the bridge as a whole. Suppose that E and R_B are varied in such a way that $di_G=0$; this requires $di_B=0$, which in turn requires that $dE=i_B dR_B$. Hence, from the above expression for di_G,

$$0=(S_E i_B+S_B)dR_B,$$

and the desired result is given by the simple relation [2]

$$S_B=-i_B S_E. \qquad (44)$$

The expressions for the sensitivities calculated above simplify somewhat when evaluated for $r=r_0$. It may be observed that

$$(S_{rf})_0=\frac{E}{2P_{dc}}(S_E)_0.$$

Also, by (44),

$$(S_{rf})_0=-\frac{E}{2i_B P_{dc}}(S_B)_0.$$

These equations suggest a method of evaluating $(S_{rf})_0$ by means of direct-current measurements.

V. A Second-Order Calculation

Taking the resistance law in the form (25), separating P into its components P_{rf},P_{dc}, and replacing P_{dc} by $E'^2r/(R'+r)^2$, one obtains

$$P_{rf}=P(T,r)-E'^2r/(R'+r)^2. \qquad (45)$$

P_{rf} becomes a function of i_G through the dependence of r upon i_G, as given by eq 19,

$$r-r_0=-(R'+r_0)\frac{i_G/I}{1+i_G/I}. \qquad (19)$$

Equation 45, with the implied elimination of r by means of (19), represents an analytical expression for $P_{rf}(i_G)$, i. e., for the calibration curve of the bolometer bridge as used in the unbalanced bridge method of measuring radio-frequency power. For some purposes a power-series expansion of $P_{rf}(i_G)$ is useful.

Elimination of r from the last term of (45) yields

$$P_{dc}=i_0^2\left[r_0+(r_0-R')\frac{i_G}{I}-R'\left(\frac{i_G}{I}\right)^2\right]. \qquad (46)$$

Thus P_{dc} is given in general and without approximation as a quadratic in i_G. Let it be assumed that $P(T,r)$ can be expanded in the series

$$P(T,r)=P(T,r_0)+P_1(T,r_0)(r-r_0)+\frac{1}{2}P_2(T,r_0)(r-r_0)^2+\ldots,$$

[2] This result could have been obtained, with a slight gain in brevity, by employing a standard network theorem generally known as the compensation theorem. The argument given avoids any question of the applicability of the theorem to a circuit involving a nonlinear element.

convergent for $|r-r_0|<\rho$, say, where $P_1,P_2\ldots$ denote the successive derivatives of $P(T,r)$ with respect to r. The expression for $r-r_0$ can be expanded in the series

$$r-r_0=(R'+r_0)\left[-\frac{i_G}{I}+\left(\frac{i_G}{I}\right)^2-\left(\frac{i_G}{I}\right)^3+\ldots\right],$$

which converges for $|i_G|<I$. (The algebraically largest and smallest values of i_G are I and $-(R'/r_0)I$, corresponding respectively to $r\to\infty$ and $r=0$. Thus only if $R'\leqq r_0$ does the series for $r-r_0$ converge for all physically possible values of i_G.) Substituting this series into the series for $P(T,r)$, ordering according to powers of i_G, and dropping powers of i_G higher than the second, one finds

$$P(T,r)=P(T,r_0)-P_1(T,r_0)(R'+r_0)\frac{i_G}{I}+\left[\frac{1}{2}P_2(T,r_0)(R'+r_0)^2+P_1(T,r_0)(R'+r_0)\right]\left(\frac{i_G}{I}\right)^2+\cdots \tag{47}$$

Here i_G is understood to be restricted so that the conditions $|r-r_0|<\rho$ and $|i_G|<I$ are both satisfied. Equations 46 and 47 together yield the expansion of (45):

$$P_{rf}=P(T,r_0)-r_0i_0^2-[P_1(T,r_0)(R'+r_0)+i_0^2(r_0-R')]\frac{i_G}{I}+\left[\frac{1}{2}P_2(T,r_0)(R'+r_0)^2+P_1(T,r_0)(R'+r_0)+i_0^2R'\right]\left(\frac{i_G}{I}\right)^2+\cdots$$

If, as is assumed, $P_{rf}=0$ when $i_G=0$, then the constant term vanishes. Further, the coefficient of i_G is necessarily equal to $(S_{rf})^{-1}$ (to verify, note that $P_1(T,r)=1/\gamma$, and compare with (41)). Hence the final second-order expression may be written

$$P_{rf}=(S_{rf})_0^{-1}i_G+\left[\frac{1}{2}P_2(T,r_0)(R'+r_0)^2+P_1(T,r_0)(R'+r_0)+i_0^2R'\right]\left(\frac{i_G}{I}\right)^2. \tag{48}$$

VI. Appendix

In this appendix are derived several identities that are useful in various extensions of the calculations of the text. These identities involve primarily the quantities M,p,q derived from the determinant D, and the determinant D itself. All of the quantities involved (except one as noted) are as defined in section II of the text. The relationships to be obtained hold for arbitrary values of the quantities r,r_0,λ,μ,b,g appearing in the expression (5) for D. These quantities here may be, and are, considered as independent variables.

The calculations are conveniently based upon a theorem on determinants [3] that states that if D is any determinant and S is the second *minor* obtained from it by striking out its i^{th} and k^{th} rows and its j^{th} and l^{th} columns, and if A_{ij} denotes the *cofactor* of the element that stands in the i^{th} row and the j^{th} column of D, then

$$\begin{vmatrix} A_{ij} & A_{il} \\ A_{kj} & A_{kl} \end{vmatrix}=(-1)^{i+j+k+l}DS.$$

This theorem, applied to the determinant (5) with $i=j=1$, $k=l=3$, yields

$$\begin{vmatrix} M_B & M \\ M & q \end{vmatrix}=(g+\mu+\mu\lambda)D.$$

Now $g+\mu+\mu\lambda$ is equal to $\partial q/\partial b$, and M_B is equal to $\partial D/\partial b$. Hence the above equation may be written

$$M^2=q\frac{\partial D}{\partial b}-D\frac{\partial q}{\partial b}. \tag{49}$$

This identity is a key to the establishment of others of more immediate physical significance. Thus, the derivative of the equivalent resistance R' with respect to battery-branch resistance R_B is

$$\frac{\partial}{\partial b}\left(\frac{p}{q}\right)=\frac{\partial}{\partial b}\left(\frac{D}{q}\right)=\left(q\frac{\partial D}{\partial b}-D\frac{\partial q}{\partial b}\right)/q^2$$

Therefore, by (49),

$$\frac{\partial}{\partial b}\left(\frac{p}{q}\right)=\left(\frac{M}{q}\right)^2. \tag{50}$$

The derivative of the quantity $\eta=(R'-r)/(R'+r)$ (introduced in connection with eq 37) with respect to the parameter b is easily obtained:

$$\frac{\partial\eta}{\partial b}=\frac{\partial\eta}{\partial R'}\frac{\partial R'}{\partial b}=\frac{2rr_0}{(R'+r)^2}\left(\frac{M}{q}\right)^2;$$

upon noting that $q(R'+r)=r_0(p+qr/r_0)=r_0D$, one has

$$\frac{\partial\eta}{\partial b}=2\left(\frac{r}{r_0}\right)\left(\frac{M}{D}\right)^2. \tag{51}$$

There are corresponding expressions for the derivatives of R' and η with respect to galvanometer resistance. These are readily obtained by making use of the fact that the interchanges

$$g\to b,\quad \lambda\to\mu,$$
$$b\to g,\quad \mu\to\lambda,$$

[3] M. Bôcher, Introduction to higher algebra, p. 33 (Macmillan Co., New York, N. Y., 1907).

leave the quantities p and q unchanged. That is, if (*) denotes the quantity as transformed by the set of interchanges, then

$$q^*=q,\ p^*=p.$$

From this property and from eq 50 and 51, it follows that

$$\frac{\partial}{\partial g}\left(\frac{p}{q}\right)=\left[\frac{\partial}{\partial b}\left(\frac{p}{q}\right)\right]^*=\frac{(M^2)^*}{q^2},$$

and that

$$\left(\frac{\partial \eta}{\partial g}\right)=\left(\frac{\partial \eta}{\partial b}\right)^*=2\left(\frac{r}{r_0}\right)\frac{(M^2)^*}{D^2}.$$

These two results are put into final form by making use of the relation $MM^*=\lambda\mu D_0$, which is evident from the explicit formulas for M and D_0. One obtains

$$\frac{\partial}{\partial g}\left(\frac{p}{q}\right)=\left(\frac{\lambda\mu D_0}{Mq}\right)^2, \tag{52}$$

$$\frac{\partial \eta}{\partial g}=2\left(\frac{r}{r_0}\right)\left(\frac{\lambda\mu D_0}{MD}\right)^2. \tag{53}$$

Equations 51 and 53 simplify to some extent when, in particular, $r=r_0$. In some cases one might wish to make use of the fact that M/λ is a factor of D_0.

The author is grateful to Harold Lyons, Chief of the Microwave Standards Section, National Bureau of Standards, for encouragement in the preparation of this paper.

WASHINGTON, October 6, 1948.

U. S. Department of Commerce
National Bureau of Standards

Research Paper RP2052
Volume 43, December 1949

Part of the Journal of Research of the National Bureau of Standards

A Method and Apparatus for Determining the Ignition Characteristics of Plastics

By Nicholas P. Setchkin

A method for the determination of the ignition temperatures of plastics is described. It is suitable for the determination of flash-, as well as self- or autogenous-ignition temperatures. The flash temperature is that temperature at which the specimen yields combustible gases ignitible by a flame. The self-ignition temperature is the lowest temperature of supplied air, under optimum conditions of air flow, at which a reaction of the specimen, or of its decomposition products, begins and is self-accelerated to the state of combustion. The described method generally results in lower and more consistently reproducible values of the self-ignition temperature than those reported by several other investigators.

Twenty-seven different specimens of plastics, covering a wide range in characteristics, were tested by the method described.

I. Introduction

An apparatus and method for determining the ignition characteristics and behavior of plastics under well-controlled conditions have been developed at this Bureau from a consideration of the fundamental principles of ignition. Twenty-seven specimens of plastics with a wide range of physical properties and ignition characteristics were tested in order to determine the validity of the method and the adaptability of the apparatus.

It is doubtful whether methods heretofore proposed for measuring the ignition temperatures of plastics actually indicate the lowest ignition temperatures. Stokes and Weber [1] [1] measured the ignitability of plastics by bringing the specimen into contact with a heated porcelain rod just removed from a furnace, or with a molten lead bath heated in a furnace to the required temperature. The estimated temperature of the porcelain rod or of the lead, at which the specimen "instantly" ignited, was accepted by them as the ignition temperature. Delmonte and Azam [2] later substituted molten sodium hydroxide for the lead bath. In their tests, the bath temperature at which a plastic specimen ignited instantly, or within 10 sec, when in contact with the bath was considered as the ignition temperature of the material. More recently, Schoenborn and Weaver [3] used a method in which the specimen was placed in a furnace heated to a temperature definitely above the ignition temperature of the material. The ignition temperature was defined by the estimated surface temperature of the specimen at the instant of the ignition and was called by them the "apparent ignition temperature." The estimate of this temperature was made by analytical extrapolation of temperatures measured within the specimen, to yield those at the surface at the moment of ignition.

In this method, observation of the temperatures and the extrapolation from them to the actual locus of ignition did not give consistent and reproducible results for a given material [4].

Gale, Stewart, and others [5, 6] used an electrically heated coil around the plastic specimen and observed the time lag required for gases developed from the specimen to be ignited by spark plugs. A so-called ignition temperature, (which in reality is the "flash temperature," as defined in section II) was determined by them from a "conversion curve." This curve was developed by measuring with a thermocouple the temperature at the edge of the specimen and observing the time lag for ignition. This time lag was composed of two superimposed periods; one of which was the time required to heat the coil, and the other was the time required to heat the specimen and to produce sufficient combustible gases to be ignited by the

[1] Figures in brackets indicate the literature references at the end of this paper.

spark plug. These superimposed lags are related to two entirely different phenomena, therefore the range of the ignition temperature, which indicates the accuracy of their determination (shown in table 3 of [6]), varied for a given plastic from 55° to 175° C, with an average of 127° C.

Most of the results obtained by these and similar methods differ materially in their numerical values, as well as in their consistency and reproducibility, because they were obtained under entirely different and noncomparable conditions that were unsuited for the determination of the lowest ignition temperatures. The main purpose of the studies at this Bureau was to develop a sound relation between the ignition phenomena and controllable conditions of test; and on this basis to determine the lowest values of the ignition temperatures and any other characteristics that may affect the fire hazards and therefore safety regulations.

II. Theoretical Considerations

Several years ago a constant-air-temperature method for measuring the ignition temperatures of solids, based upon the principles of ignition stated below, was developed at this Bureau. In this method, successive specimens of the material were heated in air at different constant temperatures until one of them ignited. The same method was found applicable for plastics with a wide range of thermophysical characteristics.

The following definitions of ignition characteristics of materials were employed in the development of the test method. The "flash temperature" is the initial temperature of the air passing around the specimen, at which a sufficient amount of combustible gas is developed to be ignited by an external heat source such as a flame, spark, or hot surface. The "self-ignition temperature" is the initial air temperature, at which, in the absence of an ignition source, ignition occurs of itself, as indicated by an explosion, flame, or sustained glow.

It is well known that the ignition of most combustible materials, excepting those such as cellulose nitrate that contain oxygen in an active form, can be initiated only in the presence of sufficient amounts of oxygen. Before ignition occurs, oxygen must participate in an oxidation reaction with the solid or liquid material, with the vapor, or with gases evolved at elevated temperatures from the decomposition of the material. In order to promote this reaction, the products of oxidation must be removed continuously and fresh portions of oxygen supplied. Actual ignition, as indicated by a flame, may result either from the accelerated exothermic reaction of vaporized or gaseous components of the material with oxygen, or through the self-heating within the solid or liquid material, which eventually leads to sustained glow of some of the nongaseous components or of the carbonized residue.

On the above basis, ignition can be defined as a self-perpetuating exothermic reaction that is initiated at the temperature of incipient oxidation, and that increases the temperature of the reactants above the initial air temperature until an explosion, flame, or sustained glow occurs. Because of the temperature differences existing within the reacting masses and between them and the surrounding walls, a certain part of the generated heat is dissipated to masses at lower temperatures. Also, some heat is carried away by the passing air and by the products of oxidation. The rate of the oxidation reaction, as well as the rate of its acceleration to self-ignition, is dependent upon the rate of heat dissipation. This will be evident from the following discussion of the time-temperature curves drawn in figure 1 for different initial temperatures.

If an incombustible material be subjected to heating at the constant-air-temperature, t_0, the temperature of the material will eventually be practically equal to that of the surrounding air, e. g. after the time lag l_0. This lag depends upon the mass, heat conductivity, and specific heat of the material and upon the initial temperature difference between the air and the material. At relatively low air temperatures, a similar behavior will be observed with conbustible materials. However, at a higher air temperature t_1, which is higher than the observed temperature of incipient oxidation t_x, the material begins to exidize with the generation of heat, and beyond the point t_x, the temperature of the material increases more rapidly than it would in the normal process of heating without oxidation. The temperature of the material continues to increase and eventually exceeds the air temperature, t_1. The rate of temperature increase depends upon the difference between the rates of heat generation and of heat

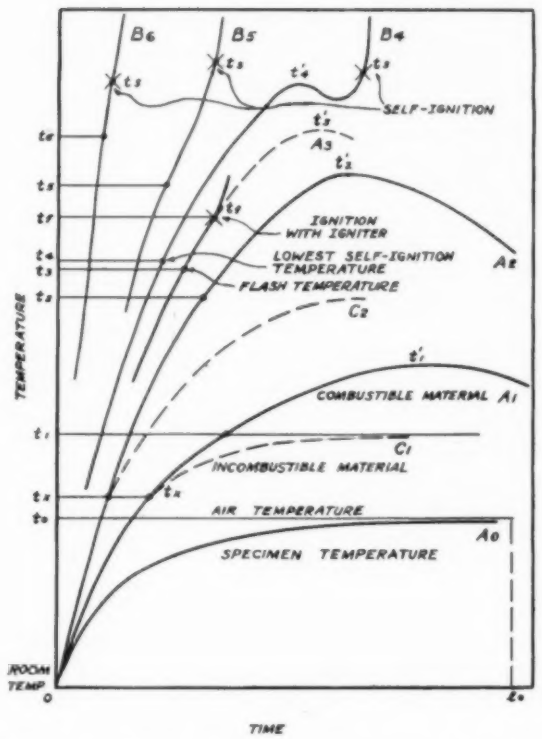

FIGURE 1. *Theoretical time-temperature curves for heating and ignition of materials.*

Curves A_0, A_1, A_2, and A_3 for nonignition reaction at air temperatures t_0, t_1, t_2, and t_3; curves B_4, B_5, and B_6 for self-ignition reaction at air temperatures t_4, t_5, and t_6; curves A_0, C_1, and C_2 for heating of noncombustible materials at air temperatures t_0, t_1, and t_2.

dissipation. The rate of heat generation depends mainly upon the temperatures of the specimen and of the air, the supply of air, the concentration of oxygen in the reacting gases, and the chemical and physical characteristics of the material. The rate of heat dissipation depends in part upon the temperature difference between the reacting mass and their surroundings, and in part upon the rate of flow of the air. An insufficient air flow leads to contamination of the air by the products of oxidation and depletes the oxygen supply. This condition hinders oxidation and lowers or stops entirely the exothermic reaction. On the other hand, an excessive air flow carries away a large amount of the generated heat and thus lessens or interrupts the exothermic reaction. The optimum rate of air flow, at which a relatively favorable rate of reaction is reached, must be established experimentally for each type of material. The temperature of the material usually continues to rise until the rate of heat generation equals the rate of heat dissipation, e. g. at a point corresponding to the maximum temperature t'_1, indicated by a thermocouple Th_3 (fig. 2) in or on the specimen. This process is often accompanied by the evolution of vapor gas, which at this particular stage may not be ignitible, either by itself or by an igniter, because of its low rate of evolution and consequent dilution with air.

At some other constant-air-temperature such as t_2, the material may self-heat by oxidation to a higher temperature such as t'_2. However, during self-heating, starting at an air temperature of t_3, the concentration of evolved combustible gases or vapors may become favorable to their ignition by the pilot flame at a particular temperature t_f, which is often below the maximum temperature t'_2 of the previous case, where the ignition could not have occurred. The air temperature t_3 in this case is called the flash temperature. In the absence of the ignition flame, self-heating may proceed to the corresponding maximum temperature t'_3 without self-ignition. Owing to these factors, regularly observed with many materials, the instantaneous temperature t_f has no important significance, even if it could be determined accurately, because this temperature, as well as the rate of heat generation and the rate of gas development and dilution, depend mainly upon the initial temperature and velocity of the air passing around the specimen.

In many cases, it was observed that the rate of the exothermic reaction was reduced beyond a temperature peak such as t'_4 by excessive contamination of the air with the decomposition products, by cooling caused by a high rate of air flow, by some endothermic reaction, or by reduction of the available reactive material. With proper adjustment of air flow (which reduces the rate of temperature rise near the point t'_4), it is possible for the rate of oxidation to be accelerated again to the self-ignition of gases at a higher temperature, such as t_s. This temperature, t_s, like the temperature t_f, has no important significance in relation to the ignition characteristics, because it depends upon both the initial air temperature t_4 and the rate of air flow. Therefore, the temperature t_4 of the air, at which with the optimum air flow and in the absence of an igni-

tion source, ignition occurs is called the self-ignition temperature of the material.

At higher initial air temperatures such as t_5 and t_6, self-ignition occurs more readily, and the ignition lag rapidly diminishes to a fraction of a second with continued increase in the initial temperature. The ignition lag for the lowest self-ignition temperature (t_4) may vary from a few minutes to a few hours, depending upon the difference between the rates of heat generation and heat dissipation, which is affected by the size of the specimen, as well as by the thermo-chemical and physical properties of the material.

The evidence of self-ignition is usually observed in the form of an explosion, flame, or sustained glow. In some plastic materials the ignition temperatures corresponding to the various types of behavior differ appreciably. The self-ignition accompanied by explosion or flame usually occurs at comparatively high initial air temperatures; however, slow decomposition and carbonization of some plastics leads to glow of the corners and edges at lower temperatures. Therefore, a secondary term, "self-ignition by glow", is proposed. The self-sustained glow may in some cases, with proper air flow, lead to ignition of the combustible gases.

The foregoing considerations indicate that "instant" ignition of the material in contact with a hot surface, as specified by some of the early methods, occurs at much higher temperatures than are observed with the constant-air-temperature method. Therefore, as explained in section V, 5 this hot-surface ignition temperature does not represent the true fire hazard of the materials.

III. Ignition Apparatus

The apparatus for the determination of the ignition characteristics of plastics was developed on the basis of the fundamentals of ignition phenomena discussed above. In the construction of the apparatus, particular attention was given to the following major requirements:

(a) The temperature of the air passing the specimen should be uniform and constant. (b) The air flow should be steady and controllable. (c) The specimen should be in a stream of air of known temperature; be visible from the outside; and be easily removable.

1. Construction of the Apparatus

The ignition apparatus shown in figure 2 consists of a vertical electrically heated furnace tube with a 4-in. (10 cm) bore, 8¾ in. (22 cm) long, made of refractory material such as a ceramic that will withstand at least 1,000° C. The furnace tube is heated by electric current passing through 50 turns of No. 16 B&S gage nichrome wire in an asbestos sleeve wound around the tube and imbedded in alundum cement. The inner refactory tube with a 3-in. (7.6-cm) bore, 8¾ in. (22 cm) long, about ⅛ in. (0.3 cm) thick is placed inside of the furnace tube and rests on small blocks in the bottom of the furnace. The space between the two tubes is used for circulation and heating of the air, admitted tangentially to the refractory tube through a copper tube. The preheated air enters the inner tube from below. The top of the latter tube is covered with a divided refractory disk with an opening for observation and for the passage of smoke and gases. If desired, a small gas flame can be lighted above the opening. An opening fitted width disk is provided at the bottom of the furnace for the removal of residue that accumulates during the tests.

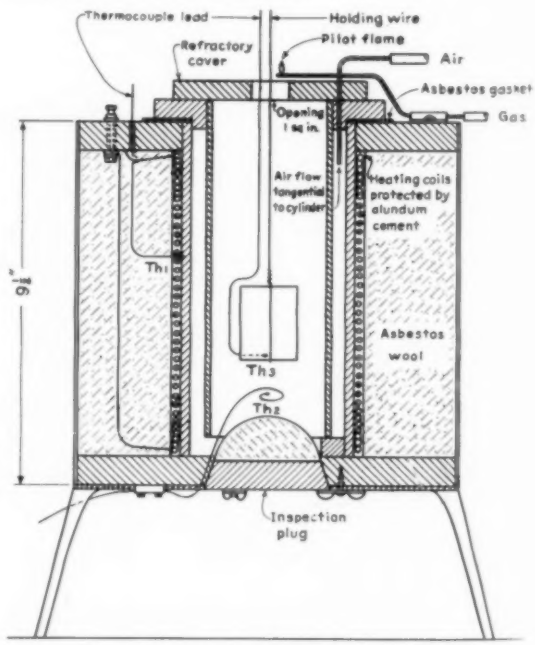

FIGURE 2. *Ignition apparatus for solids.*

Th_1—thermocouple on outer wall, Th_2—thermocouple in air stream, Th_3—thermocouple in or on the specimen.

2. Thermocouples

The temperature of air rising in the inner tube is indicated by thermocouple Th_2 placed below the specimen. It is advisable to shield this thermocouple against heat radiated from the specimen during intense oxidation reactions, especially if the thermocouple is near the specimen. However, since the temperature of the air supplied to the chamber remains substantially constant, any momentary increase of temperature shown by thermocouple Th_2 during intense oxidation reactions is not important. The temperature of the air in the inner tube is maintained constant by current supplied through a variac connected in series with the heating coils. Adjustments of the current are preferably made by reference to the readings of thermocouple Th_1 behind the coils, rather than by reference to thermocouple Th_2 (below the specimen), which always has a somewhat delayed response to current changes.

A third thermocouple, Th_3, is either attached to the surface or inserted within the lower part of the specimen. The rate of temperature rise in the specimen, indicated by this thermocouple is generally related to the rate of the oxidation reaction. The exact location of thermocouple Th_3 in the specimen is of minor importance because of the uncertainty as to the locus of ignition, but since ignition is usually initiated at the surface of the lower part of the specimen, it is desirable to locate the thermocouple junction in this region. A small bare thermocouple junction is used because of its sensitivity to small variations in temperature.

3. Size of Specimen

The size of specimen is varied with type and availability of the material. The standard size usually specified for incombustibility tests [7] is 1½ in. (3.8 cm) wide by 2 in. (5 cm) long, by the thickness of specimen, which should not exceed 1½ in. (3.8 cm). However, for determining the ignition characteristics of plastics, the preferred size of specimen is ¾ in. (1.9 cm) by ¾ in. (1.9 cm) by ¾ in. (1.9 cm) by about ½ in. (1.3 cm) thick. For materials made in thin plates, the specimen consists of a few plates with a total thickness of about ½ in. (1.3 cm) tightly bound together by wire. For materials submitted in the form of small pieces, chips, filings or powder, and for those that melt or bubble at temperatures below ignition, a wire screen basket or a porcelain crucible with a capacity of about 0.5 in.^{3} (8 ml) is used. Within these limits the ignition temperature is not appreciably affected by the size; however, the ignition time-lag varies perceptibly with the size. Small specimens of those materials that develop insignificant amounts of combustible gases, yield less consistent results for the lowest ignition temperature than do those of larger size.

4. Suspension of Specimen

The arrangement for holding the specimen is important, especially for materials whose physical state changes at temperatures below the ignition point. Materials that remain rigid during the test can be suspended on a wire; those which melt to a viscous mass and which bubble can be held in a wire-screen basket; and those which melt to a liquid state, like methyl methacrylate, polystyrene, and others; or those which foam like cellulose acetate, can be placed in a preheated porcelain crucible. Owing to a large gradient in the temperature of the air in the upper portion of the inner tube, the specimen should be placed in the region 4½ to 6½ in. (11 to 16 cm) from the top, where the air temperature around the specimen is uniform within ±3 deg. C.

IV. Test Procedure

1. Rising-Temperature Method

In tests conducted in accordance with the rising-temperature method [7, 8], the specimen is placed in the apparatus at a comparatively low temperature. In the method described in reference [8] the temperature of the apparatus is then raised at the rate of 500 deg C per hour until ignition occurs by itself, or by an igniter, or until 750° C is reached. If at this temperature ignition has not occurred, the material is considered incombustible. Some materials heated in this manner decompose or carbonize slowly without ignition of the material of the carbonized residue at temperatures higher than those obtained with the constant-temperature method. Therefore, this method is not always suitable for exact determination of the flash and self-ignition temperatures. However, it can be used to indicate the approximate ignition temperatures by the evidence of appreciable self-heating in the region of

the ignition temperature, even though actual ignition is not observed. More precise determinations of the flash and self-ignition temperatures can be made by the constant-temperature method described below.

2. Constant-Temperature Method

When the temperature of the air passing through the inner tube with a selected rate of flow has become constant at a selected value, a specimen of the material to be subjected to test is placed in the middle of the inner tube together with a thermocouple, Th_3, either attached to the surface or inserted within the specimen. The air temperature may fall slightly below the initial value, owing to the presence of the cold specimen, but within a few minutes it returns to the initial value. The uniformity of the air temperature around the specimen is quite sensitive to the velocity of air flow, especially when the size of the specimen is small. Fluctuations in temperature caused by excessive turbulence can be avoided by keeping the air velocity around the specimen at about 15 ft/min (5 m/min), particularly during the preliminary tests. However, a favorable rate of air flow is usually fixed in accordance with the trend of the exothermic reaction. The rate is generally varied from 3 to 40 ft/min (1 to 13 m/min), depending upon the material tested. A close selection of the optimum rate of air flow can be made with a series of tests in the region of the lowest ignition temperature, conducted with various constant rates of air flow.

V. Test Results

1. Test Materials

To aid in the development of an ignition apparatus and a suitable test method, 27 samples of plastics were employed. These plastics, with a wide range of physical and ignition characteristics, were divided into two basic groups: (a) thermoplastic, and (b) thermosetting. Most of the latter group were reinforced with paper, asbestos, cotton, or glass fabric. A general description of these plastics is given in table 1.

2. Ignition Characteristics of Thermoplastic Materials

The basic ignition characteristics of some of these thermoplastics, including results of hot-plate tests, are given in table 2. The plastics of the thermoplastic group, with the exception of polytetrafluoroethylene, were transparent, and the appearance of small bubbles was observed at an early stage of decomposition at comparatively low temperatures. The appearance of bubbles and the swelling of the material increased rapidly with an increase in temperature, particularly with cellulose nitrate, which suddenly, without preliminary self-heating, ignited with an explosion or burst of flame. The bubbling of cellulose acetate increased during the melting to produce a foam. Methacrylate and polystyrene melted to thin liquids and boiled similarly to water, hence these materials were held in a crucible. The first formed heavy foams of vinyl chloride-acetate yielded a hollow porous carbonized shell, inside of which the glow was usually initiated. This material was held in a wire-screen cup.

Cellulose nitrate, a material containing active oxygen, can be ignited without air flow, and therefore its lowest self-ignition temperature varied considerably with the method of heating and the impurities present. Specimens of this plastic in the ½- by ¾- by ¾-in (1.3 by 1.9 by 1.9 cm) size, heated for 6 hr under selected conditions with normal air flow, about 15 ft/min, as found favorable in the preliminary tests of most of the plastics, were not ignited at an air temperature of 140° C and during this time were self-heated to only 4° C above the air temperature. During a test with an air temperature of 141° C, the temperature of the specimen after 1 hr and 54 min reached only 150° C, when sudden decomposition and ignition occurred, as shown in figure 3. The ignition lag rapidly diminished with rise in the initial air temperature, as the two curves in figure 4, drawn for different time scales, indicate. The lower curve represents the change in the ignition lag time for air temperatures from 141° to 220° C, and the upper curve, for air temperatures above 220° C. With the air temperature at about 141° C, the ignition lag decreased at the rate of about 12 min per increase of 1 deg C. On the other hand, at air temperatures above 250° C, the ignition lag was shortened to a fraction of a minute. The ignition lag curves for other plastics are shown in figure 5. In order to produce ignition within 10 sec, as specified in some methods, the air temperature had to be above 370° C, and a 1-sec lag could be obtained only at air temperatures above 550° C. Therefore, an ignition temperature de-

TABLE 1. *Identification of plastics*

Type	Manufacturer or source	Thickness	Name or description
		in.	
THERMOPLASTIC MATERIALS			
Cellulose nitrate	Celanese Corp. of America	1/16	Celluloid, transparent.
Cellulose acetate	Monsanto Chemical Co.	1/8	Clear, special optical grade.
Methyl methacrylate:			
(a)	E. I. du Pont de Nemours & Co., Inc.	1/8	HC-202.
(b)	Rohm & Haas Co.	1/8	Plexiglas.
Vinyl chloride-acetate:			
(a)	Bakelite Corp.	1/8	Clear, VS-1310.
(b)	do	1/4	Do.
Polystyrene	Plax Corp.	1/4	Clear, Type M, compression molded.
Polytetrafluoroethylene	E. I. du Pont de Nemours & Co., Inc.	3/8	White plate.
THERMOSETTING MATERIALS			
Phenolic group:			
Paper Laminate:			
(a)	Consolidated Water Power and Paper Co.	1/8	Cross laminated Mitscherlich paper: 30 percent Bakelite phenolic resin.
(b)	Consolidated Water Power and Paper Co. (new lot).	1/8	
Cotton-cloth laminate	Synthane Corp.	1/8	Grade L, 48 percent Bakelite, BV-1112 resin.
Asbestos-cloth laminate	do	1/2	Grade AA, 47 percent Bakelite, BV2427 resin.
(a)	U. S. Plywood Corp.	1/8	6050.
(b)	do	1/8	5013.
Melamine group:			
Mineral-filled melamine	American Cyanamid Corp.	1/4	502.
Cotton-cloth laminate	do	1/4	White plate.
Glass-cloth laminate:			
(a)	Formica Insulation Co.	1/8	128, FF-55.
(b)	U. S. Plywood Corp.	1/8	Not available.
Polyester group:			
Glass-cloth laminate:			
(a)	Army Air Forces, Wright Field	1/8	ECC-11-112.
(b)	U. S. Plywood Corp.	1/8	4143.
(c)	do	1/8	4128.
(d)	do	1/8	5016.
(e)	do	1/8	4128+5 percent At.
(f)	do	1/8	5041.
(g)	do	1/8	MR-21A.
Silicone group:			
Glass-cloth silicone:			
(a)	Formica Insulation Co.	1/8	ESS-12-261, grade G-6.
(b)	U. S. Plywood Corp.	1/8	Not available.

TABLE 2. *Ignition characteristics of plastics*

Type	Ignition temperature				General behavior
	Flash	Self ignition		Hot-surface	
		Glow	Flame		
THERMOPLASTIC MATERIALS					
	°C	°C	°C	°C	
Cellulose nitrate	141	.....	141	550	Bubbled, gas exploded.
Celulose acetate	305	.....	475	600	Bubbled, melted, foamed, flamed.
Methyl methacrylate:					
(a)	280	.....	430	600	Bubbled, melted, liquefied, boiled, flamed.
(b)	300	.....	462	600	Do.
Vinyl chloride-acetate:					
(a)	320	377	557	650	Flowed, foamed, carbonized, glowed, flamed.
(b)	340	355	435	650	Do.
Polystyrene	345	.....	488	600	Bubbled, melted, liquefied, boiled, flamed.
Polytetrafluoroethylene	.....	.....	530	.....	Melted, evaporated, boiled, flamed.
REINFORCED THERMOSETTING MATERIALS					
Phenolic group:					
Paper laminate:					
(a)	300	310	430	600	Blistered, carbonized, glow, flame.
(b)	311	344	367	600	Do.
Cotton-cloth laminate	339	320	492	500	Do.
Asbestos-cloth laminate	382	.....	500	None below 750°	Blistered, carbonized, self-heated, flame.
Glass-cloth laminate:					
(a)	520	.....	571	.....	Intensely self-heated, flame.
(b)	540	.....	580	.....	Do.
Melamine group:					
Mineral-filled melamine	313	350	455	700	Glow, flame.
Cotton-cloth laminate	.....	.....	480	.....	Flame.
Glass-cloth laminate:					
(a)	500	.....	645	None below 750°	Flame below specimen.
(b)	475	.....	623	...do.....	Do.
Polyester group:					
Glass-cloth laminate:					
(a) 900	346	400	462	600	Glow, flame.
(b) 4143	394	.....	447	.....	Audible explosion.
(c) 4128	358	.....	452	.....	Do.
(d) 5016	352	.....	433	.....	Audible explosion. Flame below specimen.
(e) 4128+5%AT	355	.....	453	.....	Do.
(f) 5041	364	.....	488	.....	Audible explosion; flame.
(g) MR-21A	377	.....	475	.....	Audible explosion; flame below specimen.
Silicone group:					
Glass-cloth laminate:					
(a)	527	.....	564	None below 750°	Flame.
(b)	490	.....	550	...do.....	Do.

fined by the method that required a lag of from 1 to 10 sec was very much higher than the self-ignition temperature defined by the present method and hence did not represent the true fire hazard.

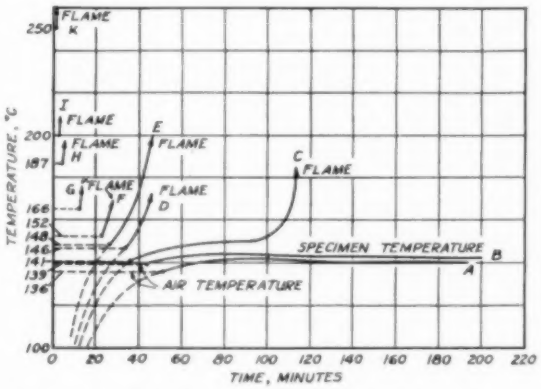

FIGURE 3. *Time-temperature curves for cellulose nitrate.*

Curves *A* and *B* for nonignition reaction; curves from *C* to *K* for self-ignition reaction. The lowest self-ignition temperature is 141° C.

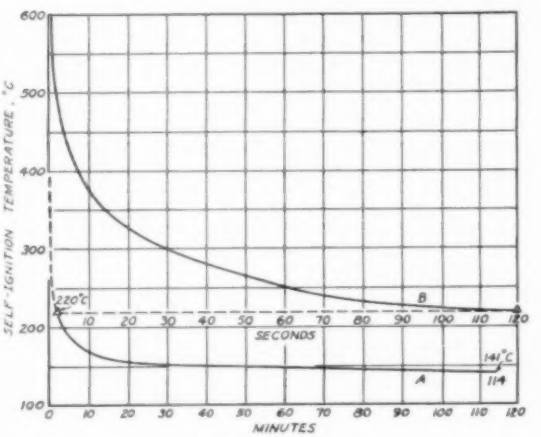

FIGURE 4. *Ignition lag curves for cellulose nitrate.*

Curve *A* at air temperatures from 141° to 220° C and curve *B* from 220° to 600° C.

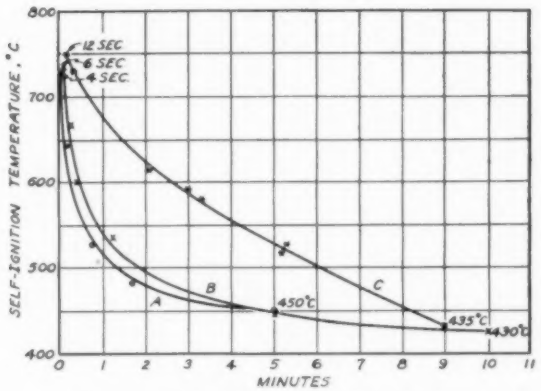

FIGURE 5. *Ignition lag curves for plastics.*

Curve *A*—methyl methacrylate (a); curve *B*—phenolic paper laminated; and *C*—vinyl chloride acetate.

A box of cellulose nitrate plastic triangles, separated by wrapping paper, was reported to have ignited after a 1-hr exposure to the sun in southern Texas. Specimens of material from the same source, about ¾ in.³ in volume, were subjected to tests in the ignition apparatus at the Bureau in a closed test tube without air circulation. During 72 hr of heating, self-heating of the specimen was observed to be about 1 deg C at 105° C, about 5 deg C at 135° C, and the rise in temperature was only 6 deg C at 141° C after 6 hr of heating. However, at a temperature of 142° C, self-heating of about 6 deg C occurred during a 32-min period, when the specimen burst into flame. These tests indicate that the temperature of incipient oxidation was about 105° C, and the self-ignition temperature was approximately 142° C. Triangles from the same lot, separated and covered by the original wrapping paper, were self-ignited after 3.5 hr of heating at a temperature of 135° C, the self-ignition temperature of the paper being about 235° C.

Physical properties of the thermosetting materials, observed at different temperatures prior to ignition, are shown in table 3.

TABLE 3. *Physical characteristics of thermosetting materials prior to ignition*

	Cellulose nitrate	Cellulose acetate	Methyl Methacrylate		Vinyl Chloride acetate	Polystyrene
			(a)	(b)		
	Temperature, °C					
Appearance of bubbles	105	130	150	200	160	160.
Loss of transparency	120	150	220	250	190	200.
State prior to ignition	Soft	Soft	Liquid	Liquid	Spongy mass	Viscous liquid.
	Rise in temperature, °C					
Self-heating of material prior to ignition.	10	40	15	20	Glow	None.
Self-heating of gases above the molten material.	None	None	Very high	Very high	Slight	None.
Apparent cause of self-ignition.	Rapid decomposition.	Self-flash of gases from inflated material.	Self-heating of gases above molten metal.	Self-heating of gases above molten material.	Glow of carbonized materials.	Self-flash of gases in 2d state of decomposition.

The appearance of bubbles and loss of transparency of the plastics rapidly increased with the temperature and duration of exposure; therefore, the extents of these changes observed within the first hour have only relative significance. In cellulose acetate the bubbles increased mainly in size, in contrast with other plastics in which they increased greatly in number. The state prior to ignition varied with the type of plastic. Both cellulose nitrate and acetate plastics are soft just before ignition. However, near the ignition temperature, cellulose nitrate remains soft indefinitely, whereas cellulose acetate inflates, melts, and evaporates. Methyl methacrylate (fig.6) and polystyrene melted below their ignition temperatures and remained in a liquid state for an appreciable time until entirely evaporated without iginition. Vinyl chloride-acetate formed a spongy semi-soft shell inside of which a glow of carbonized material occurred. The self-heating of all of these materials (with the exception of vinyl chloride-acetate) prior to ignition varied from 10 to 40 deg C above the air temperature. Vinyl chloride-acetate self-heated considerably, owing apparently to oxidation and carbonization of the spongy mass. Very intense self-heating was observed only in the vapor above molten methyl methacrylate plastics, in that the wires holding the crucible became red hot. It is doubtful whether there was a catalytic effect of these heated wires to produce self-ignition, which usually occurred at an early stage of the reaction and before the wires became red hot. However, in the nonignition zones the red hot wires did not appear to stimulate ignition. Self-ignition of cellulose nitrate, indicated by a mild audible explosion, usually occurred very suddenly, apparently owing to rapid decomposition of the soft inflated material. Cellulose acetate was ignited when gases from the inflated material escaped through a local rupture into the hot air. If the air temperature was not sufficiently high, these gases escaped without ignition and the deflated material began to melt. Methyl methacrylates (a) and (b) ignited because of an exothermic reaction of gases and hot air above the molten or foamed material. For example, methyl methacrylate (a) and (b) was ignited at air temperatures of 450° and 462° C, respectively, the liquid being at 460° and 472° C, and the foam and vapor just prior to ignition reached over 600° and 645° C, as measured by a thermocouple held just above the liquid. The self-ignition of vinyl chloride-acetate was usually indicated, as stated before, by glow of carbonized portions inside the spongy shell; however, at higher air temperatures these glowing portions ignited gases developed in the incompletely carbonized mass. At an air temperature below 340° C, polystyrene developed such an amount of incombustible gas during about the first 5 minutes that the pilot flame could not be kept lighted. However, at the next stage of decomposition this effect disappeared, and the burning of the pilot flame became normal. At an

air temperature of 345° C gases that developed during the second stage could be ignited by the pilot flame after about 13 min, and at 488° C they were self-ignited after 5.5 min. It is interesting to note that the temperature of the liquid polystyrene always was below the air temperature and when self-ignition occurred, it was only 400° C.

The ignition characteristics of polytetrafluoroethylene were determined only approximately, because of the limited size of the sample then available.

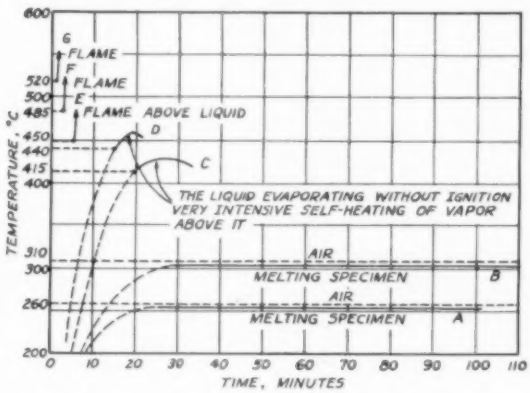

FIGURE 6. *Time-temperature curves for methyl metacrylate (a).*

Curves A to D for nonignition reaction, curves E to G for self-ignition reaction.

3. Ignition Characteristics of Reinforced Thermosetting Materials

The plastics of the thermosetting group usually changed their shape slightly because of a slow process of blistering and carbonization at temperatures below that of self-ignition. When these materials were heated at or near the ignition temperature for an appreciable time, the plastic resin evaporated or carbonized, but the asbestos and glass fabrics remained in layers. On the other hand, combustible fillers, such as paper or cotton fabrics, usually carbonized slowly into a more or less uniform mass with blisters on the surface. If, at comparatively high temperatures, then the glow started at the edges and corners or in the cracks. At still higher temperatures, the decomposition proceeded faster and the gases were self-ignited by the exothermic reaction with the passing air.

The ignition characteristics of plastics of the phenolic laminate group varied considerably with the type of filler, as shown in the second part of table 2. The flash temperature varied from 300° to 540° C. Glow was observed only if paper or cotton cloth fillers were present. Glow in other phenolic materials was not sustained after removal of the specimen from the furnace, in spite of very intense self-heating, which sometimes produced a temperature of 600° C. The lowest self-ignition temperature, characterized by a flickering flame, varied from 430° to 580° C., depending upon the type of the filler. The combustion of these fillers was usually slow and not sustained after removal of the specimen from the apparatus.

The ignition characteristics of materials of the melamine group also varied with the type of filler, as shown in table 2. The rate of oxidation of mineral-filled melamine was found very sensitive to airflow and size of specimen, as shown on the curves *F*, *G*, and *H* in figure 7, particularly in the region of glow. The specimens of normal size did not reach the state of glow with the different rates of air flow, marked on the time-temperature curves corresponding to initial air temperature of 368° and 384° C. However, the specimens of double that size were found glowing at 350°, 355° C, and higher temperatures, with practically the same variations in the air flow. The size of the cotton-cloth melamine laminate submitted for test was sufficient for the determination of the self-ignition temperature only. Therefore, data on flash and glow temperatures were not developed for this material.

Glass-cloth melamine laminate (a) was the most heat-resistant of the plastics tested. In spite of the evolution of dense smoke, the oxidation reaction was so weak that up to a temperature of 450° C the self-heating did not exceed 15 deg C above the air temperature. In the region of 500° C, the temperature of the mass of melamine laminate increased about 100 deg C above the air temperature, and the color of the mass became a dull red. Dense smoke, in which the odor of ammonia was predominant, usually disappeared in 4 min. The oxidation reaction in the gas evolved from the specimen at that time became so intense that the wires holding the specimen were heated to a bright red color, distinctly visible against the darker specimen and

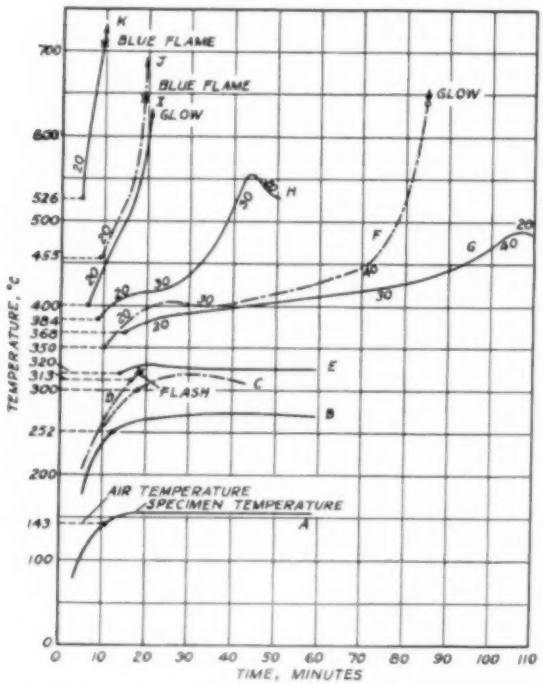

FIGURE 7. *Time-temperature curves for mineral-filled melamine.*

Curves *A*, *B*, *C*, *D*, *E*, *G*, and *H* for nonignition reaction, curves *F*, *I*, *J*, and *K* for self-ignition reaction. Figures on curves—air velocities in feet per minute, curves *F*, *G*, and *H* are taken during adjustment of air flow. ——, specimens, single size; — — — — — —, specimens, double size.

furnace wall. The intensity of self-heating in the melamine increased with air temperatures up to 660° C, at which temperature a blue flame started to flicker over the darker surface of the specimen. The red color of the self-heated mass of material did not represent a state of sustained glow, because when the specimen was moved into a cooler portion of the furnace or was removed from the furnace entirely, the mass cooled rapidly.

The self-ignition temperature of this plastic is difficult to determine exactly because of the several different types of ignition that were observed. With careful adjustment of an optimum air flow, an occasional blue or red flame was observed for type (a) at an air temperature of 645° C, a flickering of blue flame was observed at 662° C, and a continued flaming at 673° C. The lowest self-ignition temperature was 645° C. The ignition of gases by the pilot flame was obtained occasionally at 500° C and regularly at an air temperature of 544° C. For glass cloth melamine laminate (b), self-ignition was occasionally observed at 623° C and the flash temperature at 475° C.

The ignition characteristics of the polyester plastics were substantially the same. The flash temperature varied from 346° to 394° C and the self-ignition temperature from 433° to 488° C. The self-ignition was characterized by mild explosion of gases developed from the material, or by an audible flash of gases without destructive effect. The combustion of these materials varied quite appreciably: glass-cloth laminate type (d) burned readily when removed from the apparatus, whereas types (e) and (g) burned well only in the furnace and then for only a short time. The other materials of this class were slightly combustible. It is interesting to note that the combustible gases developed from some of the polyester plastics were relatively heavy, and therefore settled to the bottom of the furnace during the early states of decomposition, particularly when the rate of air flow was very low. Self-ignition usually took place below the specimen in the bottom of the furnace, and burning of these gases in the furnace continued even after the specimen had been carefully lifted out.

Both types of glass-cloth silicone laminate had about the same ignition characteristics. These withstood heating very well up to 450° C. Appreciable self-heating (115° C) was observed at 540° C. Flammable gases were developed at a temperature of 490° C for this plastic of type (b) and at 527° C for type (a). Such high flash points for gases seemed to be caused by the development of a noncombustible gas during an early stage of the decomposition of the material. This gas extinguished the pilot flame during the first 5 min. of the reaction. The self-ignition of the gases was irregular and was first observed at air temperatures of about 564° C and then only after 5-min lag, when the contamination of the combustible gases had been sufficiently reduced. At an air temperature of about 600° C, self-ignition became more regular, and the time lags varied from 2 to 3 min. During the next 3 min the plastic burned with long orange flames.

4. Reproducibility of Test Results

The reproductivity of the ignition temperature values of plastics as determined in the present

apparatus depends upon two major factors: one is uniformity of chemical composition and physical state of the plastics from which the specimens are taken; and the other is the sensitivity of the test method and the apparatus to the ignition characteristics of the material. The first factor was substantially constant for most of the plastic materials when tested and for a long time subsequently. An exception was found in cellulose nitrate, which sometimes changes under the action of sunlight and temperature. The ignition characteristics of some plastics, such as methyl methacrylate, vinyl chloride-acetate, and a few others (bearing the same names) varied with the manufacturer's lot or with their purity.

The sensitivity of the constant-temperature test method to the ignition properties characteristics of the material is high, owning to the fact that the temperature in the whole apparatus can be stabilized in advance and kept substantially constant during the test. The temperature and rate of air flow are under good control. The reproducibility of the results depends mainly upon the accuracy of the test procedure and the interpretation of the observed evidence of ignition, i. e., upon the following three factors: (1) The positioning of the specimen in the region of uniform temperature in the furnace tube (middle position); (2) correct selection of the optimum air flow for the most favorable rate of temperature rise in the reacting mass; and (3) careful bracketing of the temperatures that correspond to the types or stages of ignition, such as: explosion, flash, flame, glow, cold flame, or luminescence.

The bracketing of the lowest ignition temperature is usually made in the manner shown in table 4, with five or more determinations within the region of the boundary between ignition and nonignition zones in order to secure the desired temperature range, which is usually between 2 and 5 deg C. This range depends upon the required accuracy and the available time, since the time lag in this region may vary from a few minutes to a few hours.

TABLE 4. *Determination of the lowest self-ignition temperature*

Methyl methacrylate				Vinyl chloride acetate				Paper phenolic				Mineral filler melamine		Glass cloth polyster	
(a)		(b)		(a) clear		(b) yellowish		(a)		(b)					
Temperature	Evidence	Temperature	Evidence	Temperature	Evidence	Temperature	Evidence	Temperature	Evidence	Temperature	Evidence	Temperature	Evidence	Temperature	Evidence
°C		°C		°C		°C		°C		°C		°C		°C	
550	Flash	517	Flash	580	Flash	500	Flash	463	Flash	475	Flash	572	Flash	488	Flash.
510	Flame	470	Flame	564	Flame	475	Flame	442	Flame	469	do	545	Orange flame.	470	Flame.
470	do	464	do	560	do	440	do	433	do	467	Flame	532	Blue flame.	466	Flame.
453	do	462	do	557	do	435	do	430	do	468	Glow	455	do	462	Do.
450	do	460	No ignition.	553	Glow	432	Glow	427	Glow	463	do	453	Glow	463	Glow.
448	No ignition.	458	do	550	do	428	do	423	do	418	do	408	do	558	Do.
445	do	455	do	420	do	382	do	366	do	350	do	355	do	404	Do.
440	do	450	do	377	do	355	do	310	do	344	do	350	do	400	Do.
440	do			375	No ignition.	353	No ignition.	307	No ignition.	342	No ignition.	346	No ignition.	398	No ignition.
				370	do	350	do	303	do	338	do	344	do	392	Do.
				361	do	340	do	298	do	320	do	312	do	390	Do.

In table 4 only typical results are given, and many practically identical results observed during the tests are omitted. In some cases a nonignition state was observed 1 or 2 deg. C above the lowest self-ignition temperature, owing to accidental variation of test conditions. When the evidence of the ignition is clearly defined (as with cellulose nitrate and acetate, methyl methacrylate, and other thermoplastic materials) the results are closely reproducible. For example, a sample of methyl methacrylate plastic of type (a) was tested in October 1946 and retested in March and December 1947; the results were 450°, 451°, and 450° C. In contrast, methyl methacrylate

of another shipment, type (b) had an ignition temperature of 462° C. Yellowish vinyl chloride-acetate, type (b) was tested first in October 1946 and retested in February 1948, with the same value, 435° C, which differed from the value (557° C) for the clear type (a).

In those cases where the evidence is not clearly defined owing to a gradual change of intensity and color of the flame from a steady orange to a flickering blue, or to the appearance of flame at the end of the glowing period, the reproducibility of results depends upon the type of observed evidence. For example, the flash of the paper phenolic laminate was observed at 467° C after a 4-min lag; another specimen of the same sample glowed at 467° C, and a weak flickering flame appeared only after 16-min lag. This difference was caused by sudden exposure of a noncarbonized portion of the specimen to hot air through the opening of a crack or the separation of layers of the specimen. However, the change between glow and nonglow states was defined more clearly at 344° C, a value reproduced at other times.

The determination of the ignition state was more difficult with glass-cloth melamine laminate. In the absence of glow, the intensity of ignition gradually diminished from a bright flash at 673° C to a blue flame at 662° C, which did not appear at all at 650° C. However, the flame was observed in two of five specimens at 645° C, but in none of the five at 630° C. No explanation of this uncertainty of behavior is offered, but it could be caused by the presence of ammonia gas, which might have interfered with the ignition.

The reproducibility of the test results depends upon careful technique and accuracy of observation, as much as upon the apparatus and the principles involved.

5. Ignition by Hot Surface

Early determinations of the ignition temperature of plastics were often made by contact with hot surfaces. Basically, in the hot-surface methods, the surface is only a medium for the transmission of heat to the specimen, because the hot surface does not participate in the oxidation that usually causes ignition. The essential element in the ignition is the oxygen of the air, the temperature of which is usually considerably below that of the hot surface, particularly if the latter is not within a uniformly heated furnace. Moreover, in most cases, the ignition of plastics occurs because of intense oxidation of the gaseous components evolved during the process of heating. This process requires a time lag, which varies from hours to fractions of a second, depending upon the ambient air temperature. The air-temperature gradient from a vertical hot surface exposed to the atmosphere, as our experiments showed, varies considerably with the distance from the surface. The temperature drop in the first ⅛-in. (3-mm) zone is from 150° to 200° C when the temperature of the hot surface is 600° C. These results are in agreement with Kennard Work [9]. Combustible gaseous products from plastics, turbulently moving along the surface within the zone, usually have only a few seconds in which the oxidation reaction may be accelerated to cause ignition. Therefore, for this limited time lag the average air temperature within the ⅛-in. (3-mm) zone must be much higher to cause ignition than in a uniformly heated furnace with an unrestricted time lag. Hence, ignition by contact with a hot surface occurs only at higher temperatures than are required for ignition in uniformly heated air.

The hot-surface apparatus used in these studies consisted of a ¼-in. (0.6-cm) steel plate, heated by coiled resistance wire imbedded in the grooves of a refractory plate attached to the back of the steel plate. All sides of the assembly, except the front, were heavily insulated by asbestos wool mixed with vermiculite. The temperature of the exposed front vertical surface of the "hot plate" was indicated by a thermocouple junction imbedded in the plate. The specimen was usually held in contact with the vertical hot surface about 5 min, or until ignition took place, which might occur during the first 1 or 2 min. The temperatures of the hot plate at which different plastics were ignited are given in the fifth column of table 2. With the exception of cellulose nitrate and cotton-fabric phenolic laminate, most plastics ignited only at plate temperatures of 600° C or higher. Three thermosetting plastics, although ignited by other methods as shown in table 2, did not ignite with the maximum hot surface temperature of 750° C.

These results show that the "hot-surface-contact method" is not as suitable for indicating the lowest temperature of ignition, i. e. the fire-hazard of a material, as is the constant-air-temperature method.

VI. Summary

A new method and apparatus were developed from consideration of the principles of ignition, as explained in section II. The ignition characteristics and thermal behavior of materials were determined in this apparatus under well-controlled conditions.

Operation of this apparatus by the constant-air-temperature method is simple at temperatures up to 800° C. The air temperature around the specimen, in spite of the readily sustained constant temperature of the wall, is very sensitive to the velocity of air flow and to the heat radiated from the specimen during the exothermic reaction. The first factor can be controlled with an approximately optimum air flow, adjusted for a favorable rate of ignition as indicated by the rate of temperature rise. The second factor has no appreciable effect on the results if other temperatures in the apparatus remain constant. The effect of the second factor can be minimized, if necessary, either by shielding the thermocouple (Th_2) that indicates the temperature of air approaching the specimen, or by shifting it farther away from the specimen.

The lowest values of the temperatures defined as "flash" and "self-ignition" were selected to indicate the fire hazards of the plastics. The flash temperatures for most of the plastics listed in tables 1 and 2, are in the range from 280° to 525° C, with the exception of cellulose nitrate, which flashes at 141° C. The self-ignition temperatures for 17 of the 27 specimens tested lie in the range from 430° to 500° C. Cellulose nitrate, however, self-ignites at 141° C, whereas specimens of glass-cloth melamine laminate ignited at 623° and 645° C. The values of these temperatures were found to be reproducible to within 1 or 2 deg C.

The effect of heat on the physical state of various plastics is illustrated in figures 8, 9, and 10. Of particular interest is the ability of a material to retain its transparency and resist discoloration and carbonization. The transparency of most of the plastics in the thermoplastic group, as shown in figures 9 and 10, disappears in the range of 130° to 250° C, although cellulose nitrate loses its transparency at 105° C. For the reinforced thermosetting plastics, discoloration and carbonization depend not only upon the temperature, but also upon the duration of heating.

The specimens shown in figures 8, 9, and 10 were chosen at random and do not necessarily represent uniform steps in the process of degradation. The temperature and time data have only relative and incidental significance. The examples in figure 10 show that the most heat-resistant plastics were those consisting of glass-cloth with silicone, melamine, or polyester resins. These withstood heating to 300° C for approximately 1 hr without appreciable discoloration. The thermoplastic group, with the exception of methyl methacrylate (6), did not withstand even 200° C without considerable bubbling or melting.

The new method for the determination of ignition characteristics of materials is the first major step in evaluating the ignition properties of a material in terms of the temperature and controlable condition that may be as important as for other physical properties such as density, conductivity, etc.

VII. References

[1] H. N. Stokes and H. C. P. Weber, effect of heat on celluloid and similar materials, Techn. Pap. BS T98 (1917).

[2] J. Delmonte and M. A. Azam, Ignition points of plastic material, Mod. Plastics **20,** No. 6, 88 (Feb. 1943).

[3] E. M. Schoenborn and D. S. Weaver, Ignition temperature of rigid plastics, ASTM Bull. No. 146, 80 (May 1947).

[4] N. P. Setchkin, Discussion of paper on the ignition temperature of rigid plastics, ASTM Bull. No. 151, 66 (Mar. 1948).

[5] J. A. Gale, R. W. Stewart, and J. B. Peters, ASTM Bull. No. 131, 23 (Dec. 1944).

[6] L. B. Berger, J. P. Gale, and others, Toxicity and flame resistance of thermosetting plastic, Bureau of Mines R 14134 (Oct. 1947).

[7] C. R. Brown, The determination of the ignition temperature of solid materials (The Catholic Univ. of America, Washington, D. C., 1934).

[8] N. P. Setchkin and S. H. Ingberg, The criterion of the incombustibility of materials, ASTM Proc. **45,** 866 (1945).

[9] R. B. Kennard, An optical method for measuring temperature distribution and convective heat transfer, BS J. Research **8,** 787 (1932) RP452.

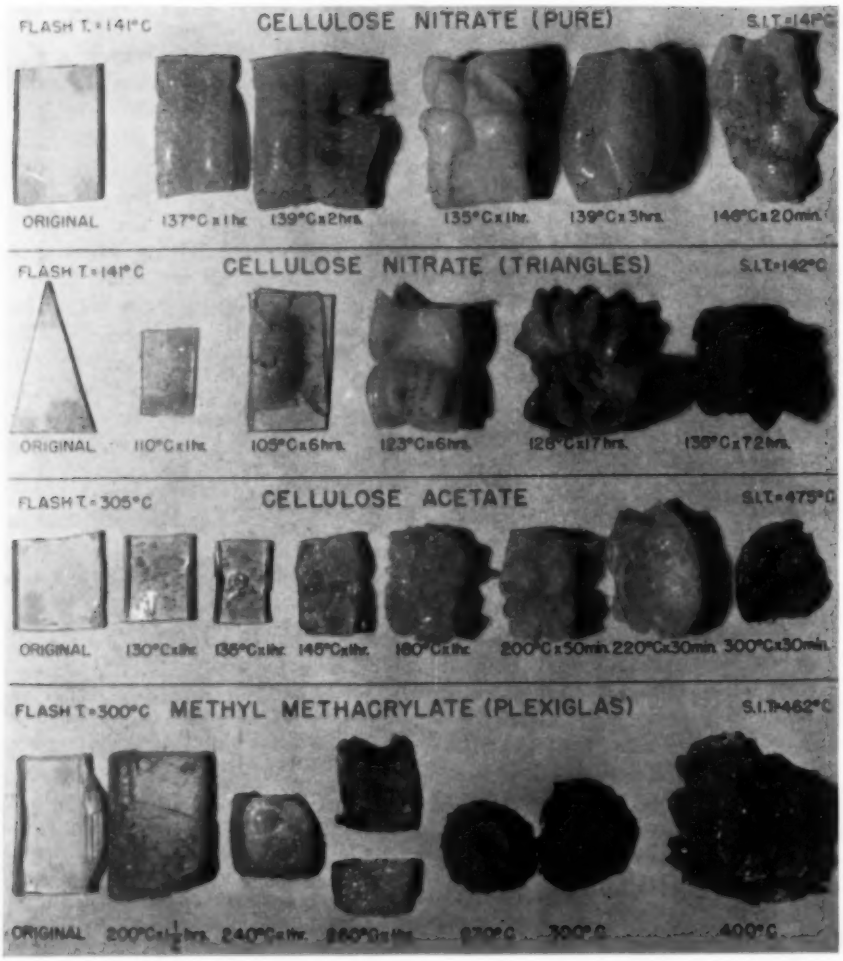

FIGURE 8. *Appearance of plastics after being heated at indicated temperatures for designated period*

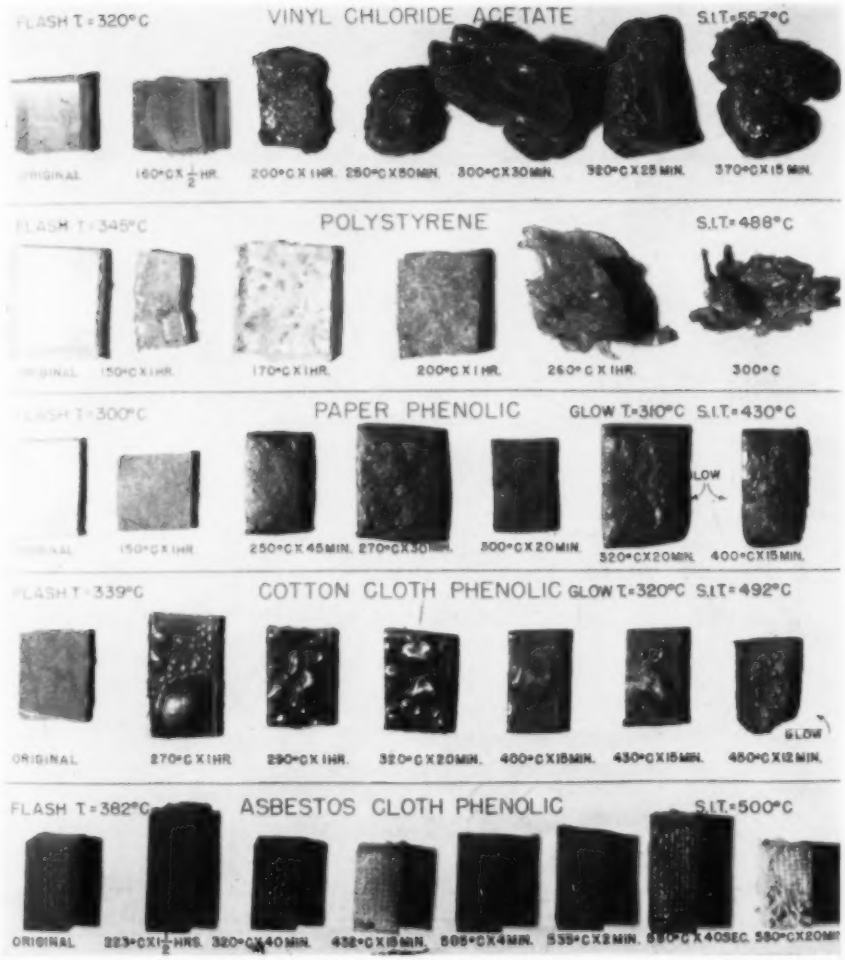

FIGURE 9. *Appearance of plastics after being heated at indicated temperatures for designated period.*

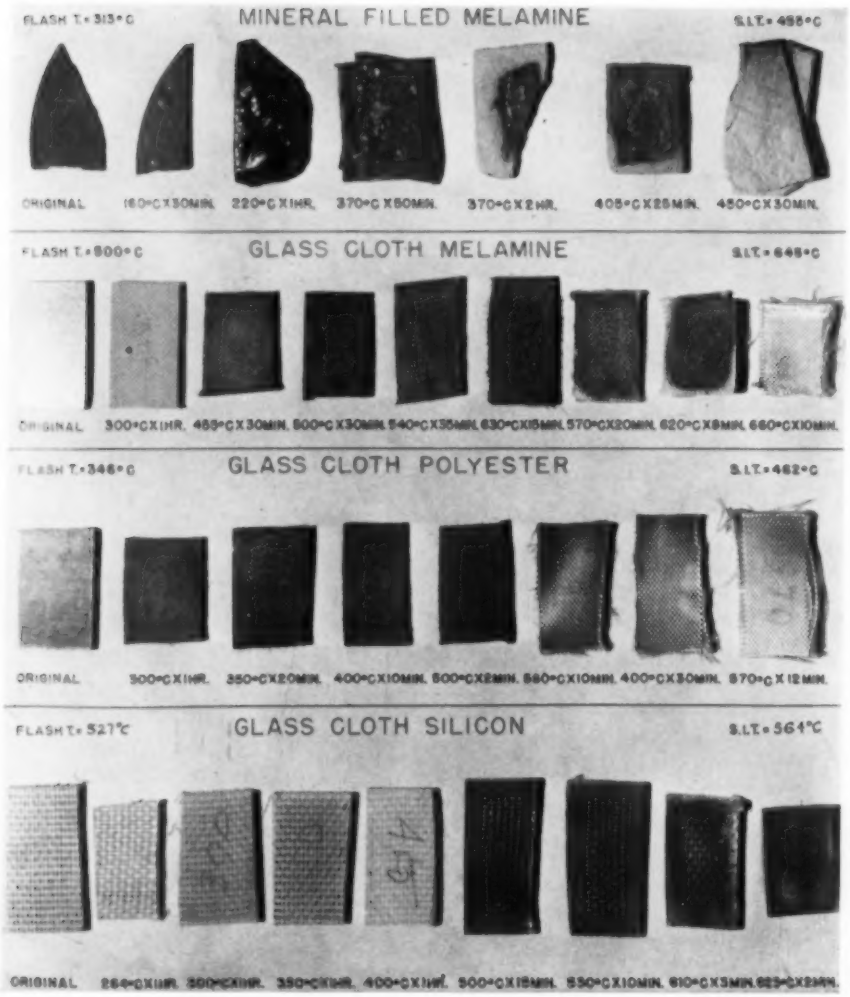

FIGURE 10. *Appearance of plastics after being heated at indicated temperatures for designated period.*

WASHINGTON, March 16, 1949.

INDEX TO VOLUME 43

A

Page

Acetyl carbohydrate derivatives, stereomeric factors in replacement reactions, RP2018 ... 161
Acetylglycosyl halides, effect of configuration, temperature, and solvent in replacement reactions, RP2018 ... 161
Acquista, Nicola Earle K. Plyler, Infrared absorption spectra of cyclohydrocarbons, RP2002 ... 37
Aircraft steels, effect of chromium plating on endurance limit, RP2011 ... 101
Albrecht, Isabelle, John J. Lamb, Benjamin M. Axilrod, Mechanical properties of laminated plastics at −70°, 77°, and 200° F, RP2028 ... 257
Antennas, broadband for vertical incidence ionosphere sounding, RP2006 ... 71
Area gage for use at low temperatures, RP2044 ... 527
Arithmetic mean, formulas for percentage points of sampling distribution of, RP2007 ... 79
Axilrod, Benjamin M., John J. Lamb, Isabelle Albrecht, Mechanical properties of laminated plastics at −70°, 77°, and 200° F, RP2028 ... 257

B

Barium-calcium titanate dielectrics, properties, RP2025 ... 237
Barrow, Gordon M., Morton B. Epstein, Kenneth S. Pitzer, Frederick D. Rossini, Heats, equilibrium constants, and free energies of formation of the dimethylcyclopentanes, RP2026 ... 251
Bars, concrete reinforcing, bond of, RP2050 ... 565
Bases, dissociation constants of tris (hydroxymethyl) aminomethane, RP2043 ... 519
Bates, Roger G., Gladys D. Pinching, Dissociation constants of weak bases from electromotive-force measurements of solutions of partially hydrolyzed salts, RP2043 ... 519
Bekkedahl, Norman, Volume dilatometry, RP2016 ... 145
Benzenes, alkyl:
Physical properties of, RP2038 ... 473
Vapor pressures and boiling points, RP2049 ... 555
Blaine, Raymond L., Charles M. Hunt, John W. Rowen, Submicroscopic structure of cellulose from nitrogen sorption measurements, RP2048 ... 547
Bloom, Evelyn G., Fred L. Mohler, C. Edward Wise, Edmunds J. Wells, Metastable transitions in mass spectra of hydrocarbons, RP2005 ... 65
—, —, *Laura Williamson, C. Edward Wise, Edmunds J. Wells*, Mass spectra of C_3H_8 isomers, RP2045 ... 533
Bogue, Robert H., William R. Eubank, Studies on the flame photometer for the determination of Na_2O and K_2O in portland cement, RP2019 ... 173
Bolometer bridge, direct-current analysis of, RP2051 ... 581
Bond, of concrete reinforcing bars, RP2050 ... 565
Bonechar, combustion of, RP2009 ... 87
Boiling points of hydrocarbons:
RP2038 ... 473
RP2049 ... 555
Borates, zinc, surface tension, RP2023 ... 221
Borysko, Emil, Sanford B. Newman, Max Swerdlow, Ultra-microtomy by a new method, RP2020 ... 183
Borey, H. L., M. R. Shafer, Laboratory flow tests of fixed-spray nozzles with hydrocarbons and with air, RP2035 ... 449
Bright, Harry A., John L. Hague, Rolf A. Paulson, Determination of nitrogen in steel, RP2021 ... 201
Bunting, Elmer N., George E. Shelton, Ansel S. Creamer, Properties of calcium-barium titanate dielectrics, RP2025 ... 237
Butenes and 1,3-butadiene, infrared absorption spectra, RP2031 ... 365
Butyl rubber, density and expansivity, RP2016 ... 145

C

Calcium-barium titanate dielectrics, properties, RP2025 ... 237
Canga, Rodrigo, Leo Shartsis, Surface tension of molten zinc borates, RP2023 ... 227
Capacitance, computation, RP2032 ... 377
Carbon adsorbents, reaction of oxygen with, RP2009 ... 87
Carwile, Nesbit L., Glenn W. Geil, A reduction-of-area gage for use at low temperatures, RP2044 ... 527
Cassel, James M., Joseph R. Kanagy, Electrophoresis of modified collagen, RP2001 ... 29
Cathode heater compensation as applied to stabilized power supplies, RP2027 ... 251
Cellulose submicroscopic structure, RP2048 ... 547
Cement, portland, flame photometer for determination of potash and soda in, RP2019 ... 173
Chand, Uttam, Formulas for the percentage points of the distribution of the arithmetic mean in random samples from certain symmetrical universes, RP2007 ... 79
Chromium plate, effect on endurance limit of steels, RP2011 ... 101
Clark, Arthur P., Bond of concrete reinforcing bar, RP2050 ... 565
Cleaves, Harold E., Andrew I. Dahl, The freezing point of uranium, RP2042 ... 513
Collagen, electrophoresis of modified, RP2001 ... 29
Colorimetry of titanium pigments, RP2024 ... 227
Combustion:
Of carbon adsorbents, RP2009 ... 87
Of cyclopropane, heat, RP2012 ... 113
Concrete:
Reinforcing bars, bond of, RP2050 ... 565
Volume behavior during freezing and thawing, RP2000 ... 1
Cones, H. N., Impedance characteristics of some experimental broadband antennas for vertical incidence ionosphere sounding, RP2006 ... 71
Coster, Irvin L., James L. Thomas, Chester Peterson, Ralph Kotter, An absolute measurement of resistance by the Wenner method, RP2029 ... 291
Carruccini, Robert J., Differences between the International Temperature Scales of 1948 and 1927, RP2014 ... 133
Cotton linters, nitrogen sorption at low temperatures, RP2048 ... 547
Creamer, Ansel S., Elmer N. Bunting, George E. Shelton, Properties of calcium-barium titanate dielectrics, RP2025 ... 237
Creep of ingot iron, influence of strain rate and temperature, RP2013 ... 117
Creitz, E. Carroll, Francis A. Smith, Infrared absorption spectra of the liquid butenes and 1,3-butadiene, RP2031 ... 365
Crystals:
Quartz oscillator, production of, RP2036 ... 359
Thallium bromide-iodide, refractive indices, RP2008 ... 81
Cyclohexanes, alkyl:
Physical properties of, RP2038 ... 473
Vapor pressures and boiling points, RP2049 ... 555
Cyclohydrocarbons, infrared absorption spectra, RP2002 ... 37
Cyclopentanes, alkyl:
Physical properties of, RP2038 ... 473
Vapor pressures and boiling points, RP2049 ... 555
Cyclopropane, heat of combustion and formation, RP2012 ... 113

D

Dahl, Andrew I., Harold E. Cleaves, The freezing point of uranium, RP2042 ... 513
Density of hydrocarbons, RP2038 ... 473
Dibeler, Vernon H., Fred L. Mohler, Laura Williamson, Robert M. Reese, Mass spectrum of pentaborane (B_5H_9), RP2010 ... 97
Dielectric properties of molded rubber, directional effects in, RP2030 ... 355
Dielectrics, calcium-barium titanate, properties, RP2025 ... 237
Digges, Thomas G., William D. Jenkins, Influence on strain rate and temperature on the creep of cold-drawn ingot iron, RP2013 ... 117
Dilatometer, mercury-displacement, measurement of volume changes in concrete cylinders during freezing and thawing, RP2000 ... 1
Dilatometry, volume, RP2016 ... 145
Dimethylcyclopentanes, heats, equilibrium constants, and free energies of formation, RP2026 ... 245
Dipole, magnetic, electron paths in field of, RP2033 ... 409
Direct-current bolometer bridge analysis of, RP2051 ... 581
Directional effects in dielectric properties of molded rubber, RP2030 ... 355

Page

Disintegration rate of sodium 22 sources, measurements, RP2047 ... 543
Dispersion, optical, of natural rubber, RP2004 ... 57
Dissociation:
Constants of weak electrolytes, RP2043 ... 519
Of pentaborane by electron impact, RP2010 ... 97

E

Electric power, precision stabilized, for ultrahigh-frequency measurements, RP2027 ... 251
Electrical resistance, absolute determination of, RP2029 ... 291
Electroformed sheet, fatigue characteristics, RP2039 ... 477
Electromotive-force measurements, determination of dissociation constants by, RP2043 ... 519
Electron:
Optical observation of magnetic field, RP2033 ... 409
Microscopy, RP2020 ... 183
Electrophoresis of modified collagen, RP2001 ... 29
Electroplated metals, fatigue characteristics, RP2039 ... 477
Electrostatic field of a conductor, computation, RP2032 ... 377
Ellenwood, Robert C., Howard E. Sorrows, Cathode heater compensation as applied to degenerative voltage-stabilized direct-current power supplies, RP2027 ... 251
Epstein, Morton B., Gordon M. Barrow, Kenneth S. Pitzer, Frederick D. Rossini, Heats, equilibrium constants, and free energies of formation of the dimethylcyclopentanes, RP2026 ... 245
Equations, differential, numerical integration:
RP2041 ... 501
RP2046 ... 537
Differential remainder in linear methods of approximation, RP2041 ... 501
Eubank, William R., Robert H. Bogue, Studies on the flame photometer for the determination of Na_2O and K_2O in portland cement, RP2019 ... 173
Expansivity of rubber from optical measurements, RP2004 ... 57

F

Fatigue properties of electroplated metals, RP2039 ... 477
Flame photometer for determination of soda and potash in portland cement, RP2019 ... 173
Flow tests of spray nozzles, RP2035 ... 449
Flows, stratified, interfacial instability and mixing in, RP2040 ... 487
Formation of cyclopropane, heat of, RP2012 ... 113
Forziati, Alphonse, F., Frederick D. Rossini, Physical properties of sixty API–NBS hydrocarbons, RP2038 ... 473
—, *William R. Harris, Frederick D. Rossini*, Vapor pressures and boiling points of sixty API–NBS hydrocarbons, RP2049 ... 555
Freezing point of uranium, RP2042 ... 513
Frequency measurements, precision stabilized power supply for, RP2027 ... 251
Frush, Harriet L., Horace S. Isbell, Mechanisms for the formation of acetylglycosides and orthoesters from acetylglycosyl halides, RP2018 ... 161

G

Gage, reduction of area, for use at low temperatures, RP2044 ... 527
Gardner, Irvine C., Relation between entrance and exit pupils of telescopic systems, RP2017 ... 157
Geil, Glenn W., Nesbit L. Carwile, A reduction-of-area gage for use at low temperatures, RP2044 ... 527
Geller, R. F., S. M. Lang, L. H. Maxwell, Some physical properties of porcelains in the systems magnesia-beryllia-zirconia and magnesia-beryllia-thoria and their phase relations, RP2034 ... 429

H

Hague, John L., Rolf A. Paulson, Harry A. Bright, Determination of nitrogen in steel, RP2021 ... 201
Halides, acetylglycosyl, effect of configuration, temperature, and solvents in replacement reactions, RP2018 ... 161
Harris, William R., Alphonse F. Forziati, Frederick D. Rossini, Vapor pressures and boiling points of sixty API–NBS hydrocarbons, RP2049 ... 555
Heats of formation of the dimethylcyclopentanes, RP2026 ... 245
Herschman, Harry K., Carrol Thomas, Fatigue characteristics of electroformed sheets with and without iron backing RP2039 ... 477
Herson, J. L., Measurement of the disintegration rate of sodium 22 by the coincidence method, RP2047 ... 543
Howard, Walter J., Leland T. Sogn, Mechanical production of very thin oscillator plates, RP2036 ... 459
Hunt, Charles M., Raymond L. Blaine, John W. Rowen, Submicroscopic structure of cellulose from nitrogen sorption measurements, RP2048 ... 547

Page

Hydrocarbons:
Air flow tests of spray nozzles with, RP2035 ... 449
Cyclopropane, heats of combustion and formation, RP2012 ... 113
Heats, equilibrium constants, and free energies of formation, RP2026 ... 245
Isomers (C_5H_8), mass spectra, RP2045 ... 533
Metastable transitions in mass spectra of, RP2005 ... 65
Physical properties of, RP2038 ... 473
Vapor pressures and boiling points, RP2049 ... 555
Hydrolysis of salts and determination of dissociation constants, RP2043 ... 519
Hygrometer elements, radiosonde electric, low-temperature performance, RP2003 ... 49

I

Ignition characteristics of plastics, RP2052 ... 591
Index of refraction of thallium bromide-iodide crystals, RP2008 ... 81
Inductance, standard, construction of, RP2029 ... 291
Infrared:
Absorption spectra of cyclohydrocarbons, RP2002 ... 37
Absorption spectra of the liquid butenes and 1,3-butadiene, RP2031 ... 365
Transmission and refraction data, lens and prism materials, RP2008 ... 81
Ingot iron, creep of, influence of strain rate and temperature, RP2013 ... 117
Integration, numerical, of differential equations:
RP2041 ... 487
RP2046 ... 533
Interfacial instability and mixing in stratified flows, RP2040 ... 487
International temperature scales, differences between scales of 1948 and 1927, RP2014 ... 133
Ionization constants of bases, RP2043 ... 519
Ionosphere sound, impedance characteristics of antennas for, RP2006 ... 71
Isbell, Horace S., Harriet L. Frush, Mechanisms for the formation of acetylglycosides and orthoesters from acetylglycosyl halides, RP2018 ... 161
Isomers, mass spectra of C_5H_8, RP2045 ... 533

J

Jenkins, William D., Thomas G. Digges, Influence of strain rate and temperature on the creep of cold-drawn ingot iron, RP2013 ... 117
Judd, Deane B., A comparison of direct colorimetry of titanium pigments with their indirect colorimetry based on spectrophotometry and a standard observer, RP2024 ... 227

K

Kanagy, Joseph R., James M. Cassel, Electrophoresis of modified collagen, RP2001 ... 29
Kerns, David M., Analysis of the direct-current bolometer bridge, RP2051 ... 581
Keulegan, Garbis H., Interfacial instability and mixing in stratified flows, RP2040 ... 487
Kinetics of combustion of carbon adsorbents, RP2009 ... 87
Knowlton, John W., Frederick D. Rossini, Heats of combustion and formation of cyclopropane, RP2012 ... 113
Kotter, Ralph, James L. Thomas, Chester Peterson, Irvin L. Cooter, An absolute measurement of resistance by the Wenner method, RP2029 ... 291
Kroll, Wilhelmina D., Instability in shear of simply supported square plates with reinforced hole, RP2037 ... 465

L

Lachenbruch, S. N., L. Marton, Electron optical observation of magnetic fields, RP2033 ... 409
Lamb, John J., Isabelle Albrecht, Benjamin M. Axilrod, Mechanical properties of laminated plastics at −70°, 77°, and 200° F., RP2028 ... 257
Lang, S. M., L. H. Maxwell, R. F. Geller, Some physical properties of porcelains in the systems magnesia-beryllia-zirconia and magnesia-beryllia-thoria and their phase relations, RP2034 ... 429
Lenses, spherical aberration, RP2015 ... 137
Loebenstein, William V., Neil L. Pennington, Fundamental aspects of the reaction of oxygen with carbon adsorbents, RP2009 ... 87
Logan, Hugh L., Effect of chromium plating on the endurance limit of steels used in aircraft, RP2011 ... 101

M

Magnetic fields, electron optical mapping of, RP2033 ... 409
Mapping of magnetic fields, electron optical, RP2033 ... 409
Marton, L., S. N. Lachenbruch, Electron optical observation of magnetic fields, RP2033 ... 409

Mass: Page
Spectra of C_3H_8 isomers, RP2045 ... 533
Spectra of hydrocarbons, metastable transitions, RP2005 ... 65
Spectrum of pentaborane, RP2010 ... 97
Maxwell, L. H., S. M. Lang, R. F. Geller, Some physical properties of porcelains in the systems magnesia-beryllia-zirconia and magnesia-beryllia-thoria and their phase relations, RP2034 ... 429
Mechanical properties of laminated plastics, RP2028 ... 257
Metastable transitions in mass spectra of hydrocarbons, RP2005 ... 65
Microtomy, materials and procedures for, RP2020 ... 183
Milne, W. E., A note on the numerical integration of differential equations, RP2046 ... 537
—, The remainder in linear methods of approximation, RP2041 ... 501
Mohler, Fred L., Evelyn G. Bloom, C. Edward Wise, Edmunds J. Wells, Metastable transitions in mass spectra of hydrocarbons, RP2005 ... 65
—, —, *Laura Williamson, C. Edward Wise, Edmunds J. Wells,* Mass spectra of C_3H_8 isomers, RP2045 ... 533
—, *Vernon H. Dibeler, Laura Williamson, Robert M. Reese,* Mass spectrum of pentaborane (B_5H_9), RP2010 ... 97

N

Newman, Sanford B., Emil Borysko, Max Swerdlow, Ultramicrotomy by a new method, RP2020 ... 183
Nitrogen:
In steel, determination, RP2021 ... 201
Sorption at low temperature by cotton linters, RP2048 ... 547
Norris, William R., Alphonse F. Forziati, Frederick D. Rossini, Vapor pressures and boiling points of 60 API-NBS hydrocarbons, RP2049 ... 555
Nozzles, spray, flow tests, RP2033 ... 449
Numerical analysis:
Integration of differential equations:
RP2041 ... 501
RP2046 ... 537
Remainder in linear methods of approximation, RP2041 ... 501

O

Oscillator plates, quartz, production of, RP2036 ... 459
Oxidation of carbon adsorbents, RP2009 ... 87
Oxide porcelains, physical properties, RP2034 ... 429
Ozone, seasonal variation at Washington, D. C., RP2022 ... 209

P

Paraffins:
Physical properties of, RP2038 ... 473
Vapor pressures and boiling points, RP2049 ... 555
Paulson, Rolf A., John L. Hague, Harry A. Bright, Determination of nitrogen in steel, RP2021 ... 201
Pennington, Neil L., William V. Loebenstein, Fundamental aspects of the reaction of oxygen with carbon adsorbents, RP2009 ... 87
Pentaborane, mass spectrum, RP2010 ... 97
Peterson, Chester, James L. Thomas, Irvin L. Cooter, Ralph Kotter, An absolute measurement of resistance by the Wenner method, RP2029 ... 291
Phase equilibria of oxide porcelains, RP2034 ... 429
Photometric characteristics of telescopic systems, RP2017 ... 157
Pinching, Gladys D., Roger G. Bates, Dissociation constants of weak bases from electromotive-force measurements of solutions of partially hydrolyzed salts, RP2043 ... 519
Pitzer, Kenneth S., Morton B. Epstein, Gordon M. Barrow, Frederick D. Rossini, Heats, equilibrium constants, and free energies of formation of the dimethylcyclopentanes, RP2026 ... 245
Plastics:
Laminated, mechanical properties, RP2028 ... 257
Method for determining ignition of, RP2052 ... 591
Plyler, Earle K., Leroy W. Tilton, Robert E. Stephens, Refractive indices of thallium bromide-iodide crystals for visible and infrared radiant energy, RP2008 ... 81
—, *Nicolo Acquista,* Infrared absorption spectra of cyclohydrocarbons, RP2002 ... 37
Porcelains, oxides physical properties, RP2034 ... 429
Portland cement, determination of soda and potash by flame photometry, RP2019 ... 173
Potash in portland cement, determination by flame photometry, RP2019 ... 173
Potential and capacitance of a conductor, RP2032 ... 377

Q

Quartz crystals, high frequency, production of, RP2036 ... 459

R

Radiosonde electric hydrometer elements, low-temperature performance RP2003 ... 49
Reese, Robert M., Vernon H. Dibeler, Fred L. Mohler, Laura Williamson, Mass spectrum of pentaborane (B_5H_9), RP2010 ... 97
Refractive:
Indices of hydrocarbons, RP2038 ... 473
Index of natural rubber for different wavelengths, RP2004 ... 57
Index of thallium bromide-iodide crystals, RP2008 ... 81
Power of lenses, measurement, RP2015 ... 137
Refractory oxide porcelains, some properties, RP2034 ... 429
Reinforced circular hole, instability in shear of plate with, RP2037 ... 465
Reinforcing bars, concrete, bond of, RP2050 ... 565
Remainder in linear methods of approximation, RP2041 ... 501
Resistance, absolute measurement of, RP2029 ... 291
Rossini, Frederick D., Alphonse F. Forziati, Physical properties of sixty API-NBS hydrocarbons, RP2038 ... 473
—, —, *William R. Harris,* Vapor pressures and boiling points of sixty API-NBS hydrocarbons, RP2049 ... 555
—, *John W. Knowlton,* Heats of combustion and formation of cyclopropane, RP2012 ... 113
—, *Morton, B. Epstein, Gordon M. Barrow, Kenneth S. Pitzer,* Heats, equilibrium constants, and free energies of formation of the dimethylcyclopentanes, RP2026 ... 245
Rowen, John W., Raymond L. Blaine, Charles M. Hunt, Submicroscopic structure of cellulose from nitrogen sorption measurements, RP2048 ... 547
Rubber:
Butyl, expansivity, RP2016 ... 145
Molded, directional effects in dielectric properties, RP2030 ... 355
Refractive index for different wavelengths, RP2004 ... 57

S

Sampling distribution of arithmetic mean, formulas for percentage points of, RP2007 ... 79
Scott, Arnold H., Directional effects in dielectric properties of molded rubber, RP2030 ... 355
Setchkin, Nicholas P., A method and apparatus for determining the ignition characteristics of plastics, RP2052 ... 591
Shafer, M. R., H. L. Borey, Laboratory flow tests of fixed-spray nozzles with hydrocarbons and with air, RP2035 ... 449
Shartsis, Leo, Rodrigo Canga, Surface tension of molten zinc borates, RP2023 ... 221
Shelton, George R., Elmer N. Bunting, Ansel S. Creamer, Properties of calcium-barium titanate dielectrics, RP2025 ... 237
Smith, Francis A., E. Carroll Creitz, Infrared absorption spectra of the liquid butenes and 1,3-butadiene, RP2031 ... 365
Snow, Chester, Potential problems and capacitance for a conductor bounded by two intersecting spheres, RP2032 ... 377
Soda, in portland cement, determination by flame photometry, RP2019 ... 173
Sodium 22, measurement of disintegration rate by a coincidence method, RP2047 ... 543
Sogn, Leland T., Walter J. Howard, Mechanical production of very thin oscillator plates, RP2036 ... 459
Sorrows, Howard E., Robert C. Ellenwood, Cathode heater compensation as applied to degenerative voltage-stabilized direct-current power supplies, RP2027 ... 251
Spectra, infrared absorption:
Of cyclohydrocarbons, RP2002 ... 37
Of the liquid butenes and 1,3-butadiene, RP2031 ... 365
Spectrophotometer, application to colorimetry of titanium pigments, RP2024 ... 227
Stair, Ralph, Seasonal variation of ozone at Washington, D. C., RP2022 ... 209
Steel:
Determination of nitrogen in, RP2021 ... 201
Effect of chromium plating on endurance limit, RP2011 ... 101
Stephens, Robert E., Leroy W. Tilton, Earle K. Plyler, Refractive indices of thallium bromide-iodide crystals for visible and infrared radiant energy, RP2008 ... 81
Stratosphere, ozone measurements at Washington, D. C., RP2022 ... 209
Stress, critical shear, of square plate with circular reinforced hole, RP2037 ... 465
Surface:
Area measurements on cotton linters, RP2048 ... 547
Tension of molten zinc borates, RP2023 ... 221

Page

Swerdlow, Max, Sanford B. Newman, Emil Borysko, Ultra-microtomy by a new method, RP2020 183

T

Telescopic systems, relation between entrance and exit pupils, RP2017 157
Temperature scales, international, differences between scales of 1948 and 1927, RP2014 133
Thallium bromide-iodide crystals, refractive index, RP2008 81
Thomas, Carroll, Harry K. Herschman, Fatigue characteristics of electroformed sheets with and without iron backing, RP2039 477
Thomas, James L., Chester Peterson, Irvin L. Coder, Ralph Kotter, An absolute measurement of resistance by the Wenner method, RP2029 291
Tilton, Leroy W., Earle K. Plyler, Robert E. Stephens, Refractive indices of thallium bromide-iodide crystals for visible and infrared radiant energy, RP2008 81
—, *Wood, Lawrence A.,* Refractive index of natural rubber for different wavelengths, RP2004 57

U

Ultraviolet measurements, solar, of variation of ozone at Washington, D. C., RP2022 269
Uranium, freezing point, RP2042 513

V

Valore, Rudolph C., Volume changes observed in small concrete cylinders during freezing and thawing with a mercury displacement dilatometer, RP2000 1

Page

Vapor pressures of hydrocarbons, RP2049 555
Volume changes, measurement, RP2016 145

W

Washer, Francis E., An instrument for measuring longitudinal spherical aberration of lenses, RP2015 137
Wells, Edmunds J., Evelyn G. Bloom, Fred L. Mohler, C. Edward Wise, Metastable transitions in mass spectra of hydrocarbons, RP2005 65
—, *Fred L. Mohler, Evelyn G. Bloom, Laura Williamson, C. Edward Wise,* Mass spectra of C_3H_8 isomers, RP2045 533
Wenner method for measurement of resistance, RP2029 291
Weiler, Arnold, Low-temperature performance of radiosonde electric hygrometer elements, RP2003 49
Williamson, Laura, Fred L. Mohler, Evelyn G. Bloom, C. Edward Wise, Edmunds J. Wells, Mass spectra of C_3H_8 isomers, RP2045 533
—, *Vernon H. Dibeler, Fred L. Mohler, Robert M. Reese,* Mass spectrum of pentaborane (B_5H_9), RP2010 97
Wise, C. Edward, Evelyn G., Bloom, Fred L. Mohler, Edmunds J. Wells, Metastable transitions in mass spectra of hydrocarbons, RP2005 65
—, *Fred L. Mohler, Evelyn G. Bloom, Laura Williamson, Edmunds J. Wells,* Mass spectra of C_3H_8 isomers, RP2045 533
Wood, Lawrence A., Leroy W. Tilton, Refractive index of natural rubber for different wavelengths, RP2004 57

Z

Zinc borates, surface tension, RP2023 221
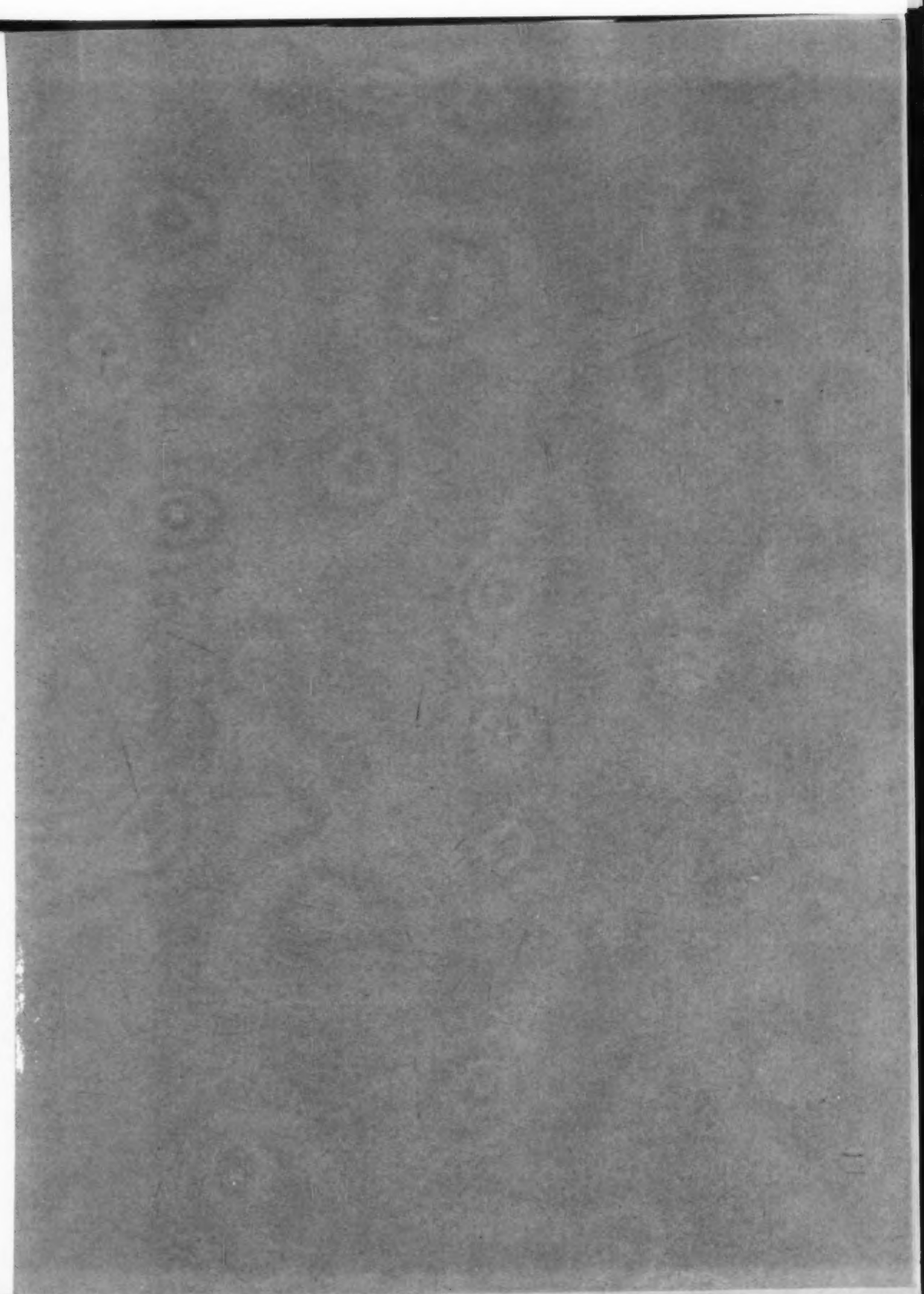
U. S. GOVERNMENT PRINTING OFFICE: 1949